Physics Reports 472 (2009) 1–76

Contents lists available at ScienceDirect

Physics Reports

journal homepage: www.elsevier.com/locate/physrep

Primordial nucleosynthesis: From precision cosmology to fundamental physics

Fabio Iocco [a,1], Gianpiero Mangano [b], Gennaro Miele [b,c,*], Ofelia Pisanti [b], Pasquale D. Serpico [d,2]

[a] INAF, Osservatorio Astrofisico di Arcetri, Largo E. Fermi 5, I-50125 Firenze, Italy

[b] Dip. Scienze Fisiche, Università di Napoli Federico II & INFN, Sez. di Napoli, Complesso Univ. Monte S. Angelo, Via Cintia, I-80126 Napoli, Italy

[c] Instituto de Física Corpuscular (CSIC-Universitat de València), Ed. Institutos de Investigación, Apartado de Correos 22085, E-46071 València, Spain

[d] Center for Particle Astrophysics, Fermi National Accelerator Laboratory, Batavia, IL 60510-0500, USA

ARTICLE INFO

Article history:
Accepted 17 February 2009
Available online 28 February 2009
editor: M.P. Kamionkowski

PACS:
98.80.Ft
26.35.+c
98.62.Ai

Keywords:
Primordial nucleosynthesis
Early universe
Physics beyond the standard model

ABSTRACT

We present an up-to-date review of Big Bang Nucleosynthesis (BBN). We discuss the main improvements which have been achieved in the past two decades on the overall theoretical framework, summarize the impact of new experimental results on nuclear reaction rates, and critically re-examine the astrophysical determinations of light nuclei abundances. We report then on how BBN can be used as a powerful test of new physics, constraining a wide range of ideas and theoretical models of fundamental interactions beyond the standard model of strong and electroweak forces and Einstein's general relativity.

Contents

* Corresponding author at: Dip. Scienze Fisiche, Università di Napoli Federico II & INFN, Sez. di Napoli, Complesso Univ. Monte S. Angelo, Via Cintia, I-80126 Napoli, Italy.
E-mail address: miele@na.infn.it (G. Miele).
1 Present address: Institut d'Astrophysique de Paris, 98bis bd Arago, 75014 Paris, France.
2 Present address: Physics Division, Theory Group, CERN, CH-1211 Geneva 23, Switzerland.

0370-1573/$ – see front matter
doi:10.1016/j.physrep.2009.02.002

1. Introduction

A remarkable scientific achievement in the second half of the 20th century has been the establishment of "Standard Models" of Particle Physics (SMPP) and Cosmology (SMC). In particular, the latter has been possible thanks to an incredibly fast growth of the amount and quality of observations over the last couple of decades. The picture revealed is at the same time beautifully simple and intriguingly mysterious: on one hand, known gauge interactions and Einstein's general relativity seem able to explain a huge wealth of information in terms of a few free parameters specifying the composition/initial conditions of the Universe; on the other hand, these numbers are not explained in terms of dynamical processes involving the known fields and interactions. This is the case of the "dark energy" density (consistent with a cosmological constant), of the non-baryonic dark matter, of the baryon–antibaryon asymmetry, the flatness, homogeneity and isotropy of the universe on large scales, etc.

The very success of the cosmological laboratory is thus providing much indirect evidence for physics beyond the SMPP. On the other hand, advances in particle physics (a very recent example being the phenomenology of massive neutrinos) have an impact at the cosmological level. This interplay has proven extremely fertile ground for the development of 'astroparticle physics', especially since many theories beyond the SMPP predict new phenomena far beyond the reach of terrestrial laboratories, but potentially testable in astrophysical and cosmological environments. In this respect, the nucleosynthesis taking place in the primordial plasma plays a twofold role: it is undoubtedly one of the observational pillars of the hot Big Bang model, being indeed known simply as "Big Bang Nucleosynthesis" (BBN); at the same time, it provides one of the earliest direct cosmological probes nowadays available, constraining the properties of the universe when it was a few seconds old, or equivalently at the MeV temperature scale. Additionally, it is special in that all known interactions play an important role: gravity sets the dynamics of the "expanding cauldron", weak interactions determine the neutrino decoupling and the neutron–proton equilibrium freeze-out, electromagnetic and nuclear processes regulate the nuclear reaction network.

The basic framework of the BBN emerged in the decade between the seminal Alpher–Bethe–Gamow (known as $\alpha\beta\gamma$) paper in 1948 [1] and the essential settlement of the paradigm of the stellar nucleosynthesis of elements heavier than ^{7}Li

with the B^{2}FH paper [2]. This pioneering period – an account of which can be found in [3] – established the basic picture that sees the four light-elements ^{2}H, ^{3}He, ^{4}He and ^{7}Li as products of the early fireball, and virtually all the rest produced in stars or as a consequence of stellar explosions.

In the following decades, the emphasis on the role played by the BBN has evolved significantly. In the simplest scenario, the only free parameters in primordial nucleosynthesis are the baryon to photon ratio η (equivalently, the baryon density of the universe) and the neutrino asymmetry parameters, η_{ν_α} (see Section 6.3). However, only neutrino asymmetries larger than η by many orders of magnitude have appreciable effects. This is why the simple case where all η_{ν_α}'s are assumed to be negligibly small (e.g., of the same order of η) is typically denoted as Standard BBN (SBBN). Since several species of 'nuclear ashes' form during BBN, SBBN is an over-constrained theory whose self-consistency can be checked comparing predictions with two or more light nuclide determinations. The agreement of predicted abundances of the light elements with their measured abundances (spanning more than nine orders of magnitude!) confirmed the credibility of BBN as a cosmological probe. At the same time, the relatively narrow range of η where a consistent picture emerged was the first compelling argument in favor of the non-baryonic nature of the "dark matter" invoked for astrophysical dynamics.

The past decade, when for the first time a redundancy of determinations of η has been possible, has stressed BBN as a consistency tool for the SMC. Beside BBN, one can infer the density of baryons from the Lyman-α opacity in quasar spectra due to intervening high redshift hydrogen clouds [4–6]; from the baryon fraction in clusters of galaxies, deduced from the hot x-ray emission [7]; most importantly, from the height of the Doppler peak in the angular power spectrum of the cosmic microwave background anisotropy (see [8] for the latest WMAP results). These determinations are not only mutually consistent with each other, but the two most accurate ones (from the CMB and BBN) agree within 5%–10%. While losing to CMB the role of "barometer of excellence", BBN made possible a remarkable test of consistency of the whole SMC.

It comes without surprise that this peculiar 'natural laboratory' has inspired many investigations, as testified by the numerous reviews existing on the subject, see e.g. [9–14]. Why then a new review? In the opinion of the authors, a new BBN review seems worthy because at present, given the robustness of the cosmological scenario, the attention of the community is moving towards a new approach to the BBN. On one hand, one uses it as a precision tool in combination with other cosmological information to reduce the number of free parameters to extract from multi-parameter fits. On the other hand, BBN is an excellent probe to explore the very early universe, constraining scenarios beyond the SMPP. The latter motivation is particularly intriguing given the perspectives of the forthcoming LHC age to shed light on the TeV scale. A new synergy with the Lab is expected to emerge in the coming years, continuing a long tradition in this sense. Finally, a wealth of data from nuclear astrophysics and neutrino physics have had a significant impact on BBN, and it is meaningful to review and assess it. In particular, the recent advances in the neutrino sector have made obsolete many exotic scenarios popular in the literature still a decade ago and improved numerous constraints, providing a clear example of the synergy we look forward to in the near future.

This review is structured as follows: in Section 2 we summarize the main cosmological notions as well as most of the symbols used in the rest of the article. Section 3 is devoted to the description of the Standard BBN scenario. Section 4 treats the status of observations of light nuclei abundances, which in Section 5 are compared with theoretical predictions. The following sections deal with exotic scenarios: Section 6 with neutrino properties, Section 7 with inhomogeneous models, Section 8 with constraints to fundamental interactions and Section 9 with massive particles. In Section 10 we report our conclusions. Although this article is a review, many analyses have been implemented ex-novo and some original results are presented here for the first time. Due to the large existing literature and to space limitation, we adopt the criterion to be as complete as possible in the post-2000 literature, while referring to previous literature only when pertinent to the discussion or when still providing the most updated result. Also, we adopt a more pedagogical attitude in introducing arguments that have rarely or never entered previous BBN reviews, as for example extra dimensions or variation of fundamental constants in Section 8, while focusing mainly on new results (as opposed to a 'theory review') in subjects that have been extensively treated in the past BBN literature (as in SUSY models leading to cascade nucleosynthesis, the gravitino 'problem', etc.). Other topics, which for observational or theoretical reasons have attracted far less interest in the past decade in relation to BBN bounds, are only briefly mentioned or omitted completely (this is the case of technicolor or cosmic strings). Older literature containing a more extensive treatment of these topics can be typically retraced from the quoted reviews. In the following, unless otherwise stated, we use natural units $\hbar = c = k_B = 1$, although conventional units in the astronomical literature (as parsec and multiples of it) are occasionally used where convenient for the context.

2. Standard cosmology

To keep this review self-contained, and fix the notation which we will be using in this paper, we summarize here the main aspects of the cosmological model which are relevant for our analysis. The standard hot Big Bang model is based on three fundamental astronomical observations: the Hubble law, the almost perfect black body spectrum of the background photon radiation, and the homogeneity and isotropy of the universe on large scales, see e.g. [15,16], The latter, also known under the spell of *Cosmological Principle* implies that the metric itself should be homogeneous and isotropic, and singles out the Friedmann–Lemaître–Robertson–Walker (FLRW) models. In comoving spherical coordinates one has:

$$\mathrm{d}s^2 = g_{\mu\nu}\mathrm{d}x^\mu \mathrm{d}x^\nu = \mathrm{d}t^2 - a^2(t)\left[\frac{\mathrm{d}r^2}{1-kr^2} + r^2(\mathrm{d}\theta^2 + \sin^2\theta\,\mathrm{d}\phi^2)\right], \tag{1}$$

where $a(t)$ is the cosmic scale-factor and $k = 1, 0, -1$ the rescaled spatial curvature signature for an elliptic, euclidean or hyperbolic space, respectively.

The Einstein field equations relate the energy–momentum tensor of the perfect fluid representing the matter-energy content of the universe,

$$T_{\mu\nu} = -P\, g_{\mu\nu} + (P + \rho) u_\mu u_\nu, \tag{2}$$

with the space–time curvature $R_{\mu\nu\rho\sigma}$,

$$R_{\mu\nu} - \frac{R}{2} g_{\mu\nu} = 8\pi\, G_N\, T_{\mu\nu} + \Lambda g_{\mu\nu}, \tag{3}$$

where $R_{\mu\nu}$ is the Ricci tensor, $R_{\mu\nu} \equiv g^{\rho\sigma} R_{\rho\mu\sigma\nu}$, R the scalar curvature, $R = g^{\mu\nu} R_{\mu\nu}$, G_N the Newton gravitational constant, and Λ the cosmological constant. Substituting the FLRW metric (1) in the Einstein's equations (3) gives the Friedmann–Lemaître (FL) equation for the Hubble parameter H,

$$H^2 \equiv \left(\frac{\dot{a}}{a}\right)^2 = \frac{8\pi\, G_N}{3}\rho - \frac{k}{a^2}. \tag{4}$$

The equation of state of the fluid filling the universe, $P = P(\rho)$, specifying the pressure as a function of the energy density, along with the covariant conservation of the energy momentum tensor (which accounts for the entropy conservation if the fluid corresponds to a thermal bath of particle excitations),

$$\frac{\mathrm{d}(\rho a^3)}{\mathrm{d}a} = -3\, P a^2, \tag{5}$$

allows one to get the evolution of ρ as function of a,

$$\rho_M \propto a^{-3}, \tag{6}$$

$$\rho_R \propto a^{-4}, \tag{7}$$

$$\rho_\Lambda \propto \text{const}, \tag{8}$$

for matter (both baryonic and dark matter, $P_B, P_{DM} \sim 0$), radiation ($P_R = \rho_R/3$), or cosmological constant ($P_\Lambda = -\rho_\Lambda$), respectively.

As usual, the present values of radiation, baryon matter, dark matter and cosmological constant energy densities will be expressed in terms of the parameters $\Omega_i = \rho_i^0/\rho_{cr}$, $i = R, B, DM, \Lambda$, with $\rho_{cr} = 3H_0^2/(8\pi G_N)$ the critical density today and $H_0 = 100$ h km s^{-1} Mpc^{-1}, with $h = 0.73^{+0.04}_{-0.03}$ [17]. To quantify the baryon density parameter we will also use $\omega_b \equiv \Omega_B h^2$ and the baryon to photon density ratio, $\eta = n_B/n_\gamma$. The latter is also proportional to the initial baryon–antibaryon asymmetry per comoving volume produced at some early stage of the universe evolution. This ratio keeps constant after the $e^+ - e^-$ annihilation phase taking place at a value of the photon temperature $T \sim 0.3$ MeV (see later). Moreover, at low energy scales there are no baryon violating interactions at work, thus the value of η can be simply related to Ω_B, see e.g. [18]

$$\eta_{10} \equiv \eta \times 10^{10} = \frac{273.45\, \Omega_B h^2}{1 - 0.007 Y_p} \left(\frac{2.725\ \mathrm{K}}{T_0}\right)^3 \left(\frac{6.708 \times 10^{-45}\ \mathrm{MeV}^{-2}}{G_N}\right), \tag{9}$$

where Y_p stands for ^{4}He mass fraction (see Section 3.1) and T_0 the photon temperature today. Note that the numerical factor multiplying Y_p takes into account the effect of the ^{4}He binding energy on the whole energy budget in baryonic matter.

Matter and radiation fluids can be usually described in terms of a bath of particle excitations of the corresponding quantum fields. In particular, at high temperatures rapid interactions among them ensures thermodynamical equilibrium and each particle specie is described by an equilibrium (homogeneous and isotropic) phase space distribution function,

$$f_i(|\mathbf{p}|, T) = \left[\exp\left(\frac{E_i(|\mathbf{p}|) - \mu_i}{T}\right) \pm 1\right]^{-1}, \tag{10}$$

where $E_i(|\mathbf{p}|) = \sqrt{|\mathbf{p}|^2 + m_i^2}$ is the energy, $+/-$ corresponds to the Fermi–Dirac/Bose–Einstein statistics, and μ_i the chemical potential, which is zero for particles which can be emitted or absorbed in any number (like photons).

In the comoving frame, the number density, energy density and pressure can be expressed as follows

$$n_i(T) = g_i \int \frac{\mathrm{d}^3\mathbf{p}}{(2\pi)^3} f_i(|\mathbf{p}|, T), \tag{11}$$

$$\rho_i(T) = g_i \int \frac{\mathrm{d}^3\mathbf{p}}{(2\pi)^3} E_i(|\mathbf{p}|) f_i(|\mathbf{p}|, T), \tag{12}$$

$$P_i(T) = g_i \int \frac{\mathrm{d}^3\mathbf{p}}{(2\pi)^3} \frac{|\mathbf{p}|^2}{3\, E_i(|\mathbf{p}|)} f_i(|\mathbf{p}|, T), \tag{13}$$

where g_i is the number of internal degrees of freedom. The BBN takes place in the radiation dominated phase, hence non-relativistic particles contribute negligibly to the total energy density, which therefore can be conveniently written in terms of the photon energy density $\rho_\gamma = \pi^2 T^4/15$,

$$\rho \sim \rho_R = g_* \frac{\rho_\gamma}{2}, \tag{14}$$

which defines g_*, the total number of relativistic degrees of freedom,

$$g_* = \sum_{B_i} g_i \left(\frac{T_i}{T}\right)^4 + \frac{7}{8} \sum_{F_i} g_i \left(\frac{T_i}{T}\right)^4, \tag{15}$$

where the first and second terms are due to all boson and fermion species, respectively. The possibility is left in the previous formula of different T_i for different species, accounting for pseudo-thermal distributions of decoupled fluids (like relativistic neutrinos at BBN times).

Finally, we will also exploit in the following the definition of the entropy density, $s(T)$, in terms of the phase space distribution function. For a given specie i one has:

$$s_i(T) = \frac{\rho_i + P_i}{T} = g_i \int \frac{\mathrm{d}^3\mathbf{p}}{(2\pi)^3} \frac{3m_i^2 + 4|\mathbf{p}|^2}{3\,T\,E_i(|\mathbf{p}|)} f_i(|\mathbf{p}|, T). \tag{16}$$

The total entropy density is conventionally written as

$$s(T) = \frac{\pi^4}{45\,\zeta(3)} g_{*s}(T) n_\gamma = \frac{2\pi^2}{45} g_{*s}(T) T^3, \tag{17}$$

where $n_\gamma = (2\,\zeta(3)/\pi^2)\,T^3$ is the number density of photons and

$$g_{*s}(T) = \sum_{B_i} g_i \left(\frac{T_i}{T}\right)^3 + \frac{7}{8} \sum_{F_i} g_i \left(\frac{T_i}{T}\right)^3. \tag{18}$$

Use of Eq. (5) implies that entropy per comoving volume is a conserved quantity, $s(t)a^3 = \text{const}$.

3. Big bang nucleosynthesis

3.1. Overview

Extrapolating the present universe back in the past, we infer that during its early evolution, before the epoch of nucleosynthesis, it was hot and dense enough for electrons, positrons, photons, neutrinos and nucleons, as well heavier nuclei, to be in kinetic and chemical equilibrium due to the high (weak, strong and electromagnetic) interaction rates. In particular, the initial values of all nuclear densities are set by Nuclear Statistical Equilibrium (NSE). NSE implies that they constitute a completely negligible fraction of the total baryon density, which is all in the form of free neutrons and protons. As expansion proceeds, weak process rates become eventually smaller than the expansion rate H at that epoch, hence some particle species can depart from thermodynamical equilibrium with the remaining plasma. This is the case of neutrinos which only interact via weak processes and *freeze out* at a temperature of about 2–3 MeV. Soon after, at a temperature $T_D \sim 0.7$ MeV, neutron–proton charged-current weak interactions also become too slow to guarantee neutron–proton chemical equilibrium. The n/p density ratio departs from its equilibrium value and freezes out at the value $\mathrm{n/p} = \exp(-\Delta m/T_D) \sim 1/7$, with $\Delta m = 1.29$ MeV the neutron–proton mass difference, and is then only reduced by subsequent neutron decays. At this stage, the photon temperature is already below the deuterium binding energy $B_D \simeq 2.2$ MeV, thus one would expect sizable amounts of ^{2}H to be formed via $\mathrm{n} + \mathrm{p} \to {}^2\mathrm{H} + \gamma$ process. However, the large photon-nucleon density ratio η^{-1}, which is of the order of 10^9, delays deuterium synthesis until the photo–dissociation process become ineffective (deuterium *bottleneck*). This takes place at a temperature T_N such that $\exp(B_D/T_N)\eta \sim 1$, i.e. $T_N \sim 100$ keV, which states the condition that the high energy tail in the photon distribution with energy larger than B_D has been sufficiently diluted by the expansion.

Once ^{2}H starts forming, a whole nuclear process network sets in, leading to heavier nuclei production, until BBN eventually stops, see Section 4. An estimate of the main BBN outcome, i.e. ^{4}He, can be obtained with very simple arguments, yet it provides quite an accurate result. Indeed, the final density $n_{^4\mathrm{He}}$ of ^{4}He is very weakly sensitive to the whole nuclear network, and a very good approximation is to assume that all neutrons which have not decayed at T_N are eventually bound into helium nuclei, see e.g. [19,12]. This leads to the famous result for the helium mass fraction $Y_p \equiv 4\,n_{^4\mathrm{He}}/n_B$

$$Y_p \sim \frac{2}{1 + \exp(\Delta m/T_D)\exp(t(T_N)/\tau_n)} \sim 0.25, \tag{19}$$

with $t(T_N)$ the value of time at T_N and τ_n the neutron lifetime.

Table 1
Nuclides which are typically considered in BBN numerical studies.

Z \ N	0	1	2	3	4	5	6	7	8
0		n							
1	H	^{2}H	^{3}H						
2		^{3}He	^{4}He						
3				^{6}Li	^{7}Li	^{8}Li			
4				^{7}Be		^{9}Be			
5				^{8}B		^{10}B	^{11}B	^{12}B	
6						^{11}C	^{12}C	^{13}C	^{14}C
7						^{12}N	^{13}N	^{14}N	^{15}N
8							^{14}O	^{15}O	^{16}O

On the other hand, the determination of all light nuclei produced during BBN, and a more accurate determination of ^{4}He as well, can be only pursued by a simultaneous solution of a set of coupled kinetic equations which rule the evolution of the various nuclei, supplemented by Einstein's equations, covariant conservation of total energy momentum tensor, as well as conservation of baryon number and electric charge. This is typically obtained numerically, although nice semi-analytical studies have been also recently performed [20].

To summarize the general BBN setting, we start with some definitions. We consider N_{nuc} species of nuclides, whose number densities, n_i, are normalized with respect to the total number density of baryons n_B,

$$X_i = \frac{n_i}{n_B} \quad i = p, {}^{2}\mathrm{H}, {}^{3}\mathrm{He}, \ldots . \tag{20}$$

The list of nuclides which are typically considered in BBN analysis is reported in Table 1. To quantify the most interesting abundances, those of ^{2}H, ^{3}He, ^{4}He and ^{7}Li, we also use in the following the short convenient definitions

$$^{2}\mathrm{H/H} \equiv X_{^{2}\mathrm{H}}/X_p, \qquad ^{3}\mathrm{He/H} \equiv X_{^{3}\mathrm{He}}/X_p, \qquad Y_p \equiv 4X_{^{4}\mathrm{He}}, \qquad ^{7}\mathrm{Li/H} \equiv X_{^{7}\mathrm{Li}}/X_p, \tag{21}$$

i.e. the ^{2}H, ^{3}He and ^{7}Li number density normalized to hydrogen, and the ^{4}He mass fraction, Y_p. Notice that, although the above definition of Y_p is widely used, it is only approximately related to the real helium mass fraction, since the ^{4}He mass is not given by 4 times the atomic mass unit. The difference is quite small, of the order of 0.5% due to the effect of ^{4}He binding energy. However, in view of the present precision of theoretical analysis on ^{4}He yield, this difference cannot be neglected, and one should clearly state if one refers to the conventional quantity Y_p (as we do here, too) or the "true" helium mass fraction. In the (photon) temperature range of interest for BBN, 10 MeV $\gtrsim T \gtrsim$ 10 keV, electrons and positrons are kept in thermodynamical equilibrium with photons by fast electromagnetic interactions and are distributed according to a Fermi–Dirac function $f_{e^{\pm}}$, with chemical potential $\pm\mu_e$, parameterized in the following by the ratio $\phi_e \equiv \mu_e/T$. The chemical potential of electrons is very small, due to the universe charge neutrality [21,22],

$$\frac{\mu_e}{T} \sim \frac{n_e}{n_\gamma} = \frac{n_p}{n_\gamma} \sim 10^{-10}. \tag{22}$$

To follow the neutrino-antineutrino fluid in detail, it is necessary to write down evolution equations for their distribution in phase space, rather than simply using their energy density. This is due to the fact, as we will illustrate in details in the following, that they are slightly reheated during the $e^{+} - e^{-}$ annihilation phase and develop non-thermal momentum-dependent features. We denote these distributions by $f_{\nu_e}(|\mathbf{p}|, t), f_{\bar{\nu}_e}(|\mathbf{p}|, t)$ and

$$f_{\nu_\mu} = f_{\nu_\tau} \equiv f_{\nu_x}(|\mathbf{p}|, t), \qquad f_{\bar{\nu}_\mu} = f_{\bar{\nu}_\tau} \equiv f_{\bar{\nu}_x}(|\mathbf{p}|, t). \tag{23}$$

In the standard scenario of no extra relativistic degrees of freedom at the BBN epoch apart from photons and neutrinos, the neutrino chemical potential is bound to be a small fraction of the neutrino temperature. This bound applies to all neutrino flavors, whose distribution functions are homogenized via flavor oscillations [23–25]. In this section we focus on non-degenerate neutrinos, namely $f_{\nu_e} = f_{\bar{\nu}_e}$ and $f_{\nu_x} = f_{\bar{\nu}_x}$, while we will consider in details the effect of neutrino–antineutrino asymmetry in Section 6.3.

The set of differential equations ruling primordial nucleosynthesis is the following, see for example [26–30]:

$$\frac{\dot{a}}{a} = H = \sqrt{\frac{8\pi G_N}{3}\rho}, \tag{24}$$

$$\frac{\dot{n}_B}{n_B} = -3H, \tag{25}$$

$$\dot{\rho} = -3H\,(\rho + P), \tag{26}$$

$$\dot{X}_i = \sum_{j,k,l} N_i \left(\Gamma_{kl\to ij} \frac{X_k^{N_k} X_l^{N_l}}{N_k! N_l!} - \Gamma_{ij\to kl} \frac{X_i^{N_i} X_j^{N_j}}{N_i! N_j!} \right) \equiv \Gamma_i, \tag{27}$$

$$n_B \sum_j Z_j X_j = n_{e^-} - n_{e^+} \equiv L\left(\frac{m_e}{T}, \phi_e\right) \equiv T^3\, \hat{L}\left(\frac{m_e}{T}, \phi_e\right), \tag{28}$$

$$\left(\frac{\partial}{\partial t} - H|\mathbf{p}| \frac{\partial}{\partial |\mathbf{p}|} \right) f_{\nu_\alpha}(|\mathbf{p}|, t) = I_{\nu_\alpha}\left[f_{\nu_e}, f_{\bar{\nu}_e}, f_{\nu_x}, f_{\bar{\nu}_x}, f_{e^-}, f_{e^+} \right], \tag{29}$$

where ρ and P denote the total energy density and pressure, respectively,

$$\rho = \rho_\gamma + \rho_e + \rho_\nu + \rho_B, \tag{30}$$

$$P = P_\gamma + P_e + P_\nu + P_B. \tag{31}$$

Eq. (24) is the definition of the Hubble parameter H, whereas Eqs. (25) and (26) state the total baryon number and entropy conservation per comoving volume, respectively. The set of N_{nuc} Boltzmann equations (27) describes the density evolution of each nuclide specie, Eq. (28) states the universe charge neutrality in terms of the electron chemical potential, with $L\,(m_e/T, \phi_e)$ the charge density in the lepton sector in unit of the electron charge, and finally Eqs. (29) are the Boltzmann equations for neutrino species, with $I_{\nu_\alpha}\left[f_{\nu_e}, f_{\nu_x}\right]$ standing for the collisional integral which contains all microscopic processes creating or destroying the specie ν_α.

Since electromagnetic and nuclear scatterings keep the non-relativistic baryons in kinetic equilibrium their energy density ρ_B and pressure P_B are given by

$$\rho_B = \left[M_u + \sum_i \left(\Delta M_i + \frac{3}{2} T \right) X_i \right] n_B, \tag{32}$$

$$P_B = T\, n_B \sum_i X_i, \tag{33}$$

with ΔM_i and M_u the i-th nuclide mass excess and the atomic mass unit, respectively.

The pressure and energy density of the electromagnetic plasma ($e^\pm$ and γ) receives a contribution at first order in the fine structure coupling α when considering QED finite temperature corrections which change the electromagnetic plasma equation of state via the appearance of a thermal mass for both photons and $e^\pm$, which in turn change the particle dispersion relation $E_{e,\gamma}(p)$. This has been studied e.g. in [31–33]. These corrections also enter Eq. (26), the expression of the expansion rate H, as well as the thermal averaged n–p weak conversion rates, which depend upon electron–positron distribution function (see later). It has been shown that at the time of BBN, all these effects slightly influence the ^{4}He abundance, at the level of per mille [32].

In Eq. (27) i, j, k, l denote nuclear species, N_i the number of nuclides of type i entering a given reaction (and analogously N_j, N_k, N_l), while the Γ's denote symbolically the reaction rates. For example, in the case of decay of the species i, $N_i = 1, N_j = 0$ and $\sum \Gamma_{i\to kl}$ is the inverse lifetime of the nucleus i. For two-body collisions $N_i = N_j = N_k = N_l = 1$ and $\Gamma_{ij\to kl} = \langle \sigma_{ij\to kl}\, v \rangle$, the thermal averaged cross-section for the reaction is $i + j \to k + l$ times the i–j relative velocity. In Eq. (28), Z_i is the charge number of the i-th nuclide, and the function $\hat{L}(\xi, \omega)$ is defined as

$$\hat{L}(\xi, \omega) \equiv \frac{1}{\pi^2} \int_\xi^\infty \mathrm{d}\zeta\, \zeta \sqrt{\zeta^2 - \xi^2} \left(\frac{1}{e^{\zeta - \omega} + 1} - \frac{1}{e^{\zeta + \omega} + 1} \right). \tag{34}$$

Eqs. (24)–(29) constitute a set of coupled differential equations which have been implemented in numerical codes since the pioneering works of Wagoner, Fowler and Hoyle [26] and Kawano [34,35]. Before discussing some details of this implementation and its present status, we describe two crucial phenomena which take place before the BBN, the freezing out of neutrino distribution functions and of the neutron–proton density ratio, when the weak charged current n–p processes become too slow to ensure chemical equilibrium between the two nucleon species. At the time these two phenomena occur the synthesis of deuterium, and thus of the whole nuclear chain, is still strongly forbidden by photo–dissociation processes, and all baryon density is in the form of free neutrons and protons. This means that in principle they could be treated *independently* of the whole set of nuclear processes which leads to the proper BBN phase. In particular, once obtained the shape of neutrino distribution functions, they can be used as given inputs when solving the set of Eqs. (24)–(25), thus significantly simplifying the problem.

3.2. The role of neutrinos in BBN and neutrino decoupling

At early epochs neutrinos were kept in thermal contact with the electromagnetic primordial plasma by rapid weak interactions with electrons and positrons, controlled by a rate $\Gamma_w \simeq \langle \sigma_w\, v \rangle n_{e^\pm} \sim G_F^2\, T^2 \times T^3$. When the temperature dropped

below a few MeV, these weak processes became too slow compared to the Hubble expansion rate ($\Gamma_w < H \sim \sqrt{G_N} T^2$) and the process of neutrino decoupling took place. An accurate estimate for the neutrino decoupling temperature is 2.3 MeV for the electron neutrino and slightly larger for $\nu_{\mu,\tau}$, 3.5 MeV [36], since the latter only interact with the electromagnetic plasma via neutral current processes.

Shortly after, the $e^{\pm}$ pairs began to annihilate almost entirely into photons, thus producing a difference between the temperatures of the relic photons and neutrinos. The MeV to 0.1 MeV range is crucial for BBN physics, and in particular for the neutron–proton fraction, so it comes without surprise that BBN is sensitive to the properties of neutrinos: it derives from the basic facts that the neutrino decoupling, the deuterium binding energy, the n–p mass difference and the electron mass all fall in the MeV range. In more detail, neutrinos enter BBN equations in three ways:

I the momentum distributions of the ν_e and $\bar{\nu}_e$ entering the n–p inter-conversion weak rates;
II their overall energy density content ρ_ν, which determines the Hubble expansion rate;
III their overall pressure P_ν, which enters the energy–momentum conservation law. *Assuming* the equation of state of relativistic species $P_\nu = \rho_\nu/3$, this effect is not independent from the previous one, and we shall not discuss it further.

The effect (I) is clearly model-dependent, in the sense that it can be quantified and parameterized only on the basis of a physically-motivated hypothesis. One popular example where the effect of neutrinos is dominated by this distortion is the case of a $\nu_e - \bar{\nu}_e$ asymmetry, see Section 6.3. Concerning the effect (II), it is customary to parameterize it via an effective number of neutrinos $N_{\rm eff}$ [37,38], defined by the relation

$$\rho_\nu \equiv \frac{N_{\rm eff}}{3} \rho_{\nu,0}, \tag{35}$$

where $\rho_{\nu,0}$ is the energy density in neutrinos in the limit of instantaneous decoupling from the e^+, e^-, γ plasma and no radiative or plasma corrections (see Eq. (40) below). Nowadays, precision electroweak measurements at the Z^0-resonance pin down the number of *light active* neutrino species with high accuracy, $N_\nu = 2.9840 \pm 0.0082$ [39], consistent within $\sim 2\,\sigma$ with the known three families of the SMPP. However, well before these measurements were available, BBN was already invoked to favor 3 light, thermalized (and thus probably active with respect to weak interactions) neutrino families, with a range not wider than 2-4 (see Refs. in the reviews [12,13,11]). While this connection between collider physics and cosmology has been historically important, we would like here to clarify some common misunderstanding and ambiguities on the BBN bound on $N_{\rm eff}$. If the bound is derived by changing only $N_{\rm eff}$, but without including any effect of the type (I), it is incorrect to refer to it as a bound on neutrino properties. It is rather a statement on the rate of expansion of the universe at the BBN time, which may be indicative e.g. of the presence of additional (semi)relativistic species in the plasma, or of exotic thermal histories. Any reasonable BBN bound on the number of neutrino species N_ν requires a modification of the type (I) as well. Since no universal parametrization exists, this is often neglected. Yet, this should not diminish the importance of the point. For example, if we accompany the rescaling of Eq. (35) by an identical rescaling of the ν_e and $\bar{\nu}_e$ distribution function (i.e. adopting a gray-body parametrization, keeping the temperature of the spectrum unchanged but altering the normalization), the range of Y_p that for standard parameters corresponds to $2.8 \leq N_{\rm eff} \leq 3.6$ (see Section 5) translates into a more severe constraint, $2.85 \leq N_\nu \leq 3.12$. It is worth noting that no role is played in BBN by possible heavy fourth generation neutrinos, whose mass must be larger than $\sim$45 GeV to avoid the Z-width bound. Even if such a neutrino exists, it would be natural to expect it to be unstable and rather short-lived, for example due to mixing with the light neutrinos (neutrino oscillations prove that family lepton-numbers are violated). Even if some protective symmetry prevents the decay (so that it accounts for a subleading fraction of the cold dark matter), no effect on the BBN is present, and we do not discuss it further.

A major consequence of the settlement of the neutrino oscillation issue is that a very refined calculation of the neutrino decoupling is possible. The standard picture in the instantaneous decoupling limit is very simple (see e.g. [19]): coupled neutrinos had a momentum spectrum with an equilibrium Fermi–Dirac (FD) form[3] with temperature T,

$$f_{\rm eq}(|\mathbf{p}|, T) = \left[\exp\left(\frac{|\mathbf{p}|}{T} \right) + 1 \right]^{-1}, \tag{36}$$

which is preserved after decoupling. Shortly after neutrino decoupling the photon temperature drops below the electron mass, m_e, and $e^{\pm}$ annihilations heat the photons. If one assumes that this entropy transfer did not affect the neutrinos because they were already completely decoupled (instantaneous decoupling limit), using conservation of entropy per comoving volume it is easy to calculate the difference between the temperatures of relic photons and neutrinos and thus the eventual neutrino energy density $\rho_{\nu,0}$ introduced before.

[3] It was noted in [40] (and more recently the topic reanalyzed in [41]) that the ^{4}He abundance in the early Universe is sensitive to the difference between FD or an exotic Bose–Einstein (BE) distribution of the (quasi)thermal neutrino bath, a conclusion which is expected according to the spin-statistics theorem but otherwise difficult to prove in laboratory experiments. They found indeed a good sensitivity to the quantum nature of the statistics, $Y_p(\mathrm{BE}) - Y_p(\mathrm{FD}) \simeq -(3\%\text{–}4\%) Y_p(\mathrm{FD})$ (or equivalent to $N_{\rm eff} \simeq 2.4$), with the present range of Y_p thus disfavoring a BE spectral shape.

At high temperatures, $T \geq 2$–3 MeV, one can write the conservation of entropy per comoving volume in the form (we are considering a temperature range well below muon annihilation epoch)

$$\left(s_{e^{\pm},\gamma} + s_{\nu}\right) a^3 = \text{const.} \tag{37}$$

After ν-decoupling, one has instead two separate conservation conditions for neutrinos and for the electromagnetic plasma. Nevertheless, until photons are reheated by $e^{\pm}$ annihilation, both photon and neutrino temperatures redshift by the same amount and keep equal. If one specifies the entropy conservation laws at the two different epochs, a_{in} well before $e^{\pm}$ annihilation, and a_{end} well after this phase, one obtains

$$\begin{aligned} s_{\nu}(a_{in}) a_{in}^3 &= s_{\nu}(a_{end}) a_{end}^3, \\ s_{e^{\pm},\gamma}(a_{in}) a_{in}^3 &= s_{\gamma}(a_{end}) a_{end}^3, \end{aligned} \tag{38}$$

where in the second equation one takes into account that both photon and $e^{\pm}$ degrees of freedom contribute at a_{in}, while only photons are present (and reheated) at a_{end}. The ratio of these two equations using the expression of entropy density (16), gives the well known asymptotic ratio of neutrino/photon temperatures after $e^{\pm}$ annihilation phase,

$$\frac{T_{\nu}}{T} = \left(\frac{2}{2 + 4 \times 7/8}\right)^{1/3} = \left(\frac{4}{11}\right)^{1/3} \simeq 1.401, \tag{39}$$

and the instantaneous decoupling expression of the neutrino energy density in terms of ρ_{γ},

$$\rho_{\nu,0} = 3\frac{7}{8}\left(\frac{4}{11}\right)^{4/3} \rho_{\gamma}. \tag{40}$$

However, the processes of neutrino decoupling and $e^{\pm}$ annihilations are sufficiently close in time so that some relic interactions between $e^{\pm}$ and neutrinos exist. These relic processes are more efficient for larger neutrino energies, leading to non-thermal distortions in the neutrino spectra (larger for ν_e than for $\nu_{\mu,\tau}$, since ν_e also feel charged-current interactions) and a slightly smaller increase of the comoving photon temperature. Even in absence of mixing, a proper calculation of the process of non-instantaneous neutrino decoupling requires the solution of the momentum-dependent Boltzmann equations for the neutrino spectra (29), a set of integro-differential kinetic equations that are quite challenging to attack numerically. In the last two decades a series of works has been devoted to solving this system in an increasingly general and precise way, ultimately also including finite temperature QED corrections to the electromagnetic plasma (a full list of the pre-2002 works is reported in [42]). To give a feeling of the overall effect, it suffices to say that the combination of these corrections leads to an effective neutrino number $N_{\text{eff}} \simeq 3.046$, while asymptotically one finds $T_{\nu}/T = 1.398$, slightly smaller than the instantaneous decoupling value [43].

The existence of neutrino oscillations imposes modifications to these corrections. The effect of f_{ν} distortions on the Y_p yield in the simplified case of two-neutrino mixing, averaged momentum, and Maxwell–Boltzmann statistics was estimated in [44,45]. All three approximations were relaxed in [43] and a full calculation was performed with a density matrix formalism. The neutrino ensemble is described by the momentum-dependent density matrices ϱ_p [46–49]. The form of the neutrino density matrix for a mode with momentum p is

$$\varrho_p(t) = \begin{pmatrix} \varrho_{ee} & \varrho_{e\mu} & \varrho_{e\tau} \\ \varrho_{\mu e} & \varrho_{\mu\mu} & \varrho_{\mu\tau} \\ \varrho_{\tau e} & \varrho_{\tau\mu} & \varrho_{\tau\tau} \end{pmatrix}. \tag{41}$$

The diagonal elements correspond to the usual number density of the different flavors, while the off-diagonal terms are non-zero in the presence of neutrino mixing. There exists a corresponding set of equations for the antineutrino density matrix $\bar{\varrho}_p$. In absence of a neutrino asymmetry (or of additional couplings flipping ν's into $\bar{\nu}$ and vice versa) antineutrinos follow the same evolution as neutrinos, and a single matrix suffices to describe the system. The equations of motion for the density matrices are

$$i\dot{\varrho}_p = \left[H_0 + H_1, \varrho_p\right] + C[\varrho_p], \tag{42}$$

where the first commutator term includes the free Hamiltonian H_0 and the effective potential of neutrinos in medium H_1, while the last term is a collisional term of order G_F^2 describing the breaking of coherence induced by neutrino scattering and annihilation as well as neutrino production by collisions in the primeval plasma. In a FLRW universe, $\dot{\varrho}_p = \left(\partial_t - Hp\,\partial_p\right)\varrho_p$. The Hamiltonian can be written explicitly in the flavor basis as

$$H_0 = \mathcal{U}\frac{M^2}{2p}\mathcal{U}^{\dagger}, \qquad M^2 = \text{diag}(m_1^2, m_2^2, m_3^2), \tag{43}$$

where $\mathcal{U}$ is the mixing matrix which, assuming vanishing CP-violating phases, writes

$$\mathcal{U} = \begin{pmatrix} c_{12}c_{13} & s_{12}c_{13} & s_{13} \\ -s_{12}c_{23} - c_{12}s_{23}s_{13} & c_{12}c_{23} - s_{12}s_{23}s_{13} & s_{23}c_{13} \\ s_{12}s_{23} - c_{12}c_{23}s_{13} & -c_{12}s_{23} - s_{12}c_{23}s_{13} & c_{23}c_{13} \end{pmatrix}. \tag{44}$$

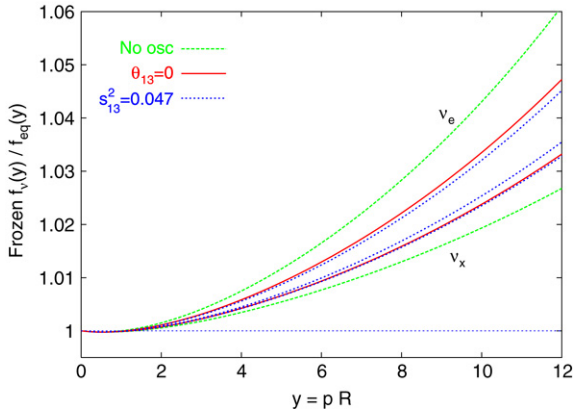

Fig. 1. Frozen distortions of the flavor neutrino spectra as a function of the comoving momentum, for the best fit solar and atmospheric mixing parameters. R is the scale factor. In the case where we allow for $\theta_{13} \neq 0$ consistently with present bounds (blue dotted lines), one can distinguish the distortions for ν_μ and ν_τ (middle and lower, respectively). From [43]. (For interpretation of the references to colour in this figure legend, the reader is referred to the web version of this article.)

Table 2
$N_{\rm eff}$ and ΔY_p obtained for different cases, with and without neutrino oscillations, as reported in [43].

Case	$N_{\rm eff}$	ΔY_p
No mixing (no QED)	3.035	1.47×10^{-4}
No mixing	3.046	1.71×10^{-4}
Mixing, $\theta_{13} = 0$	3.046	2.07×10^{-4}
Mixing, $\sin^2(\theta_{13}) = 0.047$	3.046	2.12×10^{-4}
Mixing, Bimaximal, $\theta_{13} = 0$	3.045	2.13×10^{-4}

Here $c_{ij} = \cos\theta_{ij}$ and $s_{ij} = \sin\theta_{ij}$ for $ij = 12$, 23, or 13. Apart for CP-violating phases, there are five oscillation parameters: $\Delta m^2_{21} = m^2_2 - m^2_1$, $\Delta m^2_{32} = m^2_3 - m^2_2$, θ_{12}, θ_{23} and θ_{13}. Best-fit values and uncertainties for these parameters (and upper bound for θ_{13}) can be found in [17].

Neglecting non-diagonal components of the effective potential, the matter term writes

$$H_1 = \mathrm{diag}(V_e, V_\mu, V_\tau), \tag{45}$$

where, assuming $T \ll m_\mu$,

$$V_e = -\frac{8\sqrt{2}G_F\, p}{3}\left(\frac{\rho_{\nu_e+\bar{\nu_e}}}{M_Z^2} + \frac{\rho_{e^-+e^+}}{M_W^2}\right), \tag{46}$$

$$V_\mu = -\frac{8\sqrt{2}G_F\, p}{3M_Z^2}\rho_{\nu_\mu+\bar{\nu_\mu}}, \tag{47}$$

$$V_\tau = -\frac{8\sqrt{2}G_F\, p}{3M_Z^2}\rho_{\nu_\tau+\bar{\nu_\tau}}. \tag{48}$$

Finally, the collisions of neutrinos with $e^\pm$ or among themselves are described by the term $C[\cdot]$, which is proportional to G_F^2. For the off-diagonal terms it is sufficient to adopt simple damping coefficient as reported in [23]. Instead, for the diagonal ones, in order to properly calculate the neutrino heating process one must consider the exact collision integral I_{ν_α}, that includes all relevant two-body weak reactions of the type $\nu_\alpha(1) + 2 \to 3 + 4$ involving neutrinos and $e^\pm$, see e.g. [50]. The kinetic equations for the neutrino density matrix are supplemented by the covariant conservation equation for the total energy–momentum tensor. Given the order of the effects considered, one should also include the finite temperature QED corrections to the electromagnetic plasma [33].

We show in Fig. 1 the asymptotic values of the flavor neutrino distribution, both without oscillations and with non-zero mixing. The dependence of the non-thermal distortions in momentum is well visible, which reflects the fact that more energetic neutrinos were interacting with $e^\pm$ for a longer period. Moreover, the effect of neutrino oscillations is evident, reducing the difference between the flavor neutrino distortions. Fitting formulae for these distributions are available in [43]. In Table 2 we report the effect of non-instantaneous neutrino decoupling on the radiation energy density, $N_{\rm eff}$, and on the ^{4}He mass fraction. By taking also into account neutrino oscillations, one finds a global change of $\Delta Y_p \simeq 2.1 \times 10^{-4}$ which agrees with the results in [45] due to the inclusion of QED effects. Nevertheless the net effect due to oscillations is about

Table 3
Comparison of the exact BBN results with a fixed-$\Delta N_{\rm eff}$ approximation. From [43].

Nuclide	Exact (No ν-oscillations)	Fixed $\Delta N_{\rm eff} = 0.013$
ΔY_p	1.71×10^{-4}	1.76×10^{-4}
$\Delta(^2\mathrm{H/H})$	-0.0068×10^{-5}	$+0.0044 \times 10^{-5}$
$\Delta(^3\mathrm{He/H})$	-0.0011×10^{-5}	$+0.0007 \times 10^{-5}$
$\Delta(^7\mathrm{Li/H})$	$+0.0214 \times 10^{-10}$	-0.0058×10^{-10}

a factor of 3 smaller than what was previously estimated, due to the failure of the momentum-averaged approximation to reproduce the true distortions.

It is worth remarking that the precise computation of the effect of particular neutrino decoupling scenario on primordial yields can only be performed numerically. The neutrino distribution functions, once obtained by the solution of Eq. (42), have to be substituted in Eqs. (24)–(28) which will predict the primordial abundance. The process is particularly involved, it is in fact important to follow the single neutrino distribution as a function of time because of the particular role played by the different neutrino flavors. In particular, the $N_{\rm eff}$ reported in Table 2 is the contribution of neutrinos to the whole radiation energy budget, but only at the very end of neutrino decoupling. Hence, not all the $\Delta N_{\rm eff}$ there reported will be really contributing to BBN processes. In order to clarify this subtle point, we report in Table 3 the effect on all light nuclides, of the non-instantaneous neutrino decoupling in the simple scenario of no neutrino oscillation, and compare this column with the simple *prescription* of adding a fix $\Delta N_{\rm eff} = 0.013$ contribution to radiation. Even though Y_p is reproduced (by construction), this is not the case for the other nuclear yields.

3.3. The neutron–proton chemical equilibrium and the role of weak rates

Neutrons and protons are kept in chemical equilibrium by charged current weak interactions,

$$\begin{aligned} &\text{(a)}\ \nu_e + n \to \mathrm{e}^- + p, \qquad &&\text{(d)}\ \overline{\nu}_e + p \to \mathrm{e}^+ + n,\\ &\text{(b)}\ \mathrm{e}^- + p \to \nu_e + n, \qquad &&\text{(e)}\ n \to \mathrm{e}^- + \overline{\nu}_e + p,\\ &\text{(c)}\ \mathrm{e}^+ + n \to \overline{\nu}_e + p, \qquad &&\text{(f)}\ \mathrm{e}^- + \overline{\nu}_e + p \to n, \end{aligned} \tag{49}$$

which enforce their number density ratio to follow the equilibrium value, $\mathrm{n/p} = \exp(-\Delta m/T)$. Shortly before the onset of BBN, processes (a)–(f) become too slow, chemical equilibrium is lost and the ratio n/p freezes out for temperatures lower than the decoupling temperature $T_D \sim 1$ MeV. Residual free neutrons are partially depleted by decay until deuterium starts forming at T_N and neutrons get bound in nuclei, first in deuterium and eventually in ^{4}He.

The leading role of (a)–(f) in fixing the neutron fraction at the BBN, and thus Y_p, simply means that to get an accurate theoretical prediction for ^{4}He abundance requires a careful treatment of the weak rates. Large improvements on this issue have been obtained in the last decade, which we summarize in the following. Extensive analysis can be found in e.g. [32,51].

At the lowest order, the calculation is rather straightforward, and is obtained by using V–A theory and in the limit of infinite nucleon mass (we will refer to this as the Born limit), see [52]. The latter approximation is justified in view of the typical energy scale of interest, of order $T \sim$ MeV, much smaller than the nucleon mass M_N. For example, the neutron decay rate takes the form (neglecting the very small neutrino masses)

$$\omega_B(n \to \mathrm{e}^- + \overline{\nu}_e + p) = \frac{G_F^2}{2\pi^3}\left({C_V}^2 + 3{C_A}^2\right)\int \mathrm{d}|\mathbf{p}_e||\mathbf{p}_e|^2|\mathbf{p}_\nu|^2\Theta(|\mathbf{p}_\nu|)\left[1 - f_{\overline{\nu}_e}(|\mathbf{p}_\nu|)\right]\left[1 - f_e(|\mathbf{p}_e|)\right], \tag{50}$$

where C_V and C_A are the nucleon vector and axial coupling, and $|\mathbf{p}_\nu| = \Delta m - \sqrt{|\mathbf{p}_e|^2 + m_e^2}$. The rates for all other processes (a)–(d), (f) can be simply obtained from (50) by changing the statistical factors and the expression for neutrino energy in terms of the electron energy. An average can be performed at this level of approximation over equilibrium Fermi–Dirac distribution for leptons, i.e. neglecting the effects of distortion in neutrino-antineutrino distribution functions, but taking into account the time evolution of the neutrino to photon temperature ratio T_ν/T. In Fig. 2 we report the Born rates, ω_B, for n–p processes. The accuracy of Born approximation results in being, at best, of the order of 7%. This can be estimated by comparing the prediction of Eq. (50) for the neutron lifetime at very low temperatures, with the experimental value $\tau_n^{ex} = (885.7 \pm 0.8)$ s [17].

The Born calculation can be improved by considering four classes of effects:
Electromagnetic radiative corrections. These are typically split into *outer* and *inner* terms (for a review see e.g. [53]). The first ones involve the nucleon as a whole and consist of a multiplicative factor to the squared modulus of transition amplitude of the form

$$1 + \frac{\alpha}{2\pi} g(E_e, E_\nu), \tag{51}$$

where analytic expression for $g(E_e, E_\nu)$, can be found in Ref. [54]. On the other hand, the inner corrections are deeply related to the nucleon structure. They have been estimated in Ref. [55], and applied in the BBN context in [32,51]. Furthermore, when electron and proton are both either in the initial or final state, one should also add the effect of *Coulomb correction* [56–58], due to rescattering of the electron in the proton electromagnetic field and leading to the Fermi factor

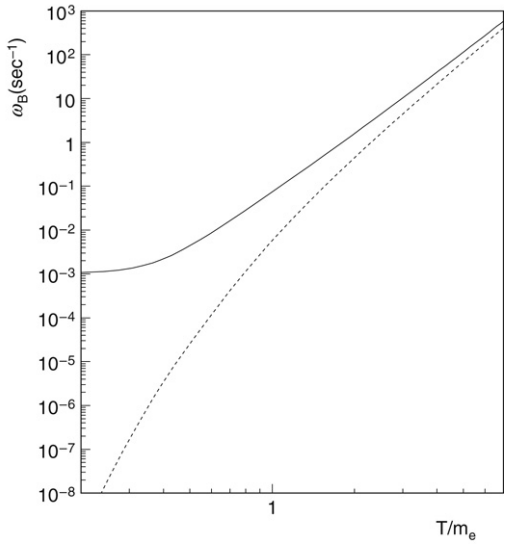

Fig. 2. The total Born rates, ω_B, for n $\to$ p (solid line) and p $\to$ n transitions (dashed line). From [51].

$$1 + \alpha\pi \frac{E_e}{|\mathbf{p}_e|}. \tag{52}$$

Finite nucleon mass corrections. For finite nucleon mass M_N and at order $1/M_N$, the weak hadronic current receives a contribution from the weak magnetic moment coupling,

$$J_\mu^{wm} = \mathrm{i}\frac{G_F}{\sqrt{2}}\frac{f_2}{M_N}\,\bar{u}_p(p)\,\sigma_{\mu\nu}\,(p-q)^\nu u_n(q), \tag{53}$$

where, from conservation of vector current (CVC), $f_2 = V_{ud}(\mu_p - \mu_n)/2 = 1.81 V_{ud}$. Both scalar and pseudoscalar contributions can be shown to be much smaller and negligible for the accuracy we are interested in. At the same order $1/M_N$ the allowed phase space for the relevant scattering and decay processes gets changed, due to nucleon recoil. Finally, one has to consider the effect of the initial nucleon thermal distribution in the comoving frame. All these effects are proportional to m_e/M_N or T/M_N, and in the temperature range relevant for BBN, can be as large as radiative corrections. This has been first pointed out in [59,60] and then also numerically evaluated in [32,51].

Thermal-Radiative corrections. The n–p rates get slight corrections from the presence of the surrounding electromagnetic plasma. To compute these corrections one may use Real Time formalism for Finite Temperature Field Theory [61] to evaluate the finite temperature contribution of the graphs of Fig. 3, for the $n \to p$ processes. Inverse processes $p \to n$ are obtained by inverting the momentum flow in the hadronic line. The first order in α is given by interference of one-loop amplitudes of Fig. 3(b) and (c) with the Born result (Fig. 3 (a)). Photon emission and absorption processes (Fig. 3 (d)), which also give an order α correction, should be included to cancel infrared divergences. Notice that photon emission (absorption) amplitudes by the proton line are suppressed as M_p^{-1} and can be neglected.

All field propagators get additional on-shell contributions proportional to the number density of that particular specie in the surrounding medium. For γ and $\mathrm{e}^\pm$ (neglecting the small electron chemical potential) we have

$$\mathrm{i}\Delta_\gamma^{\mu\nu}(k) = -\left[\frac{\mathrm{i}}{k^2} + 2\pi\,\delta(k^2)\,f_\gamma(k)\right] g^{\mu\nu}, \tag{54}$$

$$\mathrm{i}S_e(p_e) = \frac{\mathrm{i}}{\not{p}_e - m_e} - 2\pi\,\delta({p_e}^2 - m_e^2) f_e(E_e)\,(\not{p}_e + m_e), \tag{55}$$

with f_γ the photon distribution function. The whole set of thermal/radiative corrections have been computed by several authors [56,57,62–66,58,67–74]. Though they agree on the order of magnitude – which is quite small – there is nevertheless no consensus on the detailed value, due for example to different ways of treating the wave function renormalization at finite temperature. Finally, it was correctly pointed out in [75] that a (small) contribution to neutron–proton chemical equilibrium is also provided by photon–proton interactions (and inverse processes),

$$\gamma + p \to \mathrm{e}^+ + \nu_e + n, \qquad \mathrm{e}^+ + \nu_e + n \to \gamma + p. \tag{56}$$

The corresponding thermal averaged rates can be found in e.g. [18].

Non-instantaneous neutrino decoupling effects. Distortion of neutrino distribution functions changes the weak rates (a)–(f) which are enhanced by the larger mean energy of electron neutrinos. On the other hand, there is an opposite effect due to the

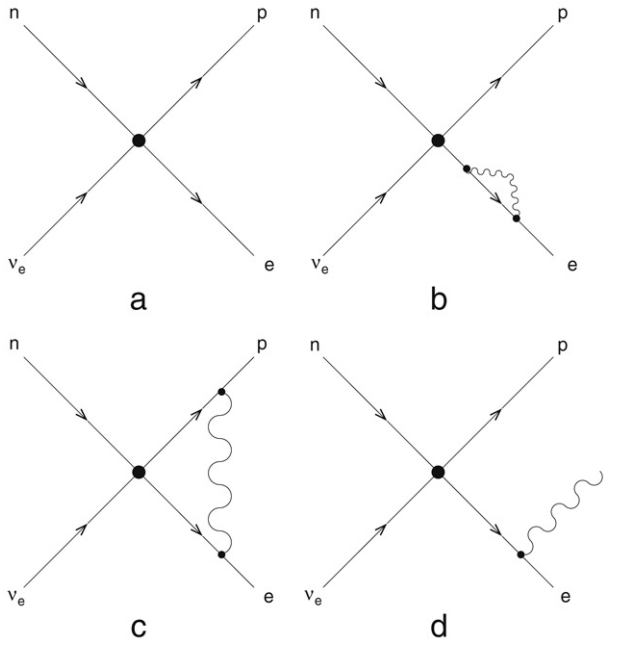

Fig. 3. The tree level Born (a), the one-loop (b), (c), and the photon emission/absorption diagrams (d) for $n \to p$ processes.

change in electron–positron temperature. Finally, since the photon temperature is reduced with respect to the instantaneous decoupling value $(11/4)^{1/3}$, the onset of BBN, via ^{2}H synthesis, takes place earlier in time. This means that fewer neutrons decay from the time of freezing out of weak interactions, and this in turn corresponds to a larger ^{4}He yield.

The effect of all corrections to the weak rates discussed so far has been considered in details in [32,51,18]. The leading contribution is given by electromagnetic radiative corrections, which decrease monotonically with increasing temperature for both $p \to n$ and $n \to p$ processes, and by finite nucleon mass effects. Their sum changes the Born estimate for a few percent correction at the freeze out temperature $T \sim$ MeV. Comparing the theoretical prediction for the neutron lifetime at zero temperature using $G_F = (1.16637 \pm 0.00001) \times 10^{-5}$ GeV^{-2}, $C_V = 0.9725 \pm 0.0013$ and the ratio $C_A/C_V = -1.2720 \pm 0.0018$, [17], one finds $\tau_n^{th} = 886.5$ s, quite an accurate result when compared with the experimental value (agreement is at the 0.1% level). It is worth commenting here on the fact that a recent measurement of the neutron lifetime exists [76], which gives $\tau_n = 878.5 \pm 0.7_{\rm stat} \pm 0.3_{\rm syst}$ and results in a 5.6σ discrepancy from the previous most precise result, which in turn is consistent with the other six determinations used in [17] to determine the best fit. According to the Particle Data Group, *[The result of* [76] *is so far from other results that it makes no sense to include it in the average. It is up to workers in this field to resolve this issue. Until this major disagreement is understood our present average of* 885.7 ± 0.8 s *must be suspect.* While implications for BBN of this different lifetime have been explored [77], in the following we shall assume that the best fit provided by the PDG is correct. Note that the PDG value also appears to be in better agreement with global electroweak fits [78]. Modulo this caveat, one might be confident that n–p weak rates are presently quite accurately computed, at per mille precision. Plasma corrections and finite temperature radiative effects are sub-leading, changing the rates at the level of (0.3%–0.6)% only. Their effect is to slightly increase Y_p by a very small amount, $\Delta Y_p \sim 1 \times 10^{-4}$, [79].

To conclude, we report a fit of the n–p rates which include all effects described in this section as a function of $z = m_e/T$, [18], accurate at the 0.01% level, which the reader might find useful:

$$\omega(n \to p) = \frac{1}{\tau_n^{ex}} \exp\left(-q_{np}/z\right) \sum_{l=0}^{13} a_l \, z^{-l} \quad 0.01 \le T/\text{MeV} \le 10, \tag{57}$$

$$\omega(p \to n) = \begin{cases} \dfrac{1}{\tau_n^{ex}} \exp\left(-q_{pn} z\right) \displaystyle\sum_{l=1}^{10} b_l z^{-l} & 0.1 \le T/\text{MeV} \le 10 \\ 0 & 0.01 \le T/\text{MeV} < 0.1, \end{cases} \tag{58}$$

with

$$\begin{array}{lll} a_0 = 1 & a_1 = 0.15735 & a_2 = 4.6172 \\ a_3 = -0.40520 \times 10^2 & a_4 = 0.13875 \times 10^3 & a_5 = -0.59898 \times 10^2 \\ a_6 = 0.66752 \times 10^2 & a_7 = -0.16705 \times 10^2 & a_8 = 3.8071 \\ a_9 = -0.39140 & a_{10} = 0.023590 & a_{11} = -0.83696 \times 10^{-4} \\ a_{12} = -0.42095 \times 10^{-4} & a_{13} = 0.17675 \times 10^{-5} & q_{np} = 0.33979, \end{array} \tag{59}$$

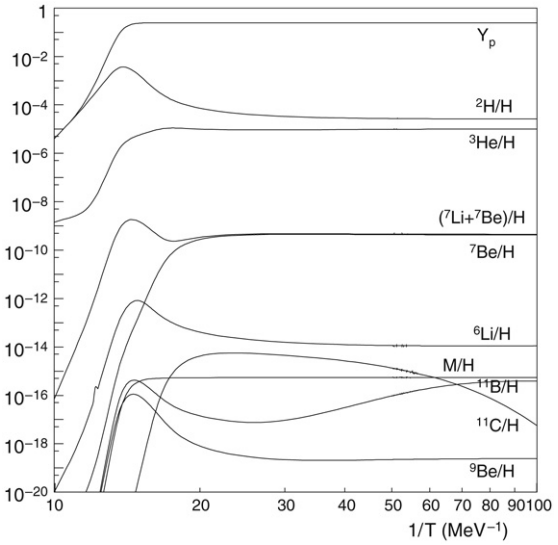

Fig. 4. The evolution of some element abundances produced during BBN. The line M/H refers to the abundance of "metals" (see text).

$$\begin{array}{lll} b_0 = -0.62173 & b_1 = 0.22211 \times 10^2 & b_2 = -0.72798 \times 10^2 \\ b_3 = 0.11571 \times 10^3 & b_4 = -0.11763 \times 10^2 & b_5 = 0.45521 \times 10^2 \\ b_6 = -3.7973 & b_7 = 0.41266 & b_8 = -0.026210 \\ b_9 = 0.87934 \times 10^{-3} & b_{10} = -0.12016 \times 10^{-4} & q_{pn} = 2.8602. \end{array} \tag{60}$$

3.4. Nuclear reaction network

Nuclear processes during the BBN proceed in an environment very different with respect to the perhaps more familiar stellar plasmas, where stellar nucleosynthesis takes place. The latter is a dense plasma where species are mostly in chemical equilibrium, the former is a hot and low density plasma with a significant population of free neutrons, which expands and cools down very rapidly, resulting in peculiar "out of equilibrium" nucleosynthetic yields. The low density of the plasma at the time of BBN is responsible for the suppression of three-body reactions and an enhanced effect of the Coulomb-barrier, which as a matter of fact inhibits any reaction with interacting nuclei charges $Z_1 Z_2 \gtrsim 6$. The most efficient categories of reactions in BBN are therefore proton, neutron and deuterium captures – $(\mathrm{p}, \gamma)(\mathrm{n}, \gamma)$, (d, γ) –, charge exchanges – (p, n) –, and proton and neutron stripping – (d, n), (d, p).

From a more technical point of view, accurate BBN predictions require a detailed knowledge of the nuclear rates entering the set of Eq. (27): a physical understanding of the basic reaction chains helps however to implement a code with a good compromise between reliability and computational time. In this section we start with the phenomenology of nuclear processes related with the choice of such nuclear network, whereas a chronology of the codes devoted to solve the whole set of equations, and related numerical issues, is reported in Section 3.4.1.

After the freeze-out of weak interactions, $p(n, \gamma)^2\mathrm{H}$ is the only reaction able to synthesize sensible amounts of nuclei, since it involves the only two nuclear species with non-vanishing abundances, protons and neutrons. The very high entropy of the primordial plasma keeps this reaction in equilibrium down to energies much lower than its Q-value, which corresponds to the deuterium binding energy of $B_D \simeq 2.2$ MeV. The deuterium *bottleneck* ends at a temperature of $T_D \sim 100$ keV, given roughly by the condition $\exp(B_D/T_D)\eta \sim 1$, which ensures that the high energy tail of the photon distribution has been sufficiently diluted by the expansion. At this point, almost instantaneously all the available neutrons are locked into deuterium nuclei. The effect of the bottleneck on the following nuclear processes is two-fold: the "delayed" population of the deuterium specie results in BBN taking place at relatively low temperatures, with consequences on the efficiency of all the following reactions. Second, but not less important, is the intervening decay of the neutron, which alters the neutron to proton ratio at the time of effective deuterium production. Efficient production of deuterium marks the effective beginning of the nuclear phase of BBN: the nuclear path towards heavier elements, before all ^{3}H, ^{3}He, ^{4}He, is enabled by the interaction of deuterium nuclei with nucleons and other ^{2}H nuclei. The bulk of the remaining ^{7}Li is produced via tritium and especially ^{3}He radiative capture on ^{4}He. The latter path leads to ^{7}Be, which eventually decays into ^{7}Li by electron capture. The evolution of light nuclide abundances as a function of the temperature of the plasma is shown in Fig. 4: they undergo the nuclear phase of departure from chemical equilibrium and, by the time the universe cools to few keV, they reach their final values. It is worth noting the dramatic change that all species undergo following the deuterium synthesis at $1/T \gtrsim 14\ \mathrm{MeV}^{-1}$.

The most important nuclear processes for the BBN were identified in [80] (reactions R_0–R_{11} in Table 4). Reaction R_9 provides actually only a sub-leading contribution to ^{7}Li for today's preferred value of η, being more relevant at lower η where

Table 4
The most relevant reactions for BBN.

Symbol	Reaction	Symbol	Reaction
R_0	τ_n	R_8	$^3\mathrm{He}(\alpha,\gamma)^7\mathrm{Be}$
R_1	$p(n,\gamma)d$	R_9	$^3\mathrm{H}(\alpha,\gamma)^7\mathrm{Li}$
R_2	$^2\mathrm{H}(p,\gamma)^3\mathrm{He}$	R_{10}	$^7\mathrm{Be}(n,p)^7\mathrm{Li}$
R_3	$^2\mathrm{H}(d,n)^3\mathrm{He}$	R_{11}	$^7\mathrm{Li}(p,\alpha)^4\mathrm{He}$
R_4	$^2\mathrm{H}(d,p)^3\mathrm{H}$	R_{12}	$^4\mathrm{He}(d,\gamma)^6\mathrm{Li}$
R_5	$^3\mathrm{He}(n,p)^3\mathrm{H}$	R_{13}	$^6\mathrm{Li}(p,\alpha)^3\mathrm{He}$
R_6	$^3\mathrm{H}(d,n)^4\mathrm{He}$	R_{14}	$^7\mathrm{Be}(n,\alpha)^4\mathrm{He}$
R_7	$^3\mathrm{He}(d,p)^4\mathrm{He}$	R_{15}	$^7\mathrm{Be}(d,p)2^4\mathrm{He}$

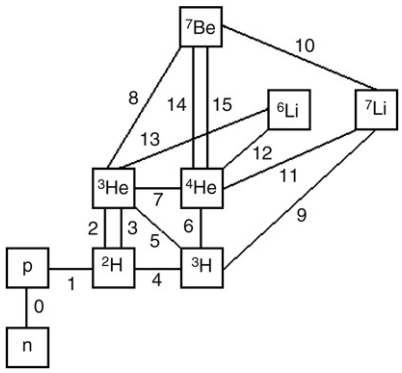

Fig. 5. The most relevant reactions for BBN.

^{7}Li production is direct rather than coming from ^{7}Be synthesis. Also, if one is concerned with the traces of ^{6}Li produced in BBN, the reactions R_{12} : $^4\mathrm{He}(d,\gamma)^6\mathrm{Li}$, and R_{13} : $^6\mathrm{Li}(p,\alpha)^3\mathrm{He}$ are relevant. Due to their larger uncertainties, even reactions as R_{14} : $^7\mathrm{Be}(n,\alpha)^4\mathrm{He}$ and perhaps R_{15} : $^7\mathrm{Be}(d,p)2^4\mathrm{He}$ are important in the ^{7}Li error budget determination. All these reactions are summarized in Table 4 and Fig. 5. Both leading and sub-leading reactions of some interest have been discussed e.g. in [18], which we mostly follow here. Other compilations can be found in [81–83].

These reactions are not only important to understand the nuclear physics of the BBN, but also to assess an error budget for its theoretical predictions. The first "modern" papers addressing these issues are [84,80]. For example, in [80], the authors performed a systematic analysis of the nuclear network in BBN, as it had been implemented in the first publicly released code [26], with the – at the time – new rates compiled in [85]. For the range of η allowed at the time, they identified the twelve leading reactions reported in Table 4. A detailed study of their rates and uncertainties led to a new code [35], implementing an updated nuclear network.

Inferring the uncertainties on the light elements yields is conceptually a three-step process. First, one has to determine the uncertainties on the cross-sections $\sigma_i(E)$ (as functions of energy) measured in the Lab or theoretically predicted. Since a first principle computation is virtually impossible for almost all processes, one has to rely on some form of theoretically motivated fitting formulae and interpolate between and extrapolate beyond the data. Indeed, the reactions in the early universe happen in a thermal plasma, so the relevant nuclear input are the temperature-dependent rates given by the convolution of the cross-sections with the Maxwell–Boltzmann distribution of nuclides, i.e. $\langle\sigma v\rangle \propto T^{-3/2}\int_0^\infty \mathrm{d}E\,\sigma(E)\,E\exp(-E/T)$. These can be approximated with analytical formulae in some simple hypotheses for the functional form of $\sigma(E)$. Although no modern compilation relies on such approximations, they are often used to suggest a fitting formula for the numerical integration results. Anyway, it is the uncertainties on these rates that ultimately propagate onto the final errors on the nuclides. The formalism/machinery to treat this problem can be found in classical papers (as [80]), textbooks [86,87] and has also been reported in several compilations of the last decade [81–83,18], so we do not repeat it here. We want to remark, however, that: (a) In the last decade, in particular following [81], a world-wide effort in obtaining new measurements at low energy for several important reactions involving light nuclei has been undergone; (b) in several cases, especially when new measurements have become available, the different experimental data sets do not seem to agree within the quoted uncertainties. In this situation, it is a tricky business to assess uncertainties in a statistically meaningful way, unless one has reason to believe that some of the datasets are affected by unaccounted systematics and decides for example to dismiss the older measurements. Here we follow the prescription illustrated in [18] and motivated on the basis of the arguments presented in [88]. While in agreement with the error estimates given in other compilations [82,83] when statistical errors dominate, we warn the reader that our procedure tends to produce smaller errors than other compilations when discrepancies among datasets exist.

An additional technical aspect arises in the way uncertainties are accounted for in the BBN calculations. A lot of attention has been paid in the last two decades to this problem. One may adopt Monte Carlo simulations directly, with various degrees

Table 5
The light nuclide abundances for WMAP 5-year result $\Omega_B h^2 = 0.02273 \pm 0.00062$ (second column). The uncertainties due to $\Omega_B h^2$ (σ_{ω_b}) and nuclear rate errors (σ_{ii}) are also shown in the third and fourth columns, respectively. The last two columns report the rates mostly contributing to the nuclear uncertainties, and their relative contributions in percent in a quadrature sum, according to [18].

Nuclide i	Central value	σ_{ω_b}	σ_{ii}	Rate	$\delta\sigma^2/\sigma^2$ (%)
Y_p	0.2480	$+0.0002$ -0.0003	± 0.0002	R_0	98.5
^{2}H/H $\times 10^5$	2.53	± 0.11	± 0.04	R_2 R_3 R_4	49 37 14
^{3}He/H $\times 10^5$	1.02	$+0.01$ -0.02	± 0.03	R_7	80.7
^{7}Li/H $\times 10^{10}$	4.7	± 0.3	± 0.4	R_2 R_{14} R_8 R_{15} R_7	16.8 40.9 25.1 16.2 8.6
^{6}Li/H $\times 10^{14}$	1.1	± 0.1	$+1.7$ -1.1	R_{13}	$\sim$100

of sophistication [84,80,89], or use an error matrix approach as in [90] and its generalization in [91]. Each one has its own advantages and disadvantages, but the agreement between the two is typically very good [90]. In Table 5 we report the light nuclide abundances for WMAP 5-year result $\Omega_B h^2 = 0.02273 \pm 0.00062$ [8] (second column), showing in the third and fourth columns, respectively, the uncertainties due to $\Omega_B h^2$ (σ_{ω_b}) and nuclear rates errors (σ_{ii}).[4] The last two columns report the rates mostly contributing to the nuclear uncertainties, and their relative contributions in percent in a quadrature sum, according to [18].

To illustrate the main dependence of the yields on the nuclear rates, we report here the scaling relations introduced in [82] and normalized with respect to the predictions of `PArthENoPE` [93] around the fiducial value of $\omega_b = 0.02273$ (WMAP 5-years). The scalings are:

$$\frac{^2\mathrm{H}}{\mathrm{H}} = 2.53 \times 10^{-5} R_3^{-0.55} R_4^{-0.45} R_2^{-0.32} R_1^{-0.20} \left(\frac{\omega_b}{0.02273}\right)^{-1.62} \left(\frac{\tau_n}{\tau_{n,0}}\right)^{0.41} \tag{61}$$

$$\frac{^3\mathrm{He}}{\mathrm{H}} = 1.02 \times 10^{-5} R_7^{-0.77} R_2^{0.38} R_4^{-0.25} R_3^{-.20} R_5^{-0.17} R_1^{0.08} \left(\frac{\omega_b}{0.02273}\right)^{-0.59} \left(\frac{\tau_n}{\tau_{n,0}}\right)^{0.15}, \tag{62}$$

$$Y_p = 0.2480\, R_3^{0.006} R_4^{0.005} R_1^{0.005} \left(\frac{\omega_b}{0.02273}\right)^{0.39} \left(\frac{\tau_n}{\tau_{n,0}}\right)^{0.72}, \tag{63}$$

$$\frac{^7\mathrm{Li}}{\mathrm{H}} = 4.7 \times 10^{-10} R_1^{1.34} R_8^{0.96} R_7^{-0.76} R_{10}^{-0.71} R_3^{0.71} R_2^{0.59} R_5^{-0.27} \left(\frac{\omega_b}{0.02273}\right)^{2.12} \left(\frac{\tau_n}{\tau_{n,0}}\right)^{0.44}. \tag{64}$$

It is clear, for example, that Y_p prediction is dominated by the neutron mean lifetime (see Section 3.3). For all the other reactions the relative weight of the different cross-sections is consistent with what is reported in Table 5, modulo a caveat: some important reactions may have a minor impact on the uncertainty due to their better determination or vice versa. This is the case of R_1, whose role does not reflect in the error budget being theoretically well under control (at the% level), or conversely the case of R_{14}, R_{15}, which contribute appreciably to the ^{7}Li error budget in Table 5 due to the assumption done in [18] that they are only known at the order of magnitude. In general, while improvements in the nuclear reaction rates would still sharpen the BBN predictions (especially for ^{7}Li), it is fair to conclude that these uncertainties are at the moment negligible compared to the observational ones (see Section 4.4). Thus an experimental campaign does not seem mandatory for BBN purposes alone. Yet, a careful assessment of the systematic uncertainties would be useful in reducing the present discrepancies in data regression protocols. A realistic account especially of scale uncertainties in the *already existing* datasets, perhaps excluding unreliable measurements and correcting underestimated error assignments would be certainly a more useful input from the experimental community.

It is worth commenting here on an additional robust prediction of BBN: elements heavier than ^{7}Li are virtually absent from the chemical composition of the early universe. This was realized from the first pioneering studies on BBN [1,94], and mostly explained in terms of the very high entropy and on the low density of the primordial plasma. They result in extremely low abundances $A \geq 2$ elements at the weak reaction freeze-out, and an inhibition of three-body reactions.[5] respectively.

[4] A recent analysis finds a larger value for $^7\mathrm{Li/H} = (5.24^{+0.71}_{-0.67})10^{-10}$, due to new determinations of the rate R_8, see [92] and references therein. This further exacerbates the ^{7}Li problem, see Sections 4.4 and 4.5.

[5] The leading reaction for the synthesis of ^{12}C in stars is the $3\alpha \rightarrow {}^{12}$C.

Table 6
A comparison of light nuclei theoretical predictions in some recent analyses. Results are either produced by public numerical tools, or obtained by using fitting formulae made available by the authors or finally, simply quoted in the papers. The theoretical errors are estimated using [93], and account for the effects of nuclear rate uncertainties. Results are shown for a baryon fraction $\Omega_B h^2 = 0.0224$.

	[35]	[90]	[97]	[82]	[14]	[93]
Y_p	0.2463	0.2479	0.2483	0.2485	0.2485	0.2479 ± 0.0002
^{2}H/H $\times 10^5$	2.57	2.60	2.60	2.55	2.59	2.58 ± 0.04
^{3}He/H $\times 10^5$	1.04	1.04	1.02	1.01	1.04	1.03 ± 0.03
^{7}Li/H $\times 10^{10}$	4.53	4.42	4.91	4.26	4.50	4.57 ± 0.4

To assess more quantitatively the robustness of this result, the present authors have recently studied the nuclear processes involved in the production of $A \geq 8$ elements in BBN [95]. It was confirmed that their synthesis can only start at $T \lesssim 60$ keV (see Fig. 4), close to the freeze-out of nuclear reactions, when they have a very small efficiency. Heavier elements in BBN are in fact produced by an α capture over ^{7}Li and subsequent build-up of ^{12}C; their final abundance, mainly produced by means of an α capture over ^{7}Li and subsequent proton capture, is to be well below 10^{-10} that of hydrogen (see Fig. 4 for details). While processes till now neglected were identified and included, their role does not alter this basic conclusion. An important implication of these results follows for the first stars in the universe, known as Population III stars, whose formation process and initial mass function is thought to be critically dependent on the carbon and oxygen content of the environment.[6] While the amount of "heavy" element predicted in SBBN is safely below the critical level to alter the standard (but yet to be tested) scenario, in exotic models this might not be true. More in general, even when roughly reproducing ^{2}H, ^{3}He, ^{4}He and ^{7}Li yields of the SBBN, exotic scenarios may differ for the predictions of ^{6}Li, ^{9}Be or elements with $A \geq 12$ ('metals' in the astrophysical jargon). Examples of this will be provided in Sections 7.1 and 9.2.3.

3.4.1. Numerical solution of the BBN set of equations

Despite of the fact that some simple estimate of BBN predictions can be made *on the back of the envelope*, detailed theoretical estimates that can be compared with experimental data require a careful numerical solution of BBN equations (24)–(27) and (29). This is particularly relevant when one considers exotic scenarios with extra parameters or where a different BBN dynamics is considered, with the aim of constraining physics beyond the SMPP. Since the original Wagoner computer code [27,28] much effort has been devoted to develop numerical tools and provide reliable numerical results [34,35,90,32,51,97,30,11,98–100,82,18,101]. In 1988, Kawano modified the BBN program of Wagoner [34], and in 1992 an updated and user friendly public version has been released [35], which has served as a reference tool for a wide number of research groups. Nuclear reaction rates were updated in 1993 [80] and radiative and Coulomb corrections to the weak rates, to which the ^{4}He abundance is very sensitive, as well plasma effects, were included as a constant multiplicative factor to n–p weak rates. In 1993 Kernan discovered a relatively large time-step systematic error in the ^{4}He abundance prediction of the public Kawano code, $\delta Y_p = 0.0017$, since then routinely added to its result. This, strictly speaking, is not fully adequate because different users use different step sizes and furthermore, numerical error is machine dependent. In 1999 Lopez and Turner wrote a new nucleosynthesis code [32], which used the same nuclear rates but incorporated more accurately the radiative, finite nucleon mass and finite temperature corrections to the weak rates. The code used by Olive, Steigman and Walker [11] agreed, over the whole range $1 \leq \eta_{10} \leq 10$, better than the 0.1% level, with the predicted ^{4}He abundance of the Lopez and Turner code. In 2000, the weak rate corrections were also calculated in [51] and included in a BBN code. This code was developed and continuously updated over almost a decade, giving particular care also to the treatment of neutrino decoupling and the nuclear reaction chain which enters the light abundances evolution [30,18]. It was eventually made public in 2008 with the name `PArthENoPE` [93]. Details can be found in [101], where particular emphasis is given to a comparison with [35]. To our knowledge, only the original Kawano code or improved versions of it[7] and `PArthENoPE` are publicly available.

To examine the concordance of theoretical predictions we have considered some recent results obtained using numerical BBN codes, either publicly available or whose outputs have been made public by the authors as fitting formulae versus the baryon density or finally, simply quoted in their papers for some reference value of $\Omega_B h^2$. These results are shown in Table 6. The list is of course largely incomplete, but we think it is representative enough to give the idea of the status of BBN theoretical accuracy. In the last column we also quote the theoretical uncertainty due to nuclear rate (experimental) errors, as estimated using [93]. We see that all results are in very good agreement, in particular Y_p agrees at the $\pm 0.1\%$ level in the most recent calculations. There is a somehow larger spread of ^{7}Li estimates which are however all compatible within the larger theoretical uncertainty (Table 6).

We report the fit of the main nuclide abundances as function of $\omega_b \equiv \Omega_B h^2$ and the number of effective degree of freedom, $N_{\rm eff}$. The fit holds for $0.015 \leq \omega_b \leq 0.029$ and $0 \leq N_{\rm eff} \leq 7$. The fitting function for all nuclei is

$$\sum_n \sum_m a_{nm}\, \omega_b^n\, N_{\rm eff}^m, \tag{65}$$

[6] For a review we address the reader to the proceedings of the last plenary conference on the topic [96].

[7] See the link http://www-thphys.physics.ox.ac.uk/users/SubirSarkar/bbn.htmlfor a version of the Kawano standard code, made Linux-friendly by S. Dodelson.

Table 7
Coefficients of the fit of Eq. (65) for the Y_p abundance.

m	n					
	0	1	2	3	4	5
0	0.24307	−14.242	1418.4	−65863.	1.4856×10^6	-1.3142×10^7
1	-3.6433×10^{-2}	14.337	−1375.0	64741.	-1.4966×10^6	1.3601×10^7
2	1.6132×10^{-2}	−4.5189	444.13	−21353.	502610.	-4.6405×10^6
3	-1.6279×10^{-3}	0.43362	−42.850	2069.4	−48890.	452740.

Table 8
Coefficients of the fit of Eq. (65) for the $^2H/H \times 10^5$ abundance.

m	n				
	0	1	2	3	4
0	14.892	−1551.6	70488.	-1.5390×10^6	1.3164×10^7
1	6.1888	−916.16	56639.	-1.6046×10^6	1.7152×10^7
2	−0.60319	118.51	−8556.3	267580.	-3.0624×10^6
3	4.5346×10^{-2}	−8.7506	624.51	−19402.	221200.

Table 9
Coefficients of the fit of Eq. (65) for the $^3He/H \times 10^5$ abundance.

m	n				
	0	1	2	3	4
0	3.1820	−298.88	15974.	−422530.	4.4031×10^6
1	0.57549	−91.210	6376.6	−201070.	2.3486×10^6
2	−0.15717	33.689	−2651.2	89571.	-1.0998×10^6
3	1.4594×10^{-2}	−3.2160	256.66	−8780.2	109100.

Table 10
Coefficients of the fit of Eq. (65) for the $^7Li/H \times 10^{10}$ abundance.

m	n				
	0	1	2	3	4
0	2.5274	−614.44	62186.	-1.5670×10^6	1.4339×10^7
1	1.9384×10^{-2}	55.173	−11365.	492710.	-6.2826×10^6
2	-8.6994×10^{-2}	16.437	−431.32	−13313.	359980.
3	2.2257×10^{-2}	−4.2339	260.16	−6277.3	55300.

and the coefficient are reported in Tables 7–10. The fit accuracy is better than 0.13% for Y_p, than 0.3% for $^2H/H$ and $^7Li/H$, and than 0.6% for $^3He/H$.

4. Observational abundances

The abundances of primordial elements are inferred from measurements performed in a large variety of astrophysical environments. What *precision cosmology era* has meant in this field is an increased number and precision of spectroscopic data over the past two decades. Presently, the situation is still quite involved due to the presence of relevant systematic errors which are comparable to (where not dominant over) the statistical uncertainties. Unfortunately, these errors are to a large extent irreducible and intrinsic to the astrophysical determinations themselves, which rely on highly evolved systems where reprocessing, astration, and contaminations from younger systems are possibly present and difficult to correct for.

Since our nearby universe is far from reflecting its primordial conditions, the methods proposed and developed in the last forty years to infer primordial yields have focused on very old and hence little evolved astrophysical regions, as well as on the capability to correct for the effect of the galactic evolution on the pristine abundances. For example, due to its very weak binding, any ^2H nucleus contained into pre-stellar nebulae is burned out during their collapse. Hence, the post-BBN deuterium evolution is expected to be a monotonic function of time and astrophysical deuterium measurements can be assumed to represent lower bounds of its primordial abundance.

Unfortunately, such a simple scheme cannot be applied to the more tightly bound ^3He nucleus. In this case, in fact, in stellar interior it can be either produced by ^2H-burning or destroyed in the hotter regions. As a consequence, all the ^3He nuclides surviving the stellar evolution phase contribute to the chemical composition of the InterStellar Medium (ISM) and thus stellar and galactic evolution models are necessary to track back the primordial ^3He abundance from the post-BBN data, at least in the regions where stellar matter is present. For this reason the inferred primordial ^3He abundance is intrinsically a model-dependent quantity.

The situation of ^{4}He is reversed with respect to that of deuterium, since in this case the hydrogen burning in the successive stellar population has increased the amount of ^{4}He as well as "metals" (nuclei with $Z > 4$) such as C, N and O. Usually, ^{4}He is measured in old and very little evolved systems versus their metallicity, and extrapolating *linearly* to zero-metallicity. While this is certainly a reasonable approach, still it could lead to some systematic uncertainty.

Finally, ^{7}Li, whose bulk is also believed to be produced in the primordial cauldron, is a very weakly bound nuclide which has an extremely involved post-BBN chemical evolution. In fact, it is easily destroyed in the interiors of stars but can survive in the cooler outer layers of stars with shallow convective zones, where it can be measured by means of absorption spectra. However, the scenario is much more involved due to the observation of enhanced lithium abundance in some red-giants. This suggests that ^{7}Li formed in the interior of some stars may be transported by convective modes to the cooler exteriors. In this case these stars behave as lithium producers and thus enrich the ISM with lithium. Furthermore, the cosmic rays scattering on ISM nuclei can contribute to the total amount of ^{7}Li and since CNO elements are necessary for spallation processes, this would imply a correlation between post-BBN ^{7}Li and the metallicity, which may help in tracking back this non-primordial component.

4.1. Deuterium

It is commonly believed that there are no astrophysical sources of deuterium since it is destroyed by stellar evolution processes [102] and non-thermal production channels have been constrained to be negligible (see e.g. [103]). Thus, any astrophysical observation can provide a lower bound for the primordial abundance. Therefore, the local ISM in the Milky Way can provide an order of magnitude more determinations of ^{2}H/H than high redshift Quasar Absorption Systems (QAS) (see Ref. [104] for the most recent compilation), given its easier observational accessibility. By using the Far-Ultraviolet Spectroscopic Explorer (FUSE) [105], a large database of Galactic ^{2}H/H measurements has been compiled. However, despite FUSE and other satellite observations, providing measurements of ^{2}H/H in almost 50 lines of sight, the picture of Galactic deuterium abundances remains puzzling. In particular, inside the Local Bubble (<100 pc from the Sun) the deuterium to hydrogen ratio seems roughly constant at $^2\mathrm{H/H}|_p = (1.56 \pm 0.04) \times 10^{-5}$ [106]. However, beyond this bound, an unexpected scatter of a factor of ∼2 in ^{2}H/H values is observed [107,106,104,108] as well as correlations with heavy element abundances, which suggest that ISM deuterium might have suffered stellar processing, namely astration (see for example [109]), but also that it may reside in dust particles which evade gas-phase observations. This is supported by a measurement in the lower halo [110] which indicates that the Galactic ^{2}H abundance has been reduced by a factor of only 1.12 ± 0.13 since its formation. As an alternative explanation, it is worth reporting the possible existence of a strong late infall of pre-galactic material with primordial composition (high ^{2}H) (see for example [111,112]) which has some observational evidence via the study of kinematics of high latitude gas regions. Finally, it is important to mention the analysis of Infrared Space Observatory spectra of H_2, H-^{2}H, CH_4, and CH_3^2H in Jupiter's atmosphere which led authors of Ref. [113] to infer the value of deuterium to hydrogen ratio for the protosolar cloud $^2\mathrm{H/H}_{psc} = (2.1 \pm 0.4) \times 10^{-5}$, which corresponds to our galaxy value when its age was two thirds of the present one.

The astrophysical environments which seem most appropriate to obtain reliable measurements of the primordial deuterium fraction are the hydrogen-rich clouds absorbing the light of background QSOs at high redshifts, as recognized already in [114]. Conventional models of galactic nucleosynthesis (chemical evolution) predict a small contamination of pristine ^{2}H/H [115]. However, a successful implementation of this method requires: (i) neutral hydrogen column density in the range $17 \lesssim \log[\mathrm{N}(\mathrm{H}_I)/\mathrm{cm}^{-2}] \lesssim 21$; (ii) low metallicity [M/H] to reduce the chances of deuterium astration; (iii) low internal velocity dispersion of the atoms of the clouds, allowing the isotope shift of only 81.6 km /s to be resolved [116]. For this reason, only a handful of determinations have been obtained since the advent of the >8 m class telescopes in the 1990s in damped Lyman-α systems and Lyman limit systems:

(i) **Q1009+2956**, with the absorber placed at $z = 2.504$, yielding $^2\mathrm{H/H} = \left(3.98^{+0.59}_{-0.67}\right) \times 10^{-5}$ ($\log{}^2\mathrm{H/H} = -4.40^{+0.06}_{-0.08}$) [117,118].

(ii) **PKS1937-1009 (I)**, with the absorber placed at $z = 3.572$, yielding $^2\mathrm{H/H} = (3.3 \pm 0.3) \times 10^{-5}$ ($\log{}^2\mathrm{H/H} = -4.49 \pm 0.04$) [117].

(iii) **HS 0105+1619**, with the absorber placed at $z = 2.536$ with metallicity [Si/H] ∼ 0.01, yielding $^2\mathrm{H/H} = (2.54 \pm 0.23) \times 10^{-5}$ ($\log{}^2\mathrm{H/H} = -4.596 \pm 0.040$) [119].

(iv) **Q2206-199**, with the absorber placed at $z = 2.0762$ with metallicity [Si/H] $= -2.23$, yielding $^2\mathrm{H/H} = (1.65 \pm 0.35) \times 10^{-5}$ ($\log{}^2\mathrm{H/H} = -4.78^{+0.08}_{-0.10}$) [120].

(v) **Q0347-3819**, with the absorber placed at $z = 3.024855$ with metallicity [Si/H] $= -0.95 \pm 0.02$, yielding $^2\mathrm{H/H} = (3.75 \pm 0.25) \times 10^{-5}$ ($\log{}^2\mathrm{H/H} = -4.43 \pm 0.03$) [121]. Note that the previous analysis in [122] yielded $^2\mathrm{H/H} = (2.24 \pm 0.67) \times 10^{-5}$ due to an incorrect velocity distribution function (see [121]). Similar considerations apply for the value discussed in (vii) below.

(vi) **Q1243+3047**, with the absorber placed at $z = 2.525659$ with metallicity [O/H] $= -2.79 \pm 0.05$, yielding $^2\mathrm{H/H} = \left(2.42^{+0.35}_{-0.25}\right) \times 10^{-5}$ ($\log{}^2\mathrm{H/H} = -4.617^{+0.058}_{-0.048}$) [118].

(vii) **PKS1937-1009 (II)**, with the absorber placed at $z = 3.256$ with metallicity [Si/H] $= -2.0 \pm 0.5$, yielding $^2\mathrm{H/H} = \left(1.6^{+0.25}_{-0.30}\right) \times 10^{-5}$ ($\log{}^2\mathrm{H/H} = -4.80^{+0.06}_{-0.09}$) [123]. Since not all the ionized deuterium (D_I) components are resolved, it is often claimed that this value of ^{2}H/H is more dependent on the precise description of the kinematics of the gas and thus less robust against systematics (see [116]).

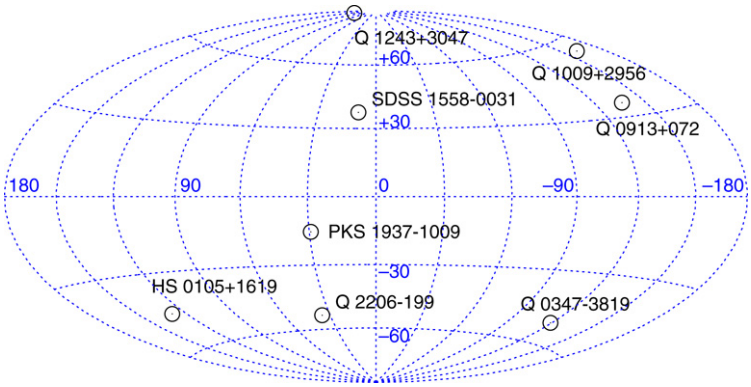

Fig. 6. Hammer–Aitoff projection in Galactic coordinates of the positions of the eight quasars along which nine measurements of deuterium abundance have been reported (see (i)–(ix), in the text).

(viii) **SDSS 1558-0031**, with the absorber placed at $z = 2.70262$ with metallicity $[\mathrm{O/H}] = -1.49$, yielding $^2\mathrm{H/H} = \left(3.31^{+0.49}_{-0.43}\right) \times 10^{-5}$ ($\log {}^2\mathrm{H/H} = -4.48 \pm 0.06$) [124].
(ix) **Q0913+072** shows six well-resolved D_I Lyman series transitions placed at $z = 2.61843$ and recently observed with the ESO VLT [116]. With an oxygen abundance of about 1/250 of the solar value the authors of Ref. [116] deduce a value of the deuterium abundance $^2\mathrm{H/H} = \left(2.75^{+0.27}_{-0.24}\right) \times 10^{-5}$ ($\log {}^2\mathrm{H/H} = -4.56 \pm 0.04$).
(x) **Q0014+813**, with the absorber placed at $z = 3.32$, yielding $^2\mathrm{H/H} \sim (1.9 \pm 0.5) \times 10^{-4}$ [125,126]. Very old and no more used after [127].
(xi) **Q0420-388**, with the absorber placed at $z = 3.08$, implying, if the deuterium identification is correct, that the $^2\mathrm{H/H}$ ratio could have any value $\leq 2 \times 10^{-5}$. Whereas, if the $\mathrm{O}_I/\mathrm{H}_I$ ratio is constant throughout the complex, then $^2\mathrm{H/H} \sim 2 \times 10^{-4}$ [128].
(xii) **BR1202-0725**, two Lyman-α systems placed at $z = 4.383$ and $z = 4.672$, yielding $^2\mathrm{H/H} \leq 1.5 \times 10^{-4}$ [129].
(xiii) **PG1718+4807**, with the absorber placed at $z = 0.701$ $^2\mathrm{H/H} \in (1.8 - 3.1) \times 10^{-4}$ [130–133], but having been criticized in past by Ref. [132].
(xiv) **Q0130-4021**, with the absorber placed at z 2.8 with metallicity $[\mathrm{Si/H}] \leq -2.6$, yielding $^2\mathrm{H/H} \leq 6.7 \times 10^{-5}$ ($\log {}^2\mathrm{H/H} \leq -4.17$) [134], considered not very interesting and thus typically neglected.

Recently, three different analysis of high-redshift systems appeared:

(1) in [124,14] quasars used are: HS 0105+1619, Q2206-199, PKS1937-1009 (I), Q1009+2956, Q1243+3047, SDSS 1558-0031, and the cumulative value reported is

$$^2\mathrm{H/H} = \left(2.68^{+0.27}_{-0.25}\right) \times 10^{-5},$$

when averaging over $^2\mathrm{H/H}$ determinations [14], or rather

$$\log {}^2\mathrm{H/H} = -4.55 \pm 0.04 \Longrightarrow {}^2\mathrm{H/H} = \left(2.82^{+0.27}_{-0.25}\right) \times 10^{-5},$$

when the log's are used;
(2) the authors of [135] use: HS 0105+1619, Q2206-199, PKS1937-1009 (I), Q1009+2956, Q1243+3047 and the cumulative value reported is

$$^2\mathrm{H/H} = (2.78 \pm 0.29) \times 10^{-5},$$

averaging over the $\log[^2\mathrm{H/H}]$ determinations;
(3) finally, in the very recent analysis of [116] the following sample is exploited: HS 0105+1619, Q0913+072, Q1009+2956, Q1243+3047, SDSS 1558-0031, PKS1937-1009 (I), Q2206-199. An average consistent with all the data is $\log[^2\mathrm{H/H}] = -4.55 \pm 0.03$ or, equivalently,

$$^2\mathrm{H/H} = (2.82^{+0.20}_{-0.19}) \times 10^{-5}.$$

The positions in the sky of the reported measurements (i)–(ix), are given in galactic coordinates in Fig. 6, and in redshift space in Fig. 7. We have performed a re-analysis of $^2\mathrm{H/H}$ using these results, averaging over the values of $\log[^2\mathrm{H/H}]$ and using the method described in Ref. [136] which has the particular advantage to give a continuous χ^2 function even in the case of asymmetric errors. In particular, let us denote with $\bar{x}_i\,{}^{+\sigma_i^+}_{-\sigma_i^-}$ the generic measurement of $\log[^2\mathrm{H/H}]$ corresponding to the i-th QSA. According to Ref. [136] one can define the following quantities:

$$\sigma_i \equiv \frac{\sigma_i^+ + \sigma_i^-}{2} \qquad A_i \equiv \frac{\sigma_i^+ - \sigma_i^-}{\sigma_i^+ + \sigma_i^-}, \tag{66}$$

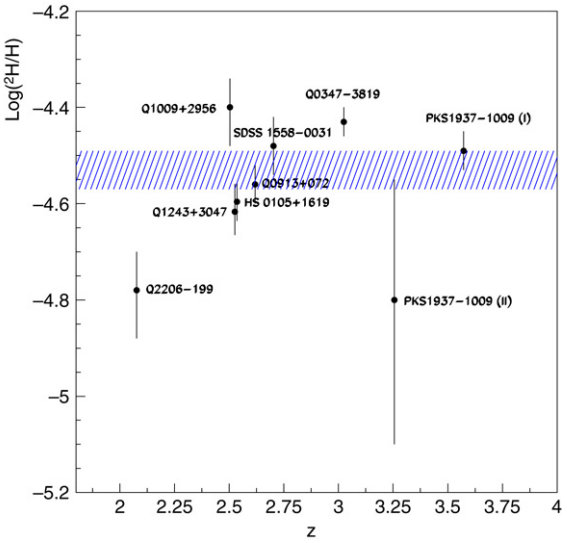

Fig. 7. The nine measurements of (i)–(ix) QSA's used in our analysis. The horizontal band represents the value of Eq. (68).

and define a total $\chi^2(\mu) = \sum_i \chi_i^2(\mu)$, where each contribution χ_i^2 is expanded up to A_i^2 terms

$$\chi_i^2(\mu) = \left(\frac{\bar{x}_i - \mu}{\sigma_i}\right)^2 \left(1 - 2A_i\left(\frac{\bar{x}_i - \mu}{\sigma_i}\right) + 5A_i^2\left(\frac{\bar{x}_i - \mu}{\sigma_i}\right)^2\right). \tag{67}$$

Using this procedure we find a value of the reduced χ^2, $\sqrt{\chi^2_{\rm min}/(9-1)} = 2.715$, which shows the effect of some systematic effects and that one or more uncertainties have been underestimated. If one chooses to treat all the data on the same footing, one can account for this by inflating each uncertainty by the multiplicative factor 2.715. In this case, after repeating the procedure, the new minimization leads to the result

$$\log {}^2{\rm H/H} = -4.53 \pm 0.04 \Longrightarrow {}^2{\rm H/H} = \left(2.98^{+0.29}_{-0.23}\right) \times 10^{-5}. \tag{68}$$

In [116] it was argued that the determinations (v) and (vii) of our list are less robust against systematics in the modeling of the cloud, due to the minor number of resolved deuterium lines. To be more conservative, one can thus exclude these two data from the regression. In this case, with the choice for central values and symmetric error bars done in [116], we reproduce their results. However, we find that it is not irrelevant to take into account the asymmetric errors in the regression procedure. When using the published asymmetric errors in $\log[{}^2{\rm H/H}]$ and applying the same procedure as above, we find a significantly lower multiplicative factor $\sqrt{\chi^2(-4.539)/6} = 1.897$, showing indeed that the dispersion of the measurements for this dataset is more consistent with a statistical one. To be conservative we multiply the error bars by the factor 1.897 and find

$$\log {}^2{\rm H/H} = -4.54 \pm 0.03 \Longrightarrow {}^2{\rm H/H} = \left(2.87^{+0.22}_{-0.21}\right) \times 10^{-5}, \tag{69}$$

which is the value we will be using in the following.

To conclude, it is worth mentioning the recent proposal to use the fluctuations in the absorption of cosmic microwave background photons by neutral gas during the cosmic dark ages, at redshifts $z \approx 7-200$, to reveal the primordial deuterium abundance of the Universe. This method is based on the strength of the cross-correlation of brightness-temperature fluctuations due to resonant absorption of CMB photons in the 21-cm line of neutral hydrogen, with those due to resonant absorption of CMB photons in the 92-cm line of neutral deuterium. This results to be proportional to the ratio ${}^2{\rm H/H}$ fixed during the BBN. Although technically challenging, this measurement could provide the cleanest possible determination of ${}^2{\rm H/H}$ [137]. A difficulty which has been pointed out – that may prevent the viability of the method at redshifts when the first UV sources turn on, $z \lesssim 40$ – is that when including Lyβ photons in the analysis, the inferred ratio ${}^2{\rm H/H}$ would not be constant, but depend sensitively on the UV spectrum [138].

4.2. Helium-3

Like deuterium, whose primordial yield is extremely sensitive to the baryon density parameter, η, ^{3}He is a crucial test of the standard BBN scenario as well. From the observational point of view, several environments are studied in order to derive its primordial abundance. Terrestrial determinations yield e.g. the ratio ${}^3{\rm He}/{}^4{\rm He} \sim 10^{-6}$ from balloon measurements or $\sim 10^{-8}$ from continental rock [139,140]. These observations, which show a large spread of values, confirm the idea that the terrestrial helium has no cosmological nature. In fact, most of it is ^{4}He produced by the radioactive decay of elements such

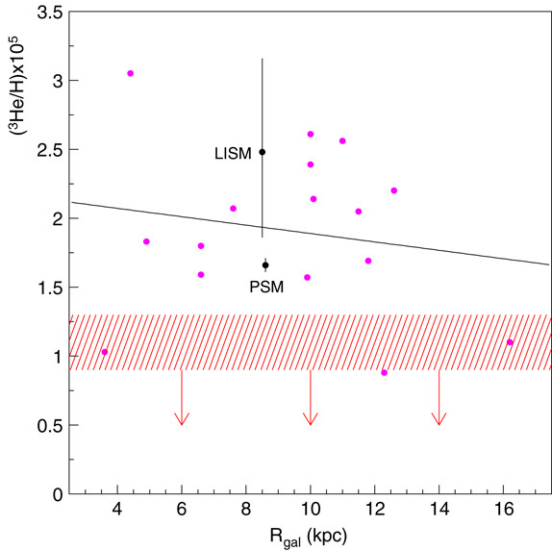

Fig. 8. The 16 purple spots represent the HII regions studied in Ref. [148] versus their distance from galactic center. Also the PSM and LISM measurements are reported. The black solid line stands for the linear fit of purple data, whereas the red band represents the upper bound obtained in [148].

as uranium and thorium. No natural radioactive decay produces ^{3}He, hence its observed terrestrial traces can be ascribed to unusual processes such as the testing of nuclear weapons or the infusion of extraterrestrial material.

In the solar system, ^{3}He is measured through the solar wind and meteorites [141]. The most accurate value was measured in Jupiter's atmosphere by the Galileo Probe [142]. These measurements support the idea of the conversion of the deuterium initially present in the outer parts of the Sun into ^{3}He via nuclear reactions. One can infer that in the ProtoSolar Material (PSM) out of which the Sun formed, $^3\mathrm{He}/^4\mathrm{He} = (1.66 \pm 0.05) \times 10^{-4}$ [142,140] and simultaneously $^2\mathrm{H/H} = (2.6 \pm 0.7) \times 10^5$ [142]. Note that in order to transform the above mentioned ratios $^3\mathrm{He}/^4\mathrm{He}$ into $^3\mathrm{He/H}$ one can use the value $^4\mathrm{He/H} \sim 0.1$ and thus derive the important ratio $^3\mathrm{He}/^2\mathrm{H} = 0.6 \pm 0.2$ which allows one to constrain electromagnetically decaying particles (see Section 9).

The previous observation of $^3\mathrm{He}/^4\mathrm{He}$ is compatible with the same measurement performed in meteoritic gases, yielding $^3\mathrm{He}/^4\mathrm{He} = (1.5 \pm 0.3) \times 10^{-4}$ [143–146]. Further information comes from Local Inter-Stellar Medium (LISM). Occasionally, LISM atoms crossing the termination shock region that separates the solar system from interstellar space get ionized. By counting the helium ions in this particular component of the solar wind, the Ulysses spacecraft has measured a $^3\mathrm{He}/^4\mathrm{He}$ ratio of $2.48^{+0.68}_{-0.62} \times 10^{-4}$ [147], which is not inconsistent with the idea that ^{3}He at our galaxy's location might have grown in the last 4.6 billion years since the birth of the Sun.

Far beyond the LISM, only one spectral transition allows the detection of ^{3}He, namely the 3.46 cm spin-flip transition of $^3\mathrm{He}^+$, the analog of the widely used 21-cm line of hydrogen; this is a powerful tool for the isotope identification, as there is no corresponding transition in $^4\mathrm{He}^+$. The emission is quite weak, hence ^{3}He has been observed outside the solar system only in a few HII regions and Planetary Nebulae (PN) in the Galaxy. The values found in PN result one order of magnitude larger than PSM and LISM determinations (for example $^3\mathrm{He/H} = (2-5) \times 10^{-4}$ is measured in NGC3242 [148]), confirming a net stellar production of ^{3}He in at least some stars. From the expected correlation between metallicity of the particular galactic environment and its distance from the center of the galaxy, one would expect a gradient in ^{3}He abundance versus metallicity and/or distance. In Ref. [148] the $^3\mathrm{He/H}$ abundance ratios are reported for the sample of simple HII regions.

Figs. 8 and 9 report the data as functions of the distance from galactic center and metallicity, respectively, together with the two determination from PSM and LISM. No significant correlation between the ^{3}He abundance and location (or metallicity) in the Galaxy is revealed. The linear fits reported in Figs. 8 and 9 as black solid lines correspond respectively to

$$(^3\mathrm{He/H}) \times 10^5 = 2.194 - 0.030\, R_{gal}(\mathrm{kpc}), \tag{70}$$

$$(^3\mathrm{He/H}) \times 10^5 = 1.910 + 0.014\, [\mathrm{O/H}], \tag{71}$$

where $[\mathrm{O/H}] \equiv \log(\mathrm{O/H}) - \log(\mathrm{O/H})_\odot$. Note that we adopt $(\mathrm{O/H})_\odot = 4.2 \times 10^{-4}$ [149], differently from [148] where $\log(\mathrm{O/H})_\odot = 6.3 \times 10^{-4}$ was used. Qualitatively, these data suggest a remarkable compensation between stellar production and destruction of ^{3}He.

The failure in observing a galactic ^{3}He dependence on metallicity, typically predicted by a chemical evolution model of the Galaxy (see [150] for a review) has been referred to as the "^{3}He problem". However, in the last years this subject received new insight [151] by the study of 3D mixing models which seem to reconcile the predictions with the data. In this scenario, by assuming a more conservative approach, the authors of Ref. [148] prefer to report an upper limit to the

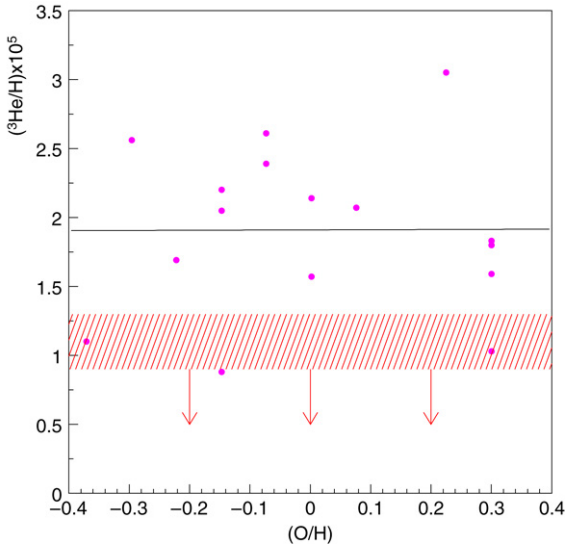

Fig. 9. The data of Ref. [148] versus metallicity are reported. The black solid line stands for the linear fit of purple data, whereas the red band represents the upper bound obtained in [148].

primordial abundance of ^{3}He by using the observations of a peculiar galactic HII region,

$$^3\mathrm{He/H} < (1.1 \pm 0.2) \times 10^{-5}. \tag{72}$$

This upper bound is reported as the red band in Figs. 8 and 9 [14].

A different approach could be based on the observation that the ratio $(^2\mathrm{H} + ^3\mathrm{He})/\mathrm{H}$ shows a high level of stability during the galactic evolution. This is partially supported by observations and chemical evolution models (see for example [152]). In this case, by using the value reported in Ref. [153] for PSM, namely $(^2\mathrm{H} + ^3\mathrm{He})/\mathrm{H} = (3.6 \pm 0.5) \times 10^{-5}$, and considering it as a good estimate for the primordial value one gets

$$\frac{^3\mathrm{He}}{\mathrm{H}} = (0.7 \pm 0.5) \times 10^{-5} \tag{73}$$

by using the primordial deuterium abundance discussed in the previous section, whose upper bound is consistent with the one derived from Eq. (72).

4.3. *Helium*-4

The post-BBN evolution of ^{4}He can be simply understood in terms of nuclear stellar processes which, through successive generations of stars, have burned hydrogen into ^{4}He and heavier elements, hence increasing the ^{4}He abundance above its primordial value [14]. Since the history of stellar processing can be tagged by measuring the *metallicity* (Z) of the particular astrophysical environment, the primordial value of ^{4}He mass fraction Y_p can be derived by extrapolating the Y_p–O/H and Y_p–N/H correlations to O/H and N/H $\to$ 0, as proposed originally in Refs. [154–156]. However, heavy elements like oxygen are produced by short-lived massive stars whereas ^{4}He is essentially synthesized in all stars, so one has to minimize model-dependent evolutionary corrections. The key data for inferring ^{4}He primordial abundance are provided by observations of helium and hydrogen emission lines generated from the recombination of ionized hydrogen and helium in low-metallicity extragalactic H_{II} regions [14]. Many attempts to determine Y_p have been made, constructing these correlations for various samples of Dwarf Irregular (DIrrs) and Blue Compact Galaxies (BCGs) [157]. These systems are the least chemically evolved known galaxies. Plausibly, they contain very little helium synthesized in stars after the BBN, minimizing the chemical evolution problems that affect e.g. the determination of ^{3}He [158].

Uncertainties in the determination of Y_p can be statistical or systematic. Statistical uncertainties can be decreased by obtaining very high signal-to-noise ratio spectra of BCGs. These BCGs are undergoing intense bursts of star formation, giving birth to high-excitation supergiant H_{II} regions and allowing an accurate determination of the helium abundance in the ionized gas through the BCG emission-line spectra. The theory of nebular emission is understood well enough not to introduce additional uncertainty. According to the standard scenario, the universe was born with zero metallicity; hence, Y_p can be determined extrapolating to $Z \to 0$ the relationship between Z and the ^{4}He abundance for a sample of objects. This procedure relies on the determination of the individual Y_p and Z values and of the slope $\mathrm{d}Y_p/\mathrm{d}Z$, which is assumed to be linear. The uncertainty affecting Y_p depends directly on the uncertainties on $\mathrm{d}Y_p/\mathrm{d}Z$ and the ensemble of the (Y_p, Z) pairs. For this reason, it has long been thought that the best results are obtained from the analysis of extremely low metallicity objects like DIrrs and BCGs, since their use minimizes the uncertainty associated with $\mathrm{d}Y_p/\mathrm{d}Z$. However, the authors of

Refs. [159,160] have noted that this advantage is outweighed by the relatively higher uncertainty on the Y_p-values, which derives from the (unknown) collisional contribution to the Balmer line intensities, an uncertainty especially affecting these objects since collisional contribution is quite important at high temperatures and rapidly fades away at intermediate and low temperatures [161]. Mostly following the analysis reported in Ref. [162] we list below the most recent estimates of Y_p.

(i) In Ref. [158] is reported the estimate $Y_p = 0.2421 \pm 0.0021$. According to Ref. [162] the differences with the previous determination are mainly systematic. One is due to the use in Ref. [162] of He_I recombination coefficients studied in Refs. [163,164], which yield Y_p values about 0.0040 higher than the previous ones. Moreover, in Ref. [162] they use some recent H_I collisional data, which further increase the Y_p values over the older H_I collisional corrections by about 0.0025.

(ii) The value quoted in Ref. [165] is $Y_p = 0.249 \pm 0.009$. The small sample size used and the large uncertainty affecting the parameters derived from the H_{II} regions considered in the analysis are responsible in this case for the very conservative error estimate. Also in this case, the systematic differences with Ref. [162] are due to the He_I recombination data used by both groups and to the estimation of the collisional contribution to the H Balmer lines.

(iii) In Ref. [166], based on a reanalysis of a sample of 33 H_{II} regions from Ref. [158], the authors determined a value of $Y_p = 0.250 \pm 0.004$. In addition to a different treatment of the underlying H and He_I absorption there are few systematic effects discussed in detail in Ref. [162].

(iv) In Ref. [162], the authors present a new ^{4}He mass fraction determination, yielding $Y_p = 0.2477 \pm 0.0029$. This result is based on new atomic physics computations of the recombination coefficients of He_I and of the collisional excitation of the H_I Balmer lines together with observations and photoionization models of metal-poor extragalactic H_{II} regions.

(v) Finally, in Ref. [167] is reported the estimate $Y_p = 0.2516 \pm 0.0011$ when using the He_I emissivity of Ref. [163].

All recent analyses of Y_p agree on the fact that the systematic error is the main responsible for the spread of the Y_p determinations. For example, in Ref. [162] three of the four main sources of error ($\Delta Y_p \geq 0.01$) in estimating Y_p are reported to be of systematic nature. Different authors however, report different error budgets (sometimes analyzing the same objects). Nevertheless, the use of new He_I recombination coefficients studied in Refs. [163,164] has sensibly changed the predictions by pushing them up a few percent as shown in Refs. [162,167]. For this reason we will use their determinations only to derive an estimate of primordial Y_p.

In particular, in Ref. [162] the uncertainty quoted on the value of Y_p seems to provide a more realistic estimate (0.003) of the residual indetermination affecting the ^{4}He mass fraction, versus the more optimistic (0.001) reported in Ref. [167], due to a very large sample of objects included in the analysis. For this reason we prefer to average the two main values as not weighted by their uncertainties, and use the more conservative error estimate of Ref. [162] at $1-\sigma$. In summary, we adopt for the ^{4}He mass fraction

$$Y_p = 0.250 \pm 0.003. \tag{74}$$

Note that this range of values totally contains the one of Ref. [167], but only partially covers the determination of Ref. [162] which points out slightly smaller values. Hence the effects of new He_I recombination coefficients [163,164] on global Y_p data analysis is to push slightly upward its estimate, and this is going to affect at a certain level the determination of cosmological parameters, as will be discussed in the following sections.

We would like to briefly point out that other constraints on Y_p can be obtained by indirect methods. For example, in [168] Y_p was bounded from studies of Galactic Globular Clusters (GGC). The value they found, $Y_p \lesssim Y_{GGC} = 0.250 \pm (0.006)_{\rm stat} \pm (0.019)_{\rm sys}$, is consistent with the above estimate. Finally, CMB anisotropies are sensitive to the reionization history, and thus to the fraction of baryons in the form of ^{4}He. Present data only allow a marginal detection of a non-zero Y_p, and even with PLANCK the error bars from CMB will be larger than the present systematic spread of the astrophysical determinations [169–173]. On the other hand, imposing a self-consistent BBN prior on Y_p would improve the diagnostic power of CMB data on other parameters, thus representing another nice synergy of CMB and BBN, besides the concordance test provided by η.

4.4. *Lithium*-7

Lithium's two stable isotopes, ^{6}Li and ^{7}Li, continue to puzzle astrophysicists and cosmologists who try to reconcile their primordial abundance as inferred from observations with the BBN predictions. From the astrophysical point of view the questions mainly concern the observation of lithium in cold interstellar gas and in all type of stars in which lithium lines are either detected or potentially detectable [174].

A chance to link primordial ^{7}Li with the BBN abundance was first proposed by Spite & Spite (1982) [175], who showed that the lithium abundance in the warmest metal-poor dwarfs was independent of metallicity for [Fe/H] < -1.5. The constant lithium abundance defining what is commonly called *the Spite plateau* suggested that this may be the lithium abundance in pre-Galactic gas provided by the BBN. The very metal-poor stars in the halo of the Galaxy or in similarly metal-poor GGC thus represent ideal targets for probing the primordial abundance of lithium. Even though lithium is easily destroyed in the hot interiors of stars, theoretical expectations supported by observational data suggest that although lithium may have been depleted in many stars, the overall trend is that its galactic abundance has increased with time [14].

There is quite a long tale of ^{7}Li determinations appearing in the literature, starting from the Spite & Spite (1982) value of $[^7{\rm Li/H}] = 2.05 \pm 0.15$ (by definition $[^7{\rm Li/H}] \equiv 12 + \log_{10}(^7{\rm Li/H})$). For the sake of brevity we will restrict our analysis

roughly to the determinations of the last decade. The implicit assumption is that, hopefully, the more recent papers have reached a better understanding of the systematics involved in the inference of the primordial ^{7}Li abundance.

In Refs. [176,177] a study of a set of very metal-poor stars showed a very small intrinsic dispersion in the ^{7}Li abundance determinations. Moreover, the authors found evidence for a decreasing trend in the ^{7}Li abundance toward lower metallicity indicating that the primordial abundance of ^{7}Li can be inferred only after allowing for nucleosynthesis processes that must have been at work in the early stages of the Galaxy. The primordial ^{7}Li abundance reported is $[^7\mathrm{Li/H}] = 2.09 \pm^{+0.19}_{-0.13}$ ($^7\mathrm{Li/H} = \left(1.23^{+0.68}_{-0.32}\right) \times 10^{-10}$). Different studies of halo and GGC stars provided higher lithium plateau abundance $[^7\mathrm{Li/H}] = 2.24 \pm 0.01$ [178,179]. A similar analysis is contained in Ref. [180], where high resolution, high signal-to-noise ratio spectra of 12 turn-off stars in the metal-poor globular cluster NGC 6397 were used. The author conclude that, within the errors, they all have the same lithium abundance $[^7\mathrm{Li/H}] = 2.34 \pm 0.06$.

In Ref. [181], a study of ^{7}Li abundance in 62 halo dwarfs was performed by using accurate equivalent widths and a temperature scale from an improved infrared flux method. For 41 plateau stars (those with $T_{\mathrm{eff}} > 6000$ K) the ^{7}Li abundance is found to be independent of temperature and metallicity, with a star-to-star scatter of only 0.06 dex over a broad range of temperatures (6000 K $< T_{\mathrm{eff}} <$ 6800 K) and metallicities ($-3.4 <$ [Fe/H] < -1). Thus they report a mean ^{7}Li plateau abundance of $[^7\mathrm{Li/H}] = 2.37 \pm 0.05$. In Ref. [182] the authors underwent a very detailed reanalysis of available observations; by means of a careful treatment of systematic uncertainties and of the error budget, they find $[^7\mathrm{Li/H}] = 2.21 \pm 0.09$ for their full sample and $[^7\mathrm{Li/H}] = 2.18 \pm 0.07$ for an analysis restricted to unevolved (dwarf) stars only. They also argued that no convincing/conclusive evidence for a correlation between ^{7}Li and metallicity can be claimed at present. More recently, the authors of Ref. [174] have studied a set of 24 very high quality spectra metal-poor halo dwarfs and subgiants, acquired with ESOs VLT/UVES. The derived one-dimensional, non-Local Thermodynamical Equilibrium (non-LTE) ^{7}Li abundances from the Li$_I$ 670.8 nm line reveal a pronounced dependence on metallicity but with negligible scatter around this trend. The estimated primordial ^{7}Li abundance is $^7\mathrm{Li/H} \in (1.1 - 1.5) \times 10^{-10}$ ($[^7\mathrm{Li/H}] = 2.095 \pm 0.055$). Recently Ref. [183] has reported the spectroscopic observations of stars in the metal poor globular cluster NGC6397 that reveal trends of atmospheric abundance with evolutionary stage for various elements. These element-specific trends are reproduced by stellar-evolution models with diffusion and turbulent mixing. They compare their observations of lithium and iron to models of stellar diffusion, finding evidence that both lithium and iron have settled out of the atmospheres of these old stars. Applying their stellar models to the data they infer for the unevolved abundances, [Fe/H] = 2.1 and $[^7\mathrm{Li/H}] = 2.54 \pm 0.10$.

The list of the last ten years estimates for ^{7}Li abundance is then the following:

(i) $[^7\mathrm{Li/H}] = 2.24 \pm 0.01$ [178,179];
(ii) $[^7\mathrm{Li/H}] = 2.09^{+0.19}_{-0.13}$ [176,177];
(iii) $[^7\mathrm{Li/H}] = 2.34 \pm 0.06$ [180];
(iv) $[^7\mathrm{Li/H}] = 2.37 \pm 0.05$ [181];
(v) $[^7\mathrm{Li/H}] = 2.21 \pm 0.09$ [182];
(vi) $[^7\mathrm{Li/H}] = 2.095 \pm 0.055$ [174];
(vii) $[^7\mathrm{Li/H}] = 2.54 \pm 0.10$ [183].

All but (marginally) the latter value are inconsistent with standard BBN predictions for the preferred range of η singled out by CMB data, which fits remarkably well deuterium abundance. It is unclear how to combine the different determinations in a single estimate, or if the value measured is truly indicative of a primordial yield. A conservative approach (similar to the one used for ^{4}He) is to quote the simple (un-weighted) average and half-width of the above distribution of data as best estimate of the average and "systematic" error on ^{7}Li/H, obtaining

$$\left[\frac{^7\mathrm{Li}}{\mathrm{H}}\right] = 2.27 \pm 0.23 \Longrightarrow \left(\frac{^7\mathrm{Li}}{\mathrm{H}}\right) = \left(1.86^{+1.30}_{-1.10}\right) \times 10^{-10}. \tag{75}$$

Note that the statistical error is much smaller (of the order of 0.01), but we will not need it since, due to its uncertain status as a tracer of the primordial value, ^{7}Li is typically excluded in "conservative" BBN statistical analyses (or rather invoked to support particular non-standard BBN scenarios).

4.5. *Lithium*-6 *and "The lithium problems"*

It is clear from the above discussion and from the substantial disagreement of almost all of the ^{7}Li observations with the standard BBN predicted value (by about 0.4 dex, assuming the central value of the quoted average) that some piece of (astro)physics is missing. For a detailed discussion of possible causes we address the reader to the excellent review given in Ref. [174] (see also [184]). Here we want to remark that: (i) a $\sim$1.5–2 lower value of η at the BBN time with respect to the best fit deduced from CMB data is excluded by the agreement between deuterium observations and CMB value of η, but also by the inferred upper limit of the primordial ^{3}He abundance; (ii) underestimated errors in the adopted nuclear reaction rates are now excluded: the laboratory measurements of the crucial $^3\mathrm{He}(\alpha, \gamma)^7\mathrm{Be}$ cross-section [185–188], its inferred rate from solar neutrino data [189], and the measurement of the proposed alternative channel for ^{7}Be destruction $^7\mathrm{Be}(d, p)2\alpha$ [190] all point to the conclusion that nuclear uncertainties cannot explain the discrepancy between observed and predicted primordial ^{7}Li abundances; (iii) systematic errors in the abundance analysis, although in principle still possible, seem very

unlikely. The introduction of 3D model atmospheres, even accounting for non-LTE, has not resulted in a significant upward revision of the lithium abundance obtained from more primitive 1D atmospheres.

The most likely causes of the "problem" are thus: (a) either some modification to the BBN scenario; (b) or, perhaps more likely, that the lithium abundance of very metal-poor stars is not the one of the primordial gas. We will illustrate later some scenarios of the type (a). Here, however, we want to point out that explanations of the type (b) are probably not trivial and might involve both reprocessing *in situ* (the observed stars) and earlier lithium synthesis/depletion in the pre-galactic, young universe environment. Indeed, even assuming that some diffusion and turbulent mixing mechanism like the one pointed out in [183] can explain the ^{7}Li problem, still an issue remains with ^{6}Li. The presence of the fragile ^{6}Li isotope, which is produced during the BBN at the level of $^6\mathrm{Li/H} \sim 10^{-15} - 10^{-14}$, has been recently confirmed in a few metal-poor halo stars, with some hint of a plateau vs. metallicity[8] with abundance as high as $^6\mathrm{Li/H} \sim 6 \times 10^{-12}$ [174]. These data (at least partially) confirm the first observations reported in literature already fifteen years ago [193–197]. In particular, in Ref. [174] ^{6}Li is detected in 9 of 24 analyzed stars at the $> 2\sigma$ significance level. However, it is worth stressing that these observations have been questioned in Ref. [198,199]. According to these papers the convective asymmetry generates an excess absorption in the red wing of the ^{7}Li absorption feature that could mimic the presence of ^{6}Li at a level comparable with published values. This would mean that only an upper limit on $^6\mathrm{Li}/^7\mathrm{Li}$ can be derived at present.

Both ^{7}Li, ^{6}Li can be produced by fusion ($\alpha + \alpha \rightarrow$ Li) and spallation (p + CNO $\rightarrow$ LiBeB) reactions by ordinary cosmic ray primaries impinging on nucleons and nuclei in the intergalactic medium (see e.g. [200]). Additionally, observations are performed not in "inert" gas clouds, but in stellar atmospheres, where thermonuclear burning depletion (of particularly fragile nuclei) is a crucial effect. It follows that primordial production mechanisms and later astrophysical effects might be competing. Viable astrophysical candidates for the acceleration of cosmic rays, able to account for the ^{6}Li observed at low metallicity include: the massive black hole in the Galactic center [201], radio-loud AGNs (one of which could have been present in our Galaxy in the past) [202], and PopIII stars [203,204] which may also explain the depletion of ^{7}Li [205], but have been recently challenged on the light of further constraints adopted in the model of [206]. The shocks developed during structure formation [207], which however conflict with astrophysical constraints [208], are not powerful enough, since in the early times of Galaxy formation, the masses of the assembling dark haloes were still quite small and the corresponding virial velocities insufficient [201].

Perhaps, the most convincing explanation proposed until now is that ^{6}Li may be produced *in situ* from stellar flares within the first billion years of the star's life [209]. In particular, the anomalously high $^3\mathrm{He}/^4\mathrm{He}$ ratio found in solar flares ($\sim$0.5) and the kinematically much more favorable process $^4\mathrm{He}(^3\mathrm{He}, p)^6\mathrm{Li}$ compared to $\alpha\,\alpha \rightarrow {}^7$Li fusion reactions provide a physical mechanism for producing large quantities of ^{6}Li without overproducing ^{7}Li. The main issue with this or other scenarios might be the difficulty to test them.

A great help in solving this issue might come from detecting lithium in a different environment. In Ref. [210], it was proposed to independently test the pre-Galactic Li abundance by looking at high velocity gas clouds falling onto our Galaxy, with metallicities as low as 10% of the solar one. If these low-metallicity clouds have a mostly pre-Galactic composition, with a small contamination from the Galaxy, they might allow probing the lithium abundance at least free of the possibility of thermonuclear depletion *in situ*. Another proposal to detect the cosmological recombination of lithium via its effect on the microwave background anisotropies [211] has been proved not to be viable [212].

We will not use ^{6}Li to derive constraints in this review. However, using the observed ^{6}Li as an upper limit to its primordial value turns out to be a powerful constraint in some regions of parameter space for exotic models. While reporting them in the following, we warn the reader that their robustness relies on the assumption that no destruction or major reprocessing of the ^{7}Li and ^{6}Li observed in the halo stars has happened, which might be overly optimistic.

5. Standard BBN theoretical predictions versus data

The goal of a theoretical analysis of BBN is to obtain a reliable estimate of the model parameters, once the experimental data on primordial abundances are known. In this section we will consider only the case of the standard BBN, where the only two free parameters are the value of the baryon energy density parameter $\Omega_B h^2$ (or equivalently the baryon to photon number density, η) and possibly, a non-standard value for the relativistic energy content during the BBN. The latter, after $e^{\pm}$ annihilation can be parameterized in terms of the effective number of neutrinos we have recalled in Section 3.2,

$$\rho_R = \left(1 + \frac{7}{8}\left(\frac{4}{11}\right)^{4/3} N_{\mathrm{eff}}\right)\rho_\gamma. \tag{76}$$

Similar analyses have been recently presented by various groups, which might be slightly different depending on the adopted values of Y_p and/or ^{2}H/H experimental determination, see e.g. [213–215,91,216,82,217–220].

In the minimal scenario the parameters reduces to the baryon density only, since ΔN_{eff} is assumed to vanish. Fig. 10 shows the dependence on η_{10} of the final value of the primordial yields, calculated using `PArthENoPE`, along with the experimental values of the abundances and their corresponding uncertainties, as discussed in the previous section.

[8] However, taking into account predictions for ^{6}Li destruction during the pre-main sequence evolution tilts the plateau suggesting a ^{6}Li increase with metallicity. Basically, fairly uncertain stellar pre-main-sequence destruction of ^{6}Li could be responsible for an apparent plateau [191,192,174].

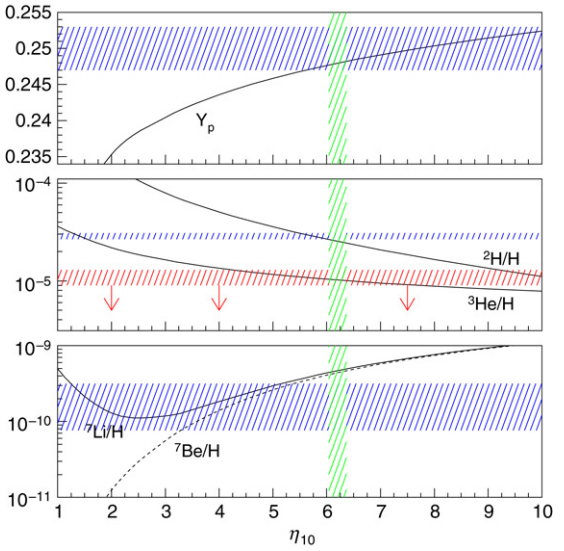

Fig. 10. Values of the primordial abundances as a function of η_{10}, calculated for $\Delta N_{\rm eff} = 0$. The hatched blue bands represent the experimental determination with $1-\sigma$ statistical errors on Y_p, ^2H, and ^{7}Li, while the red band is the upper bound obtained in Ref. [148]. Note that for a high value of η_{10} all ^{7}Li comes from ^{7}Be radioactive decay via electron capture. The vertical green band represents the WMAP 5-year result $\Omega_B h^2 = 0.02273 \pm 0.00062$ [8].

To get confidence intervals for η, one constructs a likelihood function

$$\mathcal{L}(\eta) \propto \exp\left(-\chi^2(\eta)/2\right), \tag{77}$$

with

$$\chi^2(\eta) = \sum_{ij} [X_i(\eta) - X_i^{obs}] W_{ij}(\eta) [X_j(\eta) - X_j^{obs}]. \tag{78}$$

The proportionality constant can be obtained by requiring normalization to unity, and $W_{ij}(\eta)$ denotes the inverse covariance matrix,

$$W_{ij}(\eta) = [\sigma_{ij}^2 + \sigma_{i,exp}^2 \delta_{ij} + \sigma_{ij,other}^2]^{-1}, \tag{79}$$

where σ_{ij} and $\sigma_{i,exp}$ represent the nuclear rate uncertainties and experimental uncertainties of nuclide abundance X_i, respectively (we use the nuclear rate uncertainties as in Ref. [18]), while by $\sigma_{ij,other}^2$ we denote the propagated squared error matrix due to all other input parameter uncertainties (τ_n, $G_{\rm N}$, etc.). We use the following values for the experimental yields of ^{2}H and ^{4}He (see previous section):

$$^2{\rm H/H} = \left(2.87^{+0.22}_{-0.21}\right) \times 10^{-5}, \qquad Y_p = 0.250 \pm 0.003. \tag{80}$$

We first consider ^{2}H abundance alone, to illustrate the role of deuterium as an excellent baryometer. In this case the best fit values found are $\Omega_B h^2 = 0.021 \pm 0.001$ ($\eta_{10} = 5.7 \pm 0.3$) at 68% C.L., and $\Omega_B h^2 = 0.021 \pm 0.002$ at 95% C.L.. A similar analysis can be performed using ^{4}He. In this case we get $\Omega_B h^2 = 0.028^{+0.011}_{-0.007}$ ($\eta_{10} = 7.6^{+3.0}_{-1.9}$)[9] at 68% C.L., and $\Omega_B h^2 = 0.028^{+0.024}_{-0.012}$ at 95% C.L.. Fig. 11 shows, as from our discussion in the previous section, that the determination of $\Omega_B h^2$ is mainly dominated by deuterium. In any case, the result is compatible at 2-σ with the WMAP 5-year result $\Omega_B h^2 = 0.02273 \pm 0.00062$ [8]. The slight disagreement might have some impact on the determination from CMB anisotropies of the primordial scalar perturbation spectral index n_s, as noticed in [116], where the BBN determination of $\Omega_B h^2$ from deuterium is used as a prior in the analysis of the five year data of WMAP.

In Table 11 we report the values of relevant abundances for some different baryon densities, evaluated using `PArthENoPE` [93]. Notice the very low prediction for ^{6}Li (see discussion in Section 4) and that, for these values of baryon density, almost all ^{7}Li is produced by ^{7}Be via its eventual electron capture process.

If one relaxes the hypothesis of a standard number of relativistic degrees of freedom, it is possible to obtain bounds on the largest (or smallest) amount of radiation present at the BBN epoch, in the form of decoupled relativistic particles, or non-standard features of active neutrinos (but see our previous discussion in Section 3.2). Fig. 12 displays the contour plots 68% and 95% C.L. of the total likelihood function, in the plane ($\Omega_B h^2$, $N_{\rm eff}$). After marginalization one gets $\Omega_B h^2 = 0.021 \pm 0.001$ and $N_{\rm eff} = 3.18^{+0.22}_{-0.21}$ at 68% C.L., and $\Omega_B h^2 = 0.021 \pm 0.002$ and $N_{\rm eff} = 3.18^{+0.44}_{-0.41}$ at 95% C.L.. Hence the global analysis results to be compatible with $N_{\rm eff} = 3.046$ and $\Omega_B h^2 = 0.02273$ found by WMAP at 1-σ level (see Fig. 12).

[9] Note that η_{10} reported in this section is conventionally defined, according to `PArthENoPE`, as $\eta_{10} \equiv 273.49\, \Omega_B h^2$ which is slightly different from the definition of Eq. (9), but simply connected to it.

Table 11
The theoretical values of the nuclear abundances for some value of $\Omega_B h^2$.

$\Omega_B h^2$	0.017	0.019	0.021	0.023	0.028
Y_p	0.245	0.246	0.247	0.248	0.250
^{2}H/H $\times 10^5$	4.00	3.36	2.87	2.48	1.79
^{3}He/H $\times 10^5$	1.22	1.14	1.07	1.01	0.903
^{7}Li/H $\times 10^{10}$	2.53	3.22	3.99	4.83	7.08
^{7}Be/H $\times 10^{10}$	2.15	2.89	3.69	4.56	6.88
^{6}Li/H $\times 10^{14}$	1.72	1.45	1.25	1.08	0.791

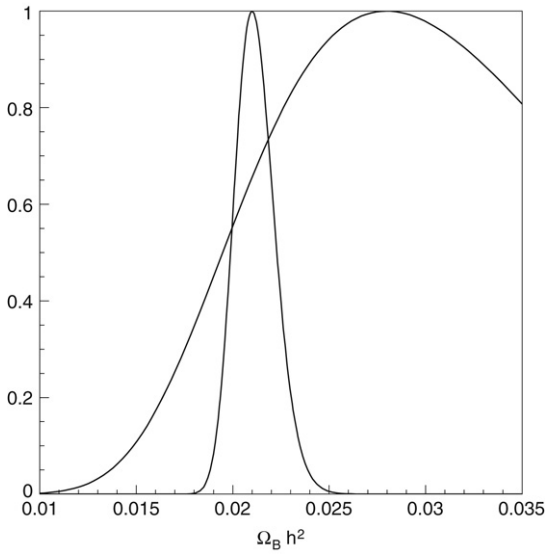

Fig. 11. Likelihood functions for ^{2}H/H (narrow) and Y_p (broad).

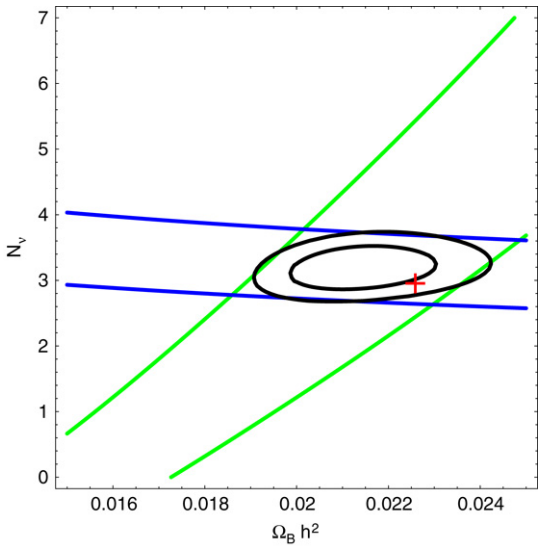

Fig. 12. Contours at 68 and 95% C.L. of the total likelihood function for deuterium and ^{4}He in the plane ($\Omega_B h^2$, $N_{\rm eff}$). The bands show the 95% C.L. regions from deuterium (almost vertical) and Helium-4 (horizontal). The red cross corresponds to the standard $N_{\rm eff}$ and $\Omega_B h^2 = 0.02273$ as indicated by WMAP 5-year results.

6. BBN and neutrino physics

We have already stressed how large is the impact of neutrino physics and neutrino properties on BBN. In fact, the discovery of neutrino masses via oscillations, combined with the stringent bounds on the effective electron neutrino mass

via tritium decay experiments, has had a profound impact on the phenomenology of active neutrinos in the early universe. At the moment we know that: (at least two) neutrinos are massive; *all* the masses are small ($m_\nu \lesssim$ eV, possibly much smaller); individual lepton numbers are violated (with mixing angles much larger than in the quark sector), although it is not known if the overall lepton number, L, is conserved. We do not know yet if the neutrino mass term in the Lagrangian is of the Dirac ($\sim[\mathcal{M}\ \bar{\nu}_L \nu_R + h.c.]$, flavor indexes omitted) or Majorana ($\sim[\mathcal{M}\ \bar{\nu}^c_L \nu_R + h.c.]$, where ν^c_L is the charge conjugate field) type, but in either case new physics is required. In the Dirac case, one is forced to introduce the yet undetected right-handed neutrino fields, ν_R. In the Majorana case, one assumes (differently from the SMPP) that the lepton number L is violated and introduces a Majorana mass operator, which is allowed for neutrinos, being the only neutral fermions in the SMPP. The important news for BBN are that even the incomplete knowledge of the mass matrix $\mathcal{M}$ that we have at present is enough to conclude that the phenomenology of active neutrinos in the BBN is greatly simplified. A plethora of cases once popular in the literature are now excluded. Among the ones which were of remarkable interest only a decade ago we can mention: (i) a lower-than-three effective number of neutrinos due to a "massive ν_τ" (improper, not being ν_τ a mass eigenstate) ; (ii) a decaying "ν_τ"; (iii) the thermalization of right-handed neutrinos (for the Dirac mass case), which is inhibited by the smallness of the neutrino masses by which they are coupled to the active states. We do not treat these issues further and address the interested reader to these historical topics to the review [42]. In the following, we focus on the bounds on electromagnetic interactions of neutrinos in Section 6.1, while Section 6.2 treats other exotic interactions. The topic of neutrino asymmetry is briefly reviewed in Section 6.3, while Section 6.4 treats the impact on BBN of sterile neutrino states.

6.1. Bounds on electromagnetic interactions of neutrinos

Dropping flavor indexes, the most general structure of effective neutrino electromagnetic interactions is

$$\mathcal{L}_{\rm int} = -e_\nu\ \bar{\nu}\ \gamma_\mu\ \nu A^\mu - a_\nu\ \bar{\nu}\ \gamma_\mu\ \gamma_5\ \nu\ \partial_\lambda F^{\mu\lambda} - \frac{1}{2}\bar{\nu}\ \sigma_{\alpha\beta}\ (\mu + \varepsilon\ \gamma_5)\ \nu F^{\alpha\beta} \tag{81}$$

where $F^{\alpha\beta}$ is the electromagnetic field tensor, $\sigma_{\alpha\beta} = [\gamma_\alpha, \gamma_\beta]$, and the form factors $\{e_\nu, a_\nu, \mu, \varepsilon\}$, which are functions of the transferred squared momentum q^2, in the limit $q^2 \to 0$ correspond to the electric charge, anapole moment, magnetic and electric dipole moment, respectively.

In principle, Dirac neutrinos may have a very small electric charge e_ν. BBN bounds may be derived by requiring both that right-handed partners are not populated and that neutrinos are not kept in equilibrium too long after the weak freeze-out, which would alter the photon–neutrino temperature relation. However, for the range of masses presently allowed, the BBN bounds are never competitive with other astrophysical or laboratory constraints, as for instance the red giant bound of $e_\nu \lesssim 2 \times 10^{-14}$ [221]. Actually, the indirect bound coming from the neutrality of matter is stronger ($e_\nu \lesssim 10^{-21}$, [222]; see also [223] and reference therein for details), so we ignore in the following a possible neutrino charge.

The possibility of a neutrino charge radius[10] (which can be negative),

$$\langle r^2 \rangle = \frac{6}{e}\left(\frac{\partial e_\nu(q^2)}{\partial q^2}\right)_{q^2=0}, \tag{82}$$

has been considered in the literature. After a long debate, it has been finally established that $\langle r^2 \rangle$ is a well-defined (gauge-independent) quantity [224–226]. The Standard Model expectations are in the range $\langle r^2 \rangle \simeq$ 1–4 nb. Differently from the case of the magnetic moment, the charge radius does not couple neutrinos to on-shell photons, so stellar cooling arguments are not very sensitive to $\langle r^2 \rangle$. Yet, for Dirac neutrinos the channel $e^- e^+ \to \nu_R \bar{\nu}_R$ is still effective, provided that new physics (NP) violates the cancelation between vector and axial contribution that otherwise applies in the SMPP. If this cancelation does not take place, the corresponding bounds from SN 1987 A [227] and nucleosynthesis [228] read

$$|\langle r^2 \rangle|^{\rm NP} \lesssim 2\ (7)\ {\rm nb}, \quad \text{from SN1987A (BBN)}. \tag{83}$$

For Majorana neutrinos, the previous bounds do not apply. In this case, however, even in the ν_τ-sector where BBN may have a sensitivity comparable to or better than laboratory experiments, even a change of one order of magnitude above the SMPP level in the channel $e^- e^+ \to \nu_\tau \bar{\nu}_\tau$ due to new physics would only bring changes at the 0.1% level in Y_p, so that only laboratory bounds are meaningful. For a further discussion of this point, see [229].

Another consequence of the existence of neutrino masses is that a neutrino magnetic moment is naturally present (and it is usually expressed in terms of Bohr magnetons, μ_B), although for Majorana particles only off-diagonal elements in flavor space are non-vanishing. There are two possible processes of interest for BBN: (i) the thermalization of Dirac neutrinos via e.g. the process $\nu_L e \to \nu_R e$; (ii) a radiative decay of the kind $\nu^i_L \to \nu^j_L\ \gamma$, the latter being possible also for Majorana neutrinos. In absence of primordial magnetic fields, the BBN bound on the diagonal elements coming from the thermalization of right-handed neutrinos is not as restrictive as the one coming from red giant cooling argument (from plasmon decay $\gamma^* \to \nu\bar{\nu}$,

[10] In complete analogy, one can define an anapole radius $\langle r^2_a \rangle$ from a_ν. For Majorana neutrinos, symmetries require some of the e.m. couplings to vanish. Since the astrophysical/cosmological bounds do not typically distinguish between $\langle r^2 \rangle$ and $\langle r^2_a \rangle$, or electric and dipole magnetic moments, we shall quote bounds on $\langle r^2 \rangle$ and μ in this loose sense.

$\mu \lesssim 3 \times 10^{-12}\,\mu_B$ [221]). The radiative decay rate for a transition $i \to j$ is

$$\Gamma_{ij}^{\gamma} = \frac{|\mu_{ij}|^2 + |\varepsilon_{ij}|^2}{8\pi}\left(\frac{m_i^2 - m_j^2}{m_i}\right)^3 \simeq 5.3\,\mathrm{s}^{-1}\left(\frac{\mu}{\mu_B}\right)^2\left(\frac{m_i^2 - m_j^2}{m_i\ \times 1\,\mathrm{eV}}\right)^3, \tag{84}$$

and typical bounds lead to a lifetime definitively too long to affect the BBN cosmology. In any case, the very cosmological bounds on the neutrino lifetime in [230] exclude any effect of the radiative neutrino decay at the BBN epoch. However, in presence of very strong primordial magnetic fields, the BBN bound via spin-precession may be as stringent as $\mu \lesssim 10^{-20}\,\mu_B$ [231]. Although very model-dependent (see [231], in particular Eqs. (50, 51)), this is to our knowledge the only bound probing the level of intensity expected for the dipole moment in the SMPP enlarged with a Dirac neutrino mass term, which is $\mu = 3\mathrm{e}\,G_F\,m_\nu/(8\sqrt{2}\pi^2) = 32 \times 10^{-20}\,(m_\nu/\mathrm{eV})\mu_B$.

6.2. Bounds on other exotic interactions of neutrinos

Besides anomalous electromagnetic interactions, neutrinos might undergo non-standard-interactions (NSI) with electrons. Ref. [232] considered low-energy four-fermions interactions of the kind

$$\mathcal{L}_{\mathrm{NSI}}^{\alpha\beta} = -2\sqrt{2}G_F[\varepsilon_{\alpha\beta}^{L}\,(\bar{\nu}_L^{\alpha}\gamma^{\mu}\nu_L^{\beta})(\bar{\mathrm{e}}_L\gamma_{\mu}\mathrm{e}_L) + \varepsilon_{\alpha\beta}^{R}(\bar{\nu}_L^{\alpha}\gamma^{\mu}\nu_L^{\beta})(\bar{\mathrm{e}}_R\gamma_{\mu}\mathrm{e}_R)], \tag{85}$$

with the NSI parameters $\varepsilon_{\alpha\beta}^{L}\,\varepsilon_{\alpha\beta}^{R}$ constrained by laboratory measurements to be at most of $\mathcal{O}(1)$. It was found that, for NSI parameters within the ranges allowed by present laboratory data, non-standard neutrino–electron interactions do not essentially modify the density of relic neutrinos nor the bounds on neutrino properties from cosmological observables. Qualitatively, this depends on the fact that a large modification of the neutrino spectra would only be achieved if the decoupling temperature were brought below the electron mass. The presence of neutrino–electron NSI within laboratory bounds may enhance the entropy transfer from electron–positron pairs into neutrinos, up to a value of $N_{\mathrm{eff}} = 3.12$ (and $\Delta Y_p \simeq 6 \times 10^{-4}$), which are almost three times the corrections due to non-thermal distortions that appear for standard weak interactions, but still probably too small to be detectable in the near future, even for PLANCK.

Another scenario is the one where neutrinos couple to a scalar or pseudoscalar particle with a Yukawa-type interaction of the kind

$$\mathcal{L}_{\nu\phi} = \frac{1}{2}\partial_{\mu}\phi\partial^{\mu}\phi - \frac{1}{2}m_{\phi}^2\phi^2 - \phi\sum_{\ell J}\bar{\nu}_L^{\ell}\lambda_{\ell J}\nu_L^{J}, \tag{86}$$

where ℓ, J are flavor indexes and, in case of pseudoscalar coupling, $\lambda_{\ell J} \to \gamma_5\lambda_{\ell J}$. We shall denote these couplings simply as λ if we ignore flavor effects and only refer to constraints within a factor of $\mathcal{O}(1)$. A famous case of this kind is the Majoron model [233–235] where the Majoron ϕ is the Goldstone boson associated to the breaking of the lepton number symmetry (and thus $m_\phi \to 0$). Although laboratory bounds rule out the original model as an explanation of the small neutrino masses, still it represents a prototype of "secret neutrino interactions", where neutrinos interact with a sector precluded from other standard model particles, and may thus have stronger interactions among themselves at low energies, than predicted by the SMPP. In the early universe, a large enough λ would allow to populate thermally the species ϕ. For $m_\phi \ll 1$ MeV, it was found in [236] that $\lambda \lesssim 10^{-5}$, if one considers one additional boson ($\Delta N_{\mathrm{eff}} = 3/7$) to be incompatible with the observations. If this is instead considered viable, the same process $\bar{\nu}\nu \leftrightarrow \phi\phi$ may be responsible for a "neutrinoless universe" well after the BBN epoch, provided that $m_\phi \ll m_\nu$ [237].

Relatively less attention has been paid to the case where the associated (pseudo)boson is massive (although a particle of this kind might have other "cosmological virtues", as providing a warm dark matter candidate, see e.g. [238]). In [239] the authors assumed MeV-scale ϕ particles produced at early epochs via additional couplings with other SMPP particles and later decaying into neutrinos in out-of-equilibrium conditions (with a rate $\Gamma(\phi \to \bar{\nu}\nu) = 3\lambda^2 m_\phi/(8\pi)$); when this happens before the photon last scattering epoch, the produced neutrino burst directly influences the CMB anisotropy spectrum, as well as the late LSS formation. They show that current cosmological observations of light element abundances, Cosmic Microwave Background (CMB) anisotropies, and Large Scale Structures (LSS) are compatible with very large deviations from the standard picture. They also calculate the bounds on non-thermal distortions which can be expected from future observations, finding that the present situation is likely to persist with future CMB and LSS data alone. On the other hand, the degeneracy affecting CMB and LSS data could be removed by additional constraints from primordial nucleosynthesis or independent neutrino mass scale measurements.

In [240], the particle ϕ was considered to be the inflaton, only coupled to neutrinos and with a mass $m_\phi \gg 1$ MeV, to determine via BBN and other cosmological observation the constraint on the lowest possible reheating temperature T_{RH}. In particular, the author derives constraints from partial thermalization as well as neutrino spectral distortions. Barring fine-tuning, the resulting bound is $T_{RH} \gtrsim 4$ MeV. A factor $\sim$2 lower bound was found in [241] if no ϕ boson is included but oscillations are taken into account. It is worth noticing that in scenarios with late-time entropy production a constraint arises anyway due to the incomplete background neutrino thermalization, even if the neutrinos do not couple to ϕ directly, as already noted in [242,243]. In [244], light scalar particles annihilating into neutrinos were considered to analyze the effect on BBN of MeV-scale dark matter particles, invoked to explain the excess of 511 keV photons from positron annihilation from the Galactic Center [245]. If such particles only couple to neutrinos, they need to be heavier than $\sim$1 MeV to be consistent

with the Y_p constraints. If they have an additional coupling to $e^+ e^-$ at the level required to explain the Galactic Center positrons, the bounds may be more stringent (but then depend on the details of the model).

We have seen that a Dirac mass term could in principle be responsible for the production of right-handed neutrinos in the primordial plasma. While this possibility is excluded by the smallness of neutrino masses, it is still possible to populate ν_R via direct right-handed currents mediated by W_R bosons, of the kind $\bar{\nu}_R \not{W}_R \nu_R$ (or analogous coupling with right-handed charged leptons). These are possible in some extensions of the standard electro-weak model. If one assumes that the right-handed interaction has the same form as the left-handed one but with heavier intermediate bosons, one can obtain from BBN a lower limit on their mass of the order of $m_{W_R} \gtrsim 75 m_W$ [246,11,247], which depends however on the exact particle spectrum of the physics beyond the SMPP up to $\sim 75\, m_W$.

6.3. Neutrino asymmetry

The origin of the most fundamental parameter in the BBN, the baryon asymmetry $\eta_B = (n_B - n_{\bar{B}})/n_\gamma$ (or simply η at late times), is not known. While SMPP and SMC contain all the ingredients required to generate it dynamically from an initially symmetric universe (B, C, and CP violating interactions, departure from thermal equilibrium) [248], the amount of CP violation and the strength of the electro-weak phase transition are insufficient to account for an asymmetry as large as $\eta \sim 6 \times 10^{-10}$. The usual theoretical attitude towards the cosmic lepton asymmetry η_L is that sphaleron effects before/at electroweak symmetry breaking equilibrate the cosmic lepton and baryon asymmetries to within a factor of order unity (the relations in the limit of ultra-relativistic SMPP particles can be found in [249]). If this is the case, for all phenomenological purposes η_L is vanishingly small. Sphaleron effects are a crucial ingredient in most baryogenesis scenarios [250,251], including leptogenesis [252,253]. Yet, no experimental evidence for or against these effects exists, and (even barring the – phenomenologically viable – alternative that η_B and its leptonic counterpart η_L are simply "initial cosmological conditions") models have been envisioned where the lepton asymmetry is large, as for example via Affleck–Dine mechanism or Q-balls [254–257]. Since charge neutrality implies that the electron density matches the proton one, we do know that a large lepton asymmetry could only reside in the neutrino sector. This asymmetry can be parameterized in terms of the chemical potentials of the different flavor species, μ_{ν_ℓ}, or better in terms of the degeneracy parameter $\xi_\ell = \mu_{\nu_\ell}/T_{\nu_\ell}$ which is constant in absence of entropy releases. For neutrinos distributed as a FD with temperature T_{ν_ℓ}, the asymmetry in each flavor is given by

$$\eta_{\nu_\ell} = \frac{n_{\nu_\ell} - n_{\bar{\nu}_\ell}}{n_\gamma} = \frac{1}{12\zeta(3)} \left(\frac{T_{\nu_\ell}}{T_\gamma}\right)^3 \left(\pi^2 \xi_\ell + \xi_\ell^3\right). \tag{87}$$

Without further input, the quantities ξ_ℓ are not determined within the Standard Model, and should be constrained observationally. Over the years, BBN with a lepton asymmetry has been studied by many authors and in different scenarios [26,258–261,30,29,262,218,263,264,215,91,265,18,266–268]. There are several effects of $\xi_\ell \neq 0$ on BBN. The most important one (at least for relatively small ξ_e) is a shift of the beta equilibrium between protons and neutrons, which is however insensitive to ξ_μ and ξ_τ. The leading flavor-blind effect amounts to a mere modification of the radiation density entering the Hubble expansion rate equation by the amount

$$\Delta N_{\rm eff} = \sum_\ell \left[\frac{30}{7}\left(\frac{\xi_\ell}{\pi}\right)^2 + \frac{15}{7}\left(\frac{\xi_\ell}{\pi}\right)^4\right]. \tag{88}$$

Moreover, for sufficiently large ξ_ℓ the neutrino decoupling temperature is higher than in the standard case [258,259], so that in principle one could get a non-standard $T_\nu(T)$ evolution. A non-zero ξ_ℓ slightly modifies the partial neutrino reheating following the e^+e^- annihilation, too [29]. Both effects are however typically negligible for the ranges of ξ_ℓ presently allowed. The greater sensitivity to ξ_e than $\xi_{\mu,\tau}$ made the constraints on the latter quantities looser, allowing on the other hand a richer phenomenology within a quasi-standard scenario.

Again, the new knowledge on neutrino mixing parameters has rescued the simplicity of the standard cosmological scenario. A few years ago it was realized that the measured neutrino oscillation parameters imply that neutrinos reach approximate chemical equilibrium before the BBN epoch. This is due to the effects of the background medium on the evolution of the neutrino matrix density. In presence of neutrino asymmetry the medium term in the Hamiltonian becomes

$$H_1 = \mathrm{diag}(V_e, V_\mu, V_\tau) \pm \sqrt{2} G_F (\varrho - \bar{\varrho}), \tag{89}$$

with the $+$ sign for ν, the $-$ sign for $\bar{\nu}$. In particular neutrino self-interactions synchronize the neutrino oscillations and drive all the potentials to the same value [23,25,24]. Assuming the standard value for $N_{\rm eff}$, from the Y_p range follows the bound $\xi_e = -0.008 \pm 0.013$.[11] In Fig. 13 we show the predictions for the primordial light-element abundances as a function of the neutrino degeneracy parameter ξ, taken to be equal for all flavors [271]. The gray band is the $1\,\sigma$ predicted range, including both the uncertainty on η of Ref. [272] and the nuclear reactions and uncertainties adopted in Ref. [18].

The bound relaxes by a factor of 2–3 (depending on other priors used) if additional degrees of freedom are present in the plasma, i.e. $N_{\rm eff}$ is allowed to vary [215,91,268]. At present, the BBN is by far the best cosmic "leptometer" available, and

[11] For some regions in parameter space, the equalization may not be complete, see [269]. Also, at least one way around the equalization of the chemical potentials has been proposed in [270]: an hypothetical neutrino-Majoron coupling of the order $g \sim 10^{-6}$ can suppress neutrino flavor oscillations in the early universe, in contrast to the usual weak interaction case.

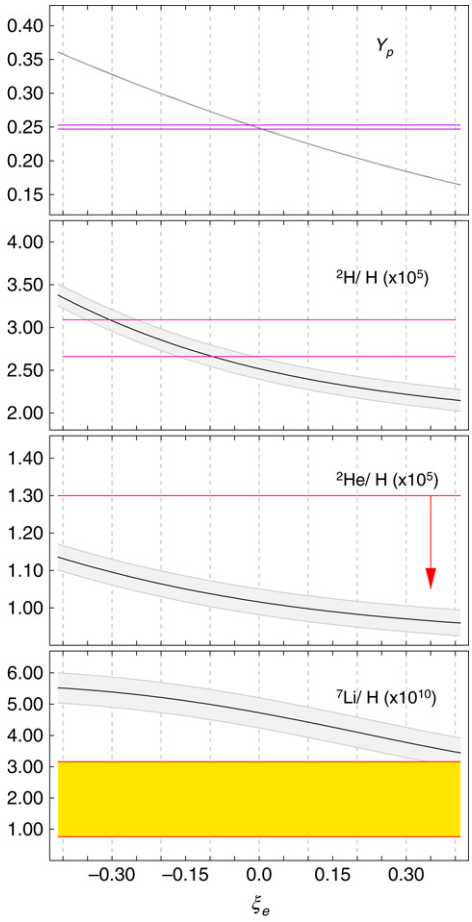

Fig. 13. Light-element abundances as a function of the neutrino degeneracy parameter. The top panel shows the primordial ^{4}He mass fraction Y_p, whereas the other panels show the ^{2}H, ^{3}He, and ^{7}Li number fractions relative to hydrogen. The gray $1\,\sigma$ error bands include the uncertainty of the WMAP determination of the baryon abundances of Ref. [272] as well as the uncertainties from the nuclear cross sections of Ref. [18]. Updated, from [271].

is virtually the only one sensitive to the sign of ξ_e. Most of its sensitivity derives however from the sensitivity of Y_p to the variation of the weak n–p rates, so in order to improve these bounds the systematic error in the determination of primordial helium remains the major obstacle. Yet, even lacking further progress in this direction, in the near future the BBN role will be still important in combination with other cosmological observables to break degeneracies among different parameters, as in the case of the PLANCK CMB mission [173,266,267].

6.4. Sterile Neutrinos and BBN

Sterile neutrinos are, by definition, standard model gauge group singlet fermions. Their only coupling to SM particles arises via their mass and mixing parameters with active neutrinos and, provided their mass is not too high and their mixing sufficiently small, they are long-lived particles.[12] Here, we shall only refer to the case where there is only one additional neutrino mass eigenstate ν_4, with mass m_4. Even in this case, the resulting 4×4 neutrino mass matrix $\mathcal{U}$ is described by 4 masses, 6 mixing angles and 3 CP-violating phases (and possibly, other 3 phases, not entering oscillations, if neutrinos are Majorana particles). Namely, one mass, three mixing angles and two more phases with respect to the 3×3 matrix for active Dirac neutrinos. Since not even the mass pattern of active neutrinos (or their complete mixing matrix) is known, it comes with no surprise that sterile neutrinos can manifest quite a rich phenomenology. This is especially true in cosmology, due to the relevance of medium effects. Basically, sterile neutrinos with a typical mixing element with the active sector of the order $\sin\theta_s$ can be populated via incoherent scattering with a rate which, under "normal" conditions, writes

$$\Gamma_s \simeq \sin^2 2\theta_s\, \Gamma_a, \tag{90}$$

[12] For a typical mixing element with the active sector of the order $\sin\theta_s$ one expects a lifetime for decay into a neutrino and a photon of the order $\tau_s \simeq 2048\,\pi^4/(9\,\alpha G_F^2 \sin^2 2\theta_s\, m_4^5)$, m_4 being the sterile mass scale [273].

$\Gamma_a \sim G_F^2 T^5$ being the active neutrino scattering rate. However, in the presence of matter with a potential V, the effective mixing angle can be efficiently enhanced whenever the resonance condition $\delta m^2_{sa}/2p \simeq V$ is fulfilled, giving rise to potentially large effects even when a small vacuum mixing would make the sterile neutrino undetectable in laboratory experiments. BBN is sensitive to sterile neutrinos through the following three effects: (i) the partial and total population of a sterile state induces $N_{\rm eff} > 3$ and thus affects the Hubble expansion rate; (ii) if ν_s are produced only after the decoupling of the active neutrinos from the cosmological plasma, they lead in general to a depletion of ν_e and $\bar{\nu}_e$, thus affecting the weak n–p rates; (iii) the depletion can be $\nu - \bar{\nu}$ asymmetric, again affecting in particular, the weak rates.

The interest in the physics of sterile neutrinos in BBN has a long history (see e.g. [274–281,213,282]). Due to the otherwise large parameter space, it has roughly followed the appeal that, from time to time, sterile neutrinos have had in explaining anomalies in the neutrino phenomenology. An incomplete account includes $m_4 \simeq$17 keV in the beta decay [283,284], the KARMEN anomaly ($m_4 \simeq$ 33.9 MeV) [285], and in the last few years, the LSND anomaly ($m_4 \simeq$ 1 eV) [286]. The recent Miniboone results [287], although not ruling out the possibility of more exotic physics, strongly disfavor or rule out the simplest sterile neutrino models to explain the LSND signal. At the moment, there is no clear theoretical or experimental argument suggesting the existence of (sufficiently light) sterile neutrinos, yet their rich physics continues to attract a lot of interest (for a review, see [288]). However, this implies that in absence of theoretical or experimental prejudice, one has to scan over a large parameter space.

Most of the old literature referred to mixing between a sterile and an active state, neglecting mixing among active neutrinos. This allowed for several simplifications, but the results are clearly unphysical given the fact that we know that neutrinos do mix, and the mixing is large. A density matrix formalism is necessary, which differs from the one we introduced in Section 3.2 in several points. The vacuum Hamiltonian H_0 includes now four mass eigenstates and a 4×4 mixing matrix. The refractive term H_1 writes now in flavor basis (considering only diagonal elements)

$$H_1 = \mathrm{diag}(V_e, V_\mu, V_\tau, 0). \tag{91}$$

The matter potentials V_ℓ for each flavor is (with $\eta_\nu \equiv \eta_{\nu_e} + \eta_{\nu_\mu} + \eta_{\nu_\tau}$)

$$V_e = \pm\sqrt{2} G_F n_\gamma \left[\eta_e - \frac{\eta_n}{2} + \eta_\nu + \eta_{\nu_e}\right] - \frac{8\sqrt{2} G_F\, p}{3}\left(\frac{\rho_{\nu_e+\bar{\nu_e}}}{M_Z^2} + \frac{\rho_{e^-+e^+}}{M_W^2}\right) \tag{92}$$

$$V_\mu = \pm\sqrt{2} G_F n_\gamma \left[-\frac{\eta_n}{2} + \eta_\nu + \eta_{\nu_\mu}\right] - \frac{8\sqrt{2} G_F\, p}{3 M_Z^2}\rho_{\nu_\mu+\bar{\nu_\mu}} \tag{93}$$

$$V_\tau = \pm\sqrt{2} G_F n_\gamma \left[-\frac{\eta_n}{2} + \eta_\nu + \eta_{\nu_\tau}\right] - \frac{8\sqrt{2} G_F\, p}{3 M_Z^2}\rho_{\nu_\tau+\bar{\nu_\tau}} \tag{94}$$

where $+$ applies to ν, $-$ to $\bar{\nu}$.

As initial conditions one assumes usually thermal populations for the active neutrinos and a vanishing one for the sterile neutrinos (this assumption is relaxed in some papers, as [289–291], where a partial filling of the initial sterile state has been considered). In general, assuming that the active-sterile mixing angles are small (to be consistent with the phenomenology in the laboratory) is the only reasonable simplification. Also, as long as $T \ll m_\mu$, in the limit $\theta_{23} = \pi/4$ and $\theta_{13} \to 0$ there is a $\mu - \tau$ symmetry which further simplifies the structure of $\mathcal{U}$. A quite thorough analysis has been performed in [292], at least for the range $\delta m^2_{4i} \lesssim 1$ eV^2 which gives rise to the majority of phenomenologically distinct cases. We summarize here the main features, while addressing to the original literature for details.

- If the terms in the square brackets are very small or have the natural value of the baryon asymmetry, $\eta_i \sim 10^{-9}$, they are dynamically negligible compared to the terms of order $\mathcal{O}(G_F/M^2_{W,Z})$ at high temperatures and to the vacuum term H_0 at low temperatures. This is also the situation considered for the standard decoupling in Section 3.2. In this case, the matter potential is always negative, and the existence of resonance conditions depends only on the mass-square differences δm^2_{4i}. If $\delta m^2_{4i} > 0$, $\forall i$, the sterile-active mixing is never resonant, and the analysis simplifies considerably. If however $\delta m^2_{4i} < 0$ for some value of i, the system may undergo one, two or three resonances, and many sub-cases are possible.
- If a large neutrino asymmetry is present, the square brackets terms may be large enough to change the impact of sterile neutrinos on BBN, typically weakening the constraints, as first noted in [293]. The reason is that the dominance of the flavor-diagonal medium term compared to the off-diagonal term due to mixing suppresses the active-sterile oscillations, producing sterile neutrinos less efficiently than in a symmetric background. Apart for larger value of the potential at a given temperature, another peculiarity of this case is that its *sign* is opposite for ν and $\bar{\nu}$: a pattern of resonances appears independently of the sign of δm^2_i, and each one only in the ν (or $\bar{\nu}$) sector. In [138], some attention has been paid to strategies to lift the cosmological bound on sterile neutrinos invoked to explain the LSND anomaly with a moderate asymmetry (say, $\eta \sim 10^{-4}$). The weakening of the BBN bounds for a growing asymmetry is represented by the shift from the solid purple line to the dashed ones in Fig. 14. Apart for the asymmetry, the distortion of the neutrino momentum distributions is negligible in the cases studied in [138]. It is well known, however, that significant deviations from a pure FD distribution could occur during the evolution. Typically they can be relevant either for relatively small mass splittings, $\delta m^2_{4i} \lesssim 10^{-8}$ eV^2 [294] or, for eV scale masses, via matter resonances post weak decoupling, which might

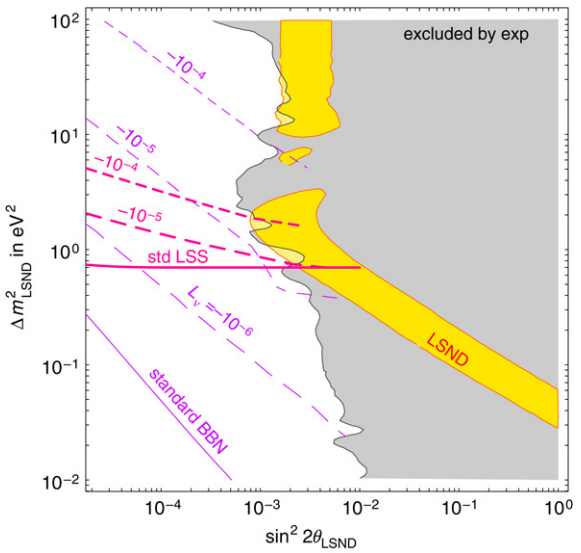

Fig. 14. The allowed LSND region at 99% C.L. (yellow/light shaded area) compared to the cosmological bounds from BBN and LSS in the presence of primordial asymmetries. The darker shaded area is already excluded at 99% C.L. by other experiments. The regions below and to the left of the thin lines are allowed by BBN because they correspond to $Y_p \leq 0.258$. The regions below and to the left of the thick lines are allowed by LSS because they correspond to $\Omega_\nu h^2 \leq 0.8\ 10^{-2}$. From [138].

leave both active and sterile neutrinos with a highly nonthermal spectrum for some choices of neutrino parameters and energies. This however requires larger initial asymmetries, $\eta_\nu \gtrsim 0.01$ [295,296].

An interesting aspect implicitly omitted above is that, even if the neutrino asymmetry is vanishingly small before the onset of the active-sterile oscillations, a large $\nu - \bar{\nu}$ asymmetry (up to $\eta \sim 0.1$) might be dynamically generated in the active neutrino sector (and compensated by an opposite one in the sterile sector) via a resonant matter effect. This scenario requires quite special choices of the parameters: the mixing must be sufficiently small, $\sin^2 2\theta_s \lesssim 10^{-4}$, $|\delta m_i^2| < 0$ for some i, and $|\delta m_i^2|\ \sin^4 2\theta_s \lesssim$ few $\times\ 10^{-9}$ eV^2. For a review we address to [42] and reference therein (see also [292] for some more details). Perhaps more general is the following consideration, which is often overlooked in the literature: once a sterile neutrino is introduced, at least two additional CP-violating phases are *naturally* introduced in the neutrino mixing matrix. The *vacuum* oscillation probability between an active and the sterile state are naturally CP-violating, even when $\theta_{13} \to 0$ and no CP violation happens in the active–active oscillations. One might generate a flavor-dependent lepton-asymmetry as large as $O(\sin^2 2\theta_s)$ – which in a large part of the allowed parameter space is much bigger than η_B – without resonances.

Finally, some BBN constraint also arises for more massive sterile neutrino states, in the keV–MeV range, by requiring that the energy density stored in the sterile states populated via mixing does not exceed e.g. $\Delta N_{\rm eff} = 1$. As reviewed in [297], the bounds are not very competitive compared with others. For significantly heavier states, the most interesting bounds may come from cascades and dissociation of light elements from the sterile neutrino decays, which we address in Section 9.

7. Inhomogeneous nucleosynthesis

In the standard scenario of nucleosynthesis all constituents are homogeneously and isotropically distributed, in accordance with the hypothesis of a FLRW universe. Anisotropic models, studied as early as in the 60's, or models with adiabatic fluctuations in the radiation energy density may affect nucleosynthesis essentially via a variation in the expansion rate. The emergence of a concordance cosmology model, supported by CMB and LSS data essentially confirm *observationally* that, apart from small initial adiabatic fluctuations ($\sim 10^{-5}$) as seed of structure formation, no significant departure from the homogeneity or isotropy is required. The logical possibility that large fluctuations existed at the horizon scales at BBN epoch (size of the order of 10^{-6} deg. in the CMB) is not well motivated either in the favored inflationary scenario to generate the perturbations. Thus, this line of research has faded away in the last decade: we address the reader to [9] for a historical overview. However, it is perfectly consistent with the present cosmological scenario to speculate on a varying baryon to photon and neutron to proton ratio on small scales. These isothermal (or isocurvature) fluctuations may alter BBN in a non-trivial way, and these scenarios are known as inhomogeneous BBN (IBBN) models. Till the 90's, the interest in IBBN was due to two aspects: (i) several theories can lead to inhomogeneous distributions of neutrons and protons at the time of nucleosynthesis: a first order quark-hadron phase transition [298–300,9], the CP violating interaction of particles with the bubble enucleated in the electroweak phase transition [301–304], the phase transition involving inflation-generated isocurvature fluctuations [305] or kaon condensation phase [306]; (ii) there was some hope that IBBN scenarios with $\Omega_B \simeq 1$ – thus consistent with a flat, matter dominated universe, or at least an open universe without non-baryonic dark matter –

were phenomenologically viable (see e.g. [307]). Both motivations have lost observational or theoretical support in the last decade. The agreement between the value of $\Omega_B h^2$ from standard BBN deuterium abundance and CMB anisotropies is indeed quite a compelling result in favor of the simplest homogeneous scenario. Theoretically, due to the high mass of the Higgs, the electroweak phase transition is a smooth cross-over for the SM particle content, and even the QCD phase transition – although less well established – appears to be a crossover or weak first order one, probably insufficient to produce significant departures from the standard BBN scenario [308].

In the following, we limit ourselves to introduce and briefly describe some recent calculations in IBBN, addressing the reader to [9] for a throughout overview of the topic. Since IBBN has to reproduce very closely the SBBN yields while requiring additional parameters, most of its phenomenological interest has declined, too. Today, perhaps the only way to discriminate IBBN vs. homogeneous BBN lies in the different predictions for the intermediate (CNO) or heavy elements.

7.1. Baryon inhomogeneous models

An important point to be considered is the sensitivity of the predictions to the form of the inhomogeneity itself. Many studies simply have a 2-phase model with a fraction f at high density and $1 - f$ at low, while in the paper [309] a more realistic distribution (log normal) is considered, which allows a bound to be placed on the variance.

If there are large fluctuations in the nucleon density, the differential transport of neutrons and protons can create neutron-rich regions where heavy elements can be formed. Neutrons diffuse by scattering on electrons and protons, protons scatter on neutrons and Coulomb scatter on electrons, but the mean free path of protons is about 10^6 times smaller than that of neutrons. The diffusion of other species is negligible with respect to neutron scattering due to their larger masses. Neutron diffusion, however, was not considered in the earliest codes of IBBN [310,311,309], where regions of different nucleon density were treated as separate homogeneous BBN models. The mass fractions from each model were then averaged, with a weight given by the corresponding size. A later generation of codes [312–314] introduced in the calculation nucleon diffusion, but only at early times and high temperatures, before the starting of nucleosynthesis. This led to the neutron enrichment of the low-density region but, once the original protons were consumed, neutrons could form ^{4}He only when other protons were produced by neutron decay. The main consequences of this situation on the light element abundances were: (a) since four neutrons (two of which decaying in two protons) were needed for each ^{4}He nucleus, the final yield of ^{4}He was reduced; (b) nucleosynthesis time scale were tuned by neutron decay rate, extending the process to cooler temperatures and allowing ^{2}H to survive in larger quantities; (c) the high neutron density could help the production of heavier elements through neutron-rich isotopes. However, once neutron diffusion during nucleosynthesis is taken into account, all the three previous effects are weakened, since when neutrons are rapidly consumed in the high density region, where nucleosynthesis begins first, the excess neutrons in the low density region diffuse back. Kurki-Suonio et al. made the significant step forward of treating nucleon diffusion both before and during nucleosynthesis, with planar symmetric baryon inhomogeneities [315] or cylindrical and spherical models [316,317]. In order to decrease the number of zones needed to obtain a high accuracy, nonuniform grids were used [318–322]. The diffusion equation is sufficient for describing the motion of particles in an IBBN model if the background fluid is stationary, as in the case of neutrons, which are much more mobile than the ions and electrons they scatter on. The evolution of ions at low temperatures is more complicated, due to momentum transfers in collisions with other ion components, which move with comparable fluid velocities. In this case, the common diffusion approximation has to be relaxed and one needs to take into account dissipative processes through hydrodynamic equations [323–325].

In an inhomogeneous code with treatment of neutron diffusion, the region considered is divided into several zones, s, where the time evolution of the number density of the specie i, $n_{i,s}$, obeys the following evolution [322,303,319]

$$\frac{\partial n_{i,s}}{\partial t} = n_{B,s} \sum_{j,k,l} N_i \left(\Gamma_{kl\to ij} \frac{Y_{k,s}^{N_k} Y_{l,s}^{N_l}}{N_k! N_l!} - \Gamma_{ij\to kl} \frac{Y_{i,s}^{N_i} Y_{j,s}^{N_j}}{N_i! N_j!} \right) - 3H\, n_{i,s} + \frac{1}{r^p} \frac{\partial}{\partial r} \left(r^p D_n \frac{\partial \xi}{\partial r} \frac{\partial n_{i,s}}{\partial \xi} \right). \tag{95}$$

The first three terms are usual, corresponding to reactions which create or destroy nuclides and to the expansion of the universe, while the last one is due to diffusion of isotope i between zones. The parameters which appear in Eq. (95) are the inhomogeneity distance scale, r, which measures the physical distance between inhomogeneity regions at the starting temperature, $T \sim 10$ MeV, the stretching function, $\xi(r)$, which implements the non-uniform grid, marking the zone edges, and the neutron diffusion coefficient, D_n, which is a function of proton density and temperature [312].[13] For small distance scales, $r < 1$ light-hour, the inhomogeneities are smeared out by neutron diffusion before nucleosynthesis starts, and the IBBN results approach standard BBN results. The constant parameter p changes with geometry (for example, for the spherical symmetry $p = 2$). Other important parameters are the density contrast, R, which is the ratio between the high and low densities, taken as high as 10^6, and the volume factor, f_v, that is the fraction of space occupied by the high density region. Note that the higher R, the larger the number of zones needed for a sufficient accuracy of the calculation.

The plots in Fig. 15 are contour maps of the ^{4}He mass fraction, and ^{2}H/H and ^{7}Li/H, taken from Ref. [322], and present the characteristic features of an IBBN prediction on light element abundances. For small values of r_i neutron diffusion

[13] Note that, as remarked in [318], in their Eq. (21) the factor $\pi/16$ is missing from the numerical value.

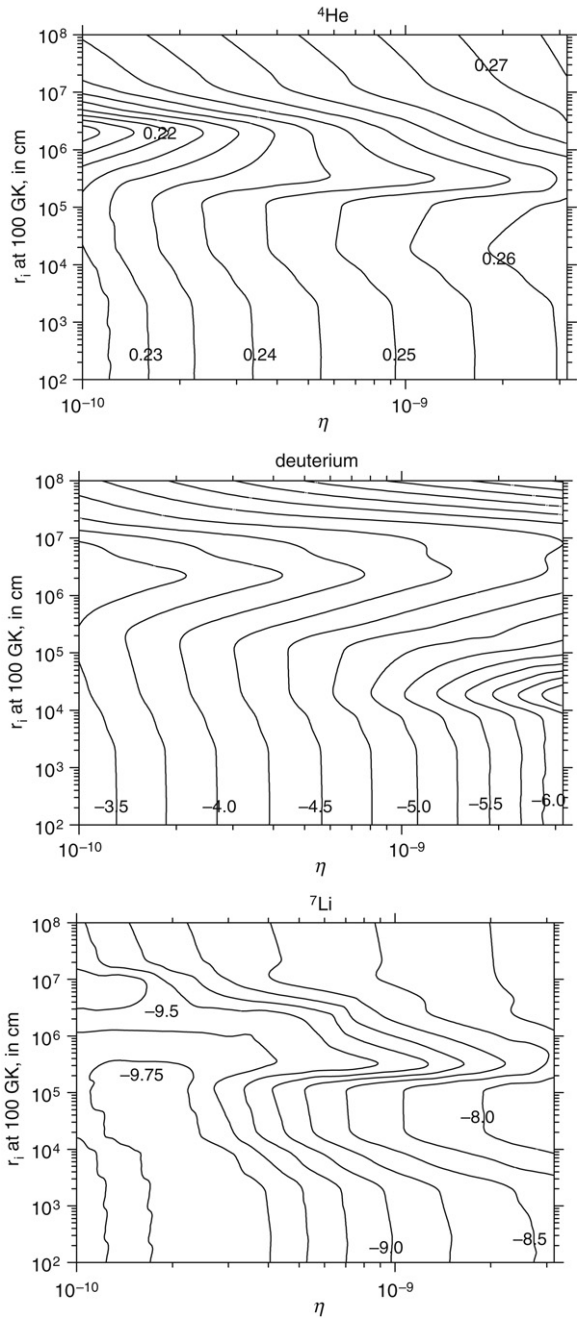

Fig. 15. Mass fraction of ^{4}He and log of the abundances Y_i/Y_p for $i = {}^2$H, ^{7}Li. From Ref. [322].

homogenizes neutrons very quickly and protons as well, since this happens before weak interactions go out of equilibrium. This means that the final abundances are the same as a homogeneous model. The shift in the contour lines towards low values of η for distance scales r_i starting from $\sim$2–3 $\times$ 10^3 cm is due to the fact that, for these values of r_i, neutron diffusion and homogenization take a time of the order of the weak interaction freeze-out. This implies that protons start to be not efficiently homogenized and nucleosynthesis occurs before in the high density shells with a larger proton density and has the characteristics of an earlier nucleosynthesis (larger ^{4}He and ^{7}Li and less ^{2}H). So, to recover the same values of the abundances of a model with lower r_i one needs lower values of η. Up to $r_i \sim 10^5$ cm the proton number density is unchanged except for a slight increase due to neutron decay, and this explains the almost vertical contour lines in this range. The depletion of neutrons in the high density shells at temperatures just after nucleon freeze-out leads to neutron back-diffusion and a more efficient nucleosynthesis (and a magnification of the production of ^{7}Be) in the high density region. Due to this overproduction of ^{7}Be, which gives ^{7}Li after decay, the contour lines in the lowest plot in Fig. 15 have a larger shift to lower η. When r_i starts

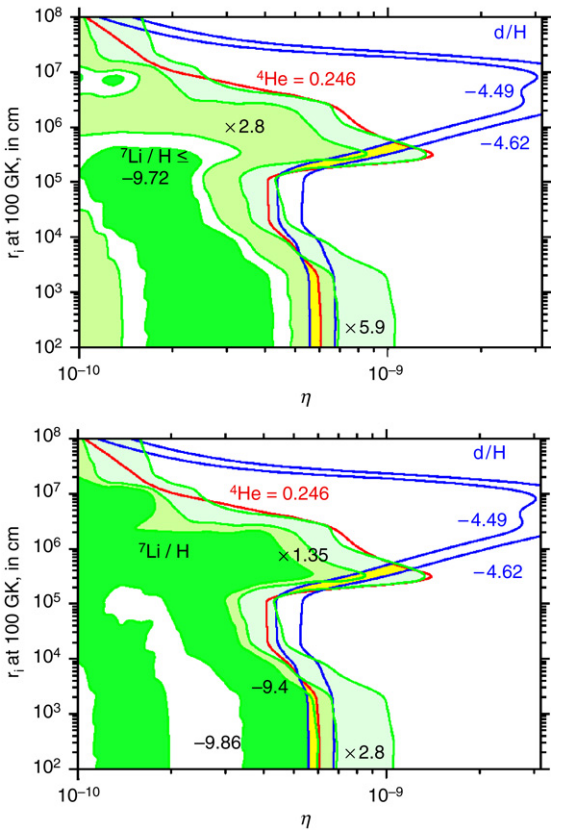

Fig. 16. Concordance between the observational constraints on ^{4}He, ^{2}H, and ^{7}Li and the model of Ref. [322]. From Ref. [322].

to be larger than 10^5 cm, neutron back-diffusion does not affect all the shells and nucleosynthesis is concentrated only in some of them. This leads to a decrease of the final ^{4}He abundance accompanied by an increase in deuterium production, which corresponds to a shift of the contour lines towards high η. Finally, contours turn back to low values of η, since for very large r_i diffusion cannot homogenize neutrons before nucleosynthesis, a large neutron density remains in the high density region, giving rise again to ^{4}He overproduction and a ^{2}H suppressed yield. In this region of r_i, results are equivalent to the average of two separate homogeneous BBN models, one of high density (with high ^{4}He and ^{7}Li and low ^{2}H) and one of low density. The basic shapes of the contour lines of Fig. 15 are common to all IBBN models: for different geometries and values of the parameters there will be regions in r_i where neutron homogenization and diffusion occur at times between weak freeze-out and nucleosynthesis or after nucleosynthesis.

Fig. 16 shows the concordance between the observational constraints on ^{4}He, ^{2}H, and ^{7}Li and the model of Ref. [322]: upper plot is for the ^{7}Li constraints from Ryan et al. [177] while lower plot is for the ^{7}Li data of Melendez & Ramirez [181]. In both plots the concordance region between ^{4}He [158] and ^{2}H data [118] is shown in yellow. While upper plot have a concordance region for ^{7}Li only for a depletion factor ranging from 2.8 to 5.9, the lower plot does not need any depletion in ^{7}Li if $r_i < 5 \times 10^3$ (see Ref. [326] for a similar analysis using $\tau_n = 878.5 \pm 0.7_{\text{stat}} \pm 0.3_{\text{syst}}$ [76]).

One interesting consequence of IBBN results is the larger range in the depletion factor one can obtain for ^{7}Li with respect to the analogous prediction of homogeneous BBN. Fig. 16 shows, moreover, that IBBN allows for larger values of η than SBBN (up to $\eta \sim 10^{-9}$), requiring at the same time a depletion factor for ^{7}Li to obtain concordance with the observational limits.

Since lithium is produced quite late in nucleosynthesis, its yield is particularly sensitive to the late-time transport phenomena such as hydrodynamic ion diffusion. In this respect, the results of codes which take into account these phenomena [325], which are not considered in [322], might explain the observed depletion of lithium. This is a consequence of late separation of elements due to Thomson drag: Thomson scattering of electrons on background photons makes the diffusion of ions inefficient which must drag electrons with them to keep charge neutrality. On the other hand, protons and helium ions, for instance, are allowed to diffuse in opposite directions. While protons diffuse out, helium and lithium get concentrated in the high density regions, leading to enhanced destruction of ^{7}Li, ^{2}H, and ^{3}He.

Heavy element production in the framework of IBBN was first investigated in Ref. [327] and then in [328,329], in the approximation of neglecting baryon diffusion. The authors claim that there is a parameter region, for the volume fraction f and density contrast R, in which heavy elements can be produced enough to affect the observation, while keeping the light element abundances consistent with observation. The results show that BBN proceeds through both the p-process and

the r-process, with the transition between the two due to the Coulomb barriers of proton-rich nuclei and the amounts of neutrons when heavy elements begin to be synthesized.

7.2. Matter–antimatter inhomogeneities

A possible scenario which gives rise to an inhomogeneous baryon-to-photon ratio is antimatter BBN (ABBN) [331–336]. Different baryogenesis models can give rise to matter–antimatter domains [337,338,305,339–342]. In the ABBN scenario, the antimatter regions have a radius r_A, while R is the antimatter-matter ratio in the universe. Antimatter regions should be small enough to be completely annihilated well before recombination, in order to satisfy CMB constraints. Their size determines the time when most of the annihilation takes place, before or after significant amounts of ^{4}He are produced by nucleosynthesis. The first case is realized for typical radii between 10^5 and 10^7 m (comoving distance at $T = 1$ KeV) [330].[14] Thanks to the different diffusion scale of protons and neutrons, the latter can more easily move to antimatter regions and annihilate. This would produce a reduced neutron to proton ratio with respect to the standard case, which can be compensated by a larger expansion rate at BBN, provided by more relativistic degrees of freedom, $N_{\rm eff} > 3$, and results in the same Y_p. Correspondingly, the speed-up of expansion shortens the time interval available for nucleosynthesis, and implies smaller yields for all other light nuclides, yet this can be compensated by the increase of the reaction rates due to a higher value of η. The net result is thus, a shift of the agreement of theory vs. data towards larger η for large $\Delta N_{\rm eff}$, see Fig. 17, but with the bonus that $N_{\rm eff}$ is no longer constrained, as shown in Fig. 18.

8. Constraints on fundamental interactions

8.1. Extra dimensions and BBN

8.1.1. A short journey to extra dimensions

The idea of introducing extra (spatial) dimensions to generalize the 4-dimensional theory of fundamental interactions and unify different forces is quite old. As early as 1919, thus shortly after the birth of General Relativity, Kaluza considered a 5-dimensional version of Einstein theory which described gravity and electromagnetism in a unique setting [343]. Shortly after, in 1926 Oskar Klein stressed the role of having a compact fifth dimension in order to evade constraints from observations of large accessible extra dimensions [344]. A nice review on Kaluza–Klein theories is [345].

Higher-dimensional theories had perhaps their golden age starting from the late 70's, after the discovery of the remarkable properties which superstring and supergravity theories have for particular spacetime dimensionalities. Quite recently, theories with one or more extra dimensions with a fundamental scale of TeV^{-1} have been advocated as possible way to address the long-standing problem of hierarchy between the electroweak and the much higher Planck scale [346–349]. In these scenarios, the fundamental gravity scale is lowered down to the TeV range, and the observed Planck mass emerges as an effective scale at low energies, smaller than the Kaluza–Klein (KK) excitation mass scale. This is due to the dilution of gravitational interactions in the large (millimeter-sized) extra dimensions (flat scenarios), or the particular configuration of the gravitational field which provides a static solution to Einstein's equations (warped extra dimensions). A general feature of these theories is to assume that ordinary matter is confined to standard $3+1$-dimensional spacetime, a brane embedded in a $(4+d)$-dimensional manifold, while gravity can propagate in the whole higher dimensional spacetime.

Interestingly, large (experimentally accessible) extra dimension models can be tested using collider physics, as for example at LHC, for a review see e.g. [350,351]. On the other hand, they may have a large impact on the cosmological evolution of our universe. The issue of understanding the phenomenological implications of "brane-cosmology" has been addressed by several scholars in the last ten years, mainly aimed at discussing how these scenarios can be constrained by cosmological observables, CMB and BBN among others. In the following, after a brief summary of the aspects of the extra dimension models which are relevant for our discussion, we (mainly) focus on the constraints which can be obtained by exploiting BBN.

We start by introducing the $D = 4 + d$ dimensional Einstein and matter action, which can be written as

$$S = \int \mathrm{d}^4x \mathrm{d}^d y \sqrt{-\overline{g}} \frac{M_D^{2+d}}{2} \overline{R} + \sqrt{-\overline{g}}\, L_m, \tag{96}$$

where the first term corresponds to the Einstein–Hilbert action, $\overline{R}$ being the $4+d$-dimensional scalar curvature for the $4+d$ metric $\overline{g}$ and M_D playing the role of the D-dimensional reduced Planck mass, while the second term contains the matter Lagrangian, with the SMPP fields localized on the $3+1$-dimensional brane $y = 0$. In the case of compact extra dimensions (we will consider the specific case of a d-dimensional torus of radius δ) and for a factorized metric, i.e. if the 4-dimensional part does not depend upon the d extra coordinates, the action can be reduced to a 4-dimensional action at low energy, smaller than the inverse compactification radius δ, by integrating over the y coordinates,

$$S = \int \mathrm{d}^4x \sqrt{-g}\, \frac{M_D^{2+d} (2\pi\delta)^d}{2} R + \sqrt{-g}\, L_m, \tag{97}$$

[14] Smaller antimatter regions would annihilate before neutrino decoupling without any effect on BBN.

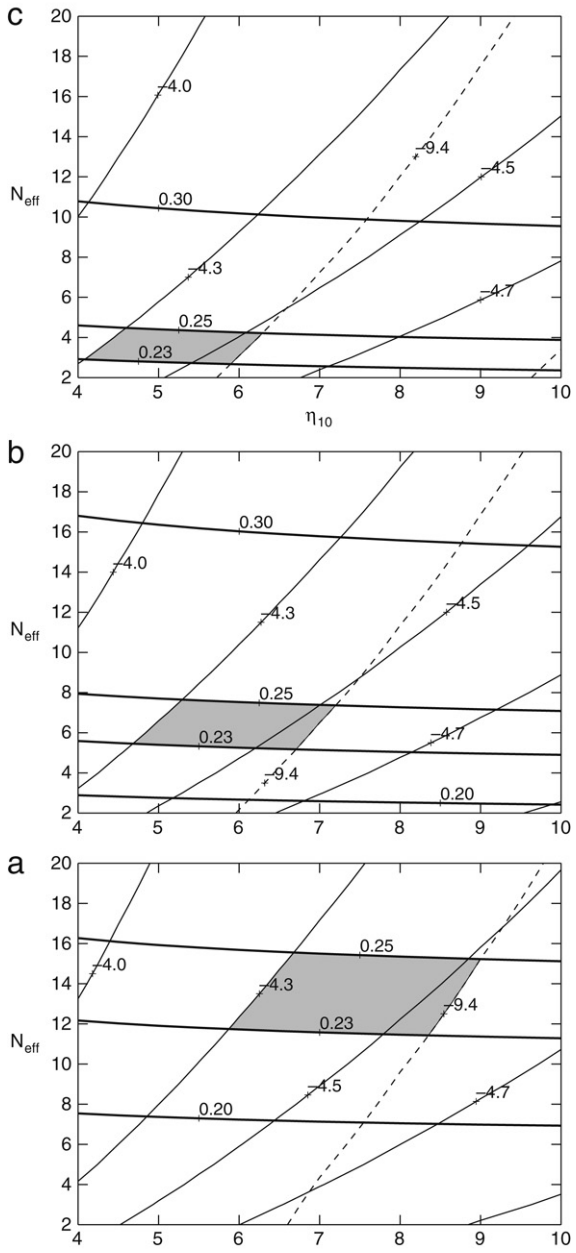

Fig. 17. Light element yields in ABBN as a function of η and $N_{\rm eff}$ for $r_A = 10^{6.9}$ m and, from top to bottom, $R = 10^{-2}$, $10^{-1.5}$, $10^{-1.2}$. Thick solid lines, thin solid lines, and dashed lines are for Y_p, $\log_{10}{}^2$H/H, and $\log_{10}{}^7$Li/H, respectively. From Ref. [330].

from which we read the expression of the Planck mass $M_P = G_N^{-1/2} = 1.2 \times 10^{19}$ GeV in terms of M_D and δ,

$$(2\pi\delta)^{-1} = M_D(\sqrt{8\pi}M_D/M_P)^{2/d}. \tag{98}$$

For $M_D \sim$ TeV, the simplest case of one extra factorized dimension is excluded as it leads to a value of δ which is too large, of the order of the scale of the solar system, while the scenario is viable for $d \geq 2$, as in this case $\delta \leq 1$ mm.

More generally, one can allow for an explicit dependence of the 4-dimensional metric on the extra coordinates. As in [352,353], and usually considered in almost the whole literature, we consider a (non-factorized) $d = 1$ model, where the extra dimension (the bulk) is compactified on the line segment S^1/Z_2. The metric (preserving 3-dimensional rotation and translation invariance) can then be written as

$$\mathrm{d}s^2 = -n^2(\tau, y)\mathrm{d}\tau^2 + a^2(\tau, y)\mathrm{d}\vec{x}^2 + b^2(\tau, y)\mathrm{d}y^2. \tag{99}$$

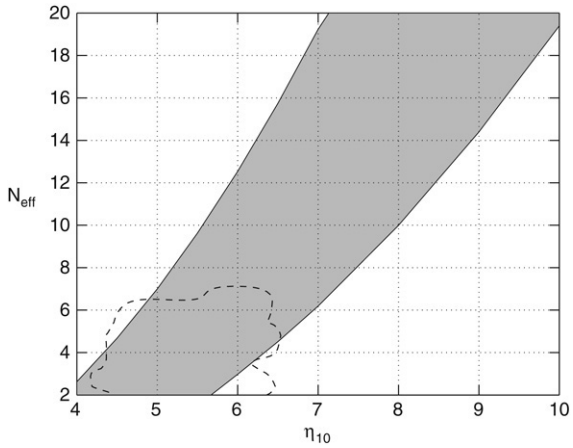

Fig. 18. Combined allowed region in $(\eta, N_{\rm eff})$. The dashed line is the CMB+SNIa constraint from [218]. From Ref. [330].

The Z_2 symmetry identifies the points y and $-y$, so one can restrict to $0 \leq y \leq 1/2$. Two three-branes are placed at $y = 0$ (our "visible" brane) and $y = 1/2$ (a hidden brane, which absorbs the gravitational flux lines of the visible brane). The metric is obtained as usual from Einstein's equations (upper case latin indexes $A, B = 0, 1, 2, 3, 5$ run over the 5-dimensional spacetime),

$$\overline{G}_{AB} = M_5^{-3}\overline{T}_{AB}, \tag{100}$$

where the stress–energy tensor is the sum of contributions of ordinary matter on the visible brane, bulk matter and fields living on the hidden brane,

$$\overline{T}^{AB} = \frac{T^{AB}_{vis}}{b(\tau, 0)}\delta(y) + \frac{T^{AB}_{hid}}{b(\tau, 1/2)}\delta(y - 1/2) + T^{AB}_{\rm bulk}. \tag{101}$$

Each term corresponds to a perfect fluid, parameterized as usual in terms of the energy density ρ and pressure P and specified by the equation of state $P = P(\rho)$, with furthermore $T^{05}_{vis} = T^{05}_{hid} = 0$, so that there is no flow of matter on the branes along the fifth dimension, and finally $T^{AB}_{\rm bulk} = {\rm diag}(-\rho_{\rm bulk}, P_{\rm bulk}, P_{\rm bulk}, P_{\rm bulk}, P_{\rm bulk,5})$.

Before considering the cosmological scenarios corresponding to this framework, one should look for the static solutions of Eq. (100), the analogous of (empty space) Minkowski spacetime. Apart for the case $T^{AB} = 0$ which leads to a (factorizable) trivial spacetime, Randall and Sundrum (RS) [348,349] found a new solution by considering a pure bulk and brane cosmological constant terms. Choosing $T^{AB}_{\rm bulk} = \Lambda\,{\rm diag}(-1, 1, 1, 1, 1)$, a static solution is in fact obtained if $\Lambda < 0$ and the two brane tensions $\rho_{vis,hid} = \Lambda_{vis,hid}$ are fine-tuned to the values

$$\Lambda_{vis} = -\Lambda_{hid} = \pm\sqrt{-6\Lambda M_5^3}, \tag{102}$$

so that the effective cosmological constant in the 3-dimensional space exactly cancels. In this case one finds [348] $b(\tau, y) = b_0 = const$ and

$$a(\tau, y) = \exp\left(\pm b_0|y|\sqrt{\frac{-\Lambda}{6M_5^3}}\right) \equiv \exp\left(\pm b_0|y|m\right). \tag{103}$$

Choosing a negative value for Λ_{vis}, so that the solution corresponds to Eq. (103) taken with the positive sign, leads to a nice solution of the hierarchy problem, since the fundamental mass scale on the invisible brane $M_5 \sim M_P$ is *red-shifted* on our visible universe by the conformal factor $\exp(-b_0 m/2)$, which can explain the large relative ratio of Planck and electroweak scales for a moderate value of $mb_0 \sim 10^2$. In other words, the non-trivial dependence of the metric upon y implies that the KK zero-mode of the graviton wavefunction is peaked around the invisible brane and has an overlap with the visible brane suppressed by the exponential "warp" factor $\exp(-mb_0/2)$. Yet the KK tower mass gap is potentially as low as the TeV scale, and thus these graviton excitations can lead to testable effects at high energy colliders as LHC, see e.g. [350] and references therein.

On the other hand RS also observed that choosing our brane with a positive cosmological constant $\Lambda_{vis} > 0$, though does not solve the hierarchy problem, nevertheless it has the nice properties of allowing for a non compact fifth-dimension, as one can take the limit $y \to \infty$ maintaining consistency with short-distance force experiments. This scenario is also the one which is more interesting from the cosmological point of view, as we will discuss soon.

8.1.2. Brane cosmology and BBN

Adding matter on the branes will lead to an evolving universe analogous to the standard FLRW model. Depending on the choice of the corresponding reference static solution one starts with, the prediction for the Friedmann-like equation governing the visible scale factor, i.e. the value of a in the vicinity of our brane $y = 0$ can be significantly different, leading to testable predictions for cosmological observables such as BBN, CMB and structure formation.

The equation governing the evolution of $a(\tau, 0) \equiv a_0(\tau)$ has been worked out in [352]. If ρ and P denote energy density and pressure on our visible universe, thus dropping the index vis in the following, one obtains the standard conservation equation,

$$\dot{\rho} + 3(\rho + P)\frac{\dot{a}_0}{a_0} = 0, \tag{104}$$

which leads to the usual power behavior for $\rho \sim a_0^{-3(1+w)}$, as well as the evolution equation for a_0,

$$\frac{\ddot{a}_0}{a_0} + \left(\frac{\dot{a}_0}{a_0}\right)^2 = -\frac{1}{36M_5^6}\rho(\rho + 3P) - \frac{1}{3b_0^2 M_5^3}T_{\mathrm{bulk},55}, \tag{105}$$

where the time derivative is with respect to t, with $\mathrm{d}t = n(\tau, 0)\mathrm{d}\tau$ and a flat metric in the ordinary 3-dimensional space has been assumed for simplicity. This expression shows two remarkable properties, namely that it is independent of the energy density and pressure of the second brane, a manifestation of the local nature of Einstein theory and, furthermore, that the energy density enters quadratically rather than linearly as in conventional cosmology.

If the dynamics is dominated by the brane energy density, so that one can neglect the last term in Eq. (105), using Eq. (104) the second order equation (105) can be put in the form

$$\frac{\mathrm{d}}{\mathrm{d}t}(\dot{a}_0^2 a_0^2) = \frac{1}{36M_5^6}\frac{\mathrm{d}}{\mathrm{d}t}(\rho^2 a_0^4), \tag{106}$$

which gives

$$H^2 = \frac{1}{36M_5^6}\rho^2 + \frac{\mathcal{C}}{a_0^4}. \tag{107}$$

The second term in the r.h.s of this expression depends upon the free integration constant $\mathcal{C}$ and behaves as a radiation term [354], thus its popular name of "dark radiation", though the sign of $\mathcal{C}$ can be also negative.

This result for the Hubble parameter strongly differs from the usual Friedmann law, unless one consider the very special case of a radiation dominated phase driven by a positive $\mathcal{C}$, while for a negligible value of $\mathcal{C}$ one gets

$$a_0(t) \sim t^{1/(3+3w)}, \tag{108}$$

thus a slower expansion rate compared to the standard result $a_0(t) \sim t^{2/(3+3w)}$. If we assume that Eq. (107) can be applied to the present universe, writing the energy density as a fraction of the critical density $\Omega \sim 1$,

$$1 = \Omega^2 \frac{H_0^2 M_P^4}{64\pi^2 M_5^6} + \frac{\mathcal{C}}{H_0^2} \sim \frac{\delta^2}{H_0^{-2}} + \frac{\mathcal{C}}{H_0^2}, \tag{109}$$

with the radius of the fifth dimension, δ (see Eq. (98)), which thus should be of the order of the present Hubble radius, H_0^{-1}. [15] This is ruled out by observations (since we could then observe five-dimensional gravity directly), as well as the possibility that dark radiation provides the dominant contribution to the expansion today.

Strong bounds on this model also come if we assume that it describes the evolution of the universe at the earliest stage we can probe in a quantitative manner, namely during BBN. A rough constraint can be obtained by considering the different behavior of the Hubble expansion parameter, which changes the neutron to proton ratio freezing temperature, T_D, as well as the time–temperature relationship in the temperature range from T_D down to the deuterium formation at $T_N \sim 0.1$ MeV [352,353]. The value of n/p at T_D is given by the standard relation $\mathrm{n/p} = \exp(-\Delta m/T_D)$, with [16]

$$G_F^2 T_D^5 \sim \frac{\rho^2}{6M_5^3}. \tag{110}$$

On the other hand, the time–temperature relationship during a radiation dominated epoch is given by Eq. (108) with $w = 1/3$, $t \sim T^{-4}$. Inserting numerical values and using the expression of the relativistic degrees of freedom, g_*, during

[15] Derivation of this result is presented in a slightly different form in [352], where the second order equation for the scale factor is used.

[16] We consider the case $\mathcal{C} = 0$. If dark radiation dominates at BBN, it would be difficult to reconcile later evolution with, say, CMB and structure formation data.

BBN one gets

$$T_D \sim 7.5 \left(\frac{\text{TeV}}{M_5}\right)^3 \text{MeV}, \tag{111}$$

and

$$t \sim 2.8 \times 10^{-4}\,\text{s} \left(\frac{M_5}{\text{TeV}}\right)^3 \left(\frac{T}{\text{MeV}}\right)^4. \tag{112}$$

Thus, assuming that all neutrons at T_N are eventually burned into ^{4}He nuclei, we have

$$\frac{\text{n}}{\text{p}}(T_N) \sim \frac{Y_p}{2 - Y_p} \sim \exp\left[-\frac{\Delta m}{7.5\ \text{MeV}} \left(\frac{M_5}{\text{TeV}}\right)^3\right] \text{e}^{-\frac{t(T_N)-t(T_D)}{\tau_n}}, \tag{113}$$

which implies that a correct mass fraction $Y_p \sim 0.25$ requires $M_5 \sim 8$ TeV and a too large compactification radius.

It should be noted that considering more than one (flat) extra dimension and an empty bulk could be potentially in better agreement with both BBN and the requirement of sub-mm extra dimensions, but a careful analysis of this scenario has not been considered in the literature in details, evaluating the whole network of light nuclei produced during BBN, in particular ^{2}H and ^{7}Li. We also mention that it has been pointed out that in general, the presence of the KK tower of gravitons may lead to overclosure of the universe, unless the highest temperature ever achieved was of the order of MeV, thus with a severe impact on the whole BBN scenario, as well as on the standard inflationary picture for early production of perturbations [45,355].

Interestingly, a much more promising brane cosmology can be obtained by exploiting the RS model. Assuming that the stress–energy tensor T^{AB}_{bulk} corresponds to a cosmological constant, $\rho_{\text{bulk}} = -P_{\text{bulk}} = -P_{\text{bulk},5}$, it has been shown in [354] that one can integrate the (0, 0) component of Einstein's equations and obtain the generalized Friedmann equation in the vicinity of the visible brane,

$$\frac{\dot{a}_0^2}{a_0^2} = \frac{1}{6M_5^2}\rho_{\text{bulk}} + \frac{1}{36M_5^6}\rho_{vis}^2 + \frac{\mathcal{C}}{a_0^4}. \tag{114}$$

This result holds independently of the metric outside and in particular of the time evolution of the scale factor b. If one assumes that the energy density ρ_{vis} can be decomposed as the sum of the contribution of ordinary matter ρ and a (positive) cosmological constant Λ_{vis}, and the latter is fine-tuned as in the RS model, see Eq. (102), one recovers a standard cosmology [356,357,353,354],

$$\frac{\dot{a}_0^2}{a_0^2} = \frac{\Lambda_{vis}}{18M_5^6}\rho + \frac{1}{36M_5^6}\rho^2 + \frac{\mathcal{C}}{a_0^4}, \tag{115}$$

if one identifies

$$8\pi G_N = \frac{\Lambda_{vis}}{6M_5^6}, \tag{116}$$

and the limit $\Lambda_{vis} \gg \rho$ is assumed.[17] Of course, choosing the original RS proposal, which provides a beautiful solution to the hierarchy problem but requires a negative tension on the visible brane, one would obtain a negative sign relative to the conventional Friedmann equation, so that the visible brane behaves as an anti-gravity world [358]. In particular, this implies that, as soon as the universe becomes matter dominated, it would collapse on a scale of the order of the matter-radiation equality time [357].

From Eq. (115) we see that adjusting the value of Λ_{vis} as in Eq. (116) for each given M_5, the Hubble rate depends on two new parameters, the fundamental scale M_5 which controls the quadratic term in ρ and the dark radiation constant $\mathcal{C}$. Bounds on both these parameters can be obtained from BBN, and have been discussed by several authors using the simple argument on ^{4}He mass fraction described above [357,356,354,359–363], namely requiring that both terms be sufficiently small that an acceptable value for Y_p be produced. A more careful analysis based on a full numerical integration of the BBN dynamics and considering the predictions for ^{2}H and ^{7}Li as well, has been instead performed in [364,365]. In particular [364] only consider the dark radiation term and its effect on both BBN and CMB, neglecting the effect of linear perturbations of dark radiation during photon decoupling and recombination. The result of [364] (and of [365] in the limit of large M_5) can be easily translated in terms of the well-known bound on the effective number of neutrino species (see Section 3),

$$\mathcal{C} = \frac{8\pi}{3} G_N \Delta N_{\text{eff}} \rho_{\nu,0} a^4. \tag{117}$$

The allowed range for $\mathcal{C}$ can be easily obtained from the result on N_{eff} of Section 3. More interestingly, if the value of M_5 is sufficiently low, the effect of the ρ^2 term can be non-negligible, but it can be compensated by a large and negative value of $\mathcal{C}$. A degeneracy is thus expected in the M_5–$\mathcal{C}$ plane which qualitatively is of the form $a/M_5^6 + \Delta N_{\text{eff}} = const$, see Fig. 19.

[17] The standard behavior is indeed recovered only in the stronger limit $\rho \ll \Lambda_{vis}^2/M_P^4$ if the bulk spacetime is not exactly anti-de Sitter [358].

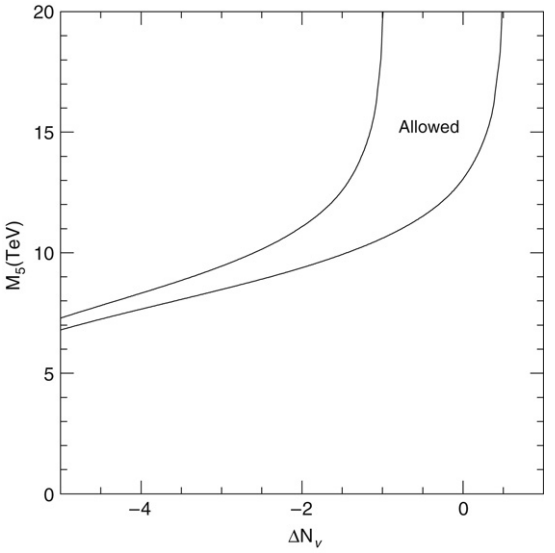

Fig. 19. The BBN-allowed range in the M_5–$\mathcal{C}$ plane. From [365].

We have assumed in the previous discussion that the size of the extra dimensional space is stabilized by some dynamical mechanism, as for example discussed in [366], but indeed it might have some dynamics during cosmological epochs. In general, for a homogeneous and isotropic model, the evolution of the extra dimensions is controlled by a single scalar field, the radion, with a canonical kinetic term which interacts with ordinary matter, see e.g. [367]. These interaction terms lead to a time dependent behavior of the Higgs vacuum expectation value, v, which in turn affects fermion masses. The BBN is extremely sensitive to such variations, since changing v produces a different Fermi coupling constant, G_F, and neutron proton mass difference, both entering the determination of the freezing temperature, T_D, as well as shifting the pion mass which influences the nucleon potential and the deuterium binding energy. We will discuss this issue in details in the next section.

Finally, BBN can be also used to put constraints on theories which consider the possibility of bulk neutrinos. As we have mentioned, in the extra dimension scenarios the SMPP particles are assumed to be localized on the visible brane, while gravitational interactions can propagate in the bulk. If the fundamental scale is of the order of TeV, this leads to a serious problem in understanding the smallness of neutrino masses, which is usually thought to be produced via a see-saw mechanism. For sub-eV neutrino masses, this scheme requires the existence of some new mass scale of order 10^{11}–10^{12} GeV, much larger than the extra dimension scale. Furthermore, operators as $LHLH/M_D$ (H and L are the Higgs and left-handed fermion doublets, respectively) could be induced in the low energy Lagrangian which lead to an unacceptable neutrino mass. This problem was realized quite early on and several solutions have been proposed [368–373], which postulate the existence of one or more gauge singlet neutrinos in the bulk which couple to the lepton doublet on the brane. Their corresponding KK modes give rise to an infinite tower of sterile neutrinos labeled by an integer n, which mix with active neutrinos and have masses typically of the order of $m_n = n\,10^{-3}$ eV for an extra dimension size of mm. This mixing has a relevant effect on both solar and atmospheric neutrino phenomenology since for each mode with mass larger than the three active neutrino with Dirac mass μ_i ($i = 1, 2, 3$) there will be a corresponding vacuum mixing angle $\theta \sim \mu_i/m_n$ (see e.g. [374] for a review and references therein).

Sizeable effects are also expected in cosmology [375–377]. In particular, KK modes of bulk neutrinos can be produced in the early universe before BBN by incoherent scatterings or coherent oscillations, thus contributing to the total radiation content parameterized by $N_{\rm eff}$. Bounds on this parameter from BBN amounts to require that the whole tower of modes should be equivalent to no more than approximately one active neutrino species. Furthermore, the photoproduction of ^{2}H and ^{6}Li by decays of modes after BBN may potentially spoil the whole standard nuclei production scenario. These effects limit the possible values for the extra dimension length scale δ as function of the Dirac active neutrino mass, see e.g. Fig. 20 (from [376]). For illustration, for a neutrino mass of order 0.1 eV [376] find from BBN $0.01\ \text{MeV} \leq \delta^{-1} \leq 10^3$ MeV.

8.2. Variation of fundamental constants

8.2.1. Introductory remarks

Already in 1937 P.A.M. Dirac first introduced the idea that the fundamental constants of physics may be indeed variable parameters characterizing the particular state of the universe [378]. Physicists have long scrutinized this possibility. On one hand, a strong effort has been devoted to embed this paradigm into a definite theoretical framework. For example, theories with extra dimensions such as Kaluza–Klein or string theories, naturally predict that 4-dimensional constants may

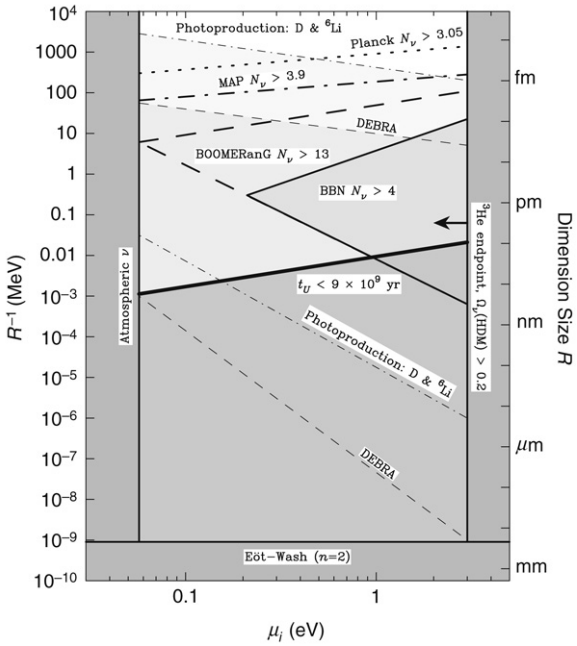

Fig. 20. Constraints on the extra dimension length scale R versus active neutrino masses μ_i for bulk neutrino scenarios. From [376].

vary (in time and space), since they represent effective values in the low energy limit, and are sensitive to the size and structures of extra dimensions. Any variation of these invisible dimensions, for example over cosmological times, would lead to varying 4-dimensional constants. On the other hand, measuring variations of fundamental constants has been pursued at the experimental level by several groups and techniques, ranging from short time laboratory based measurements, to astronomical or geological scale studies and, finally, to cosmological time variation searches. All these investigations provided quite strong constraints on the possible time evolution of e.g. the fine structure coupling, α, or the Newton gravitational constant, G_N. Both theoretical and experimental aspects of this intriguing research issue are beautifully covered in the review [379].

In the following we will summarize the impact that fundamental constant time variations have on BBN, by describing the main effects on the light nuclei abundances and the bounds which therefore is possible to obtain using BBN as a probe. Unless otherwise stated, we will limit to constrain the departure of these parameters at the BBN epoch compared to present values, independent of a specific theoretical model for their evolution (this is instead the approach considered e.g. in [380–382]). As a general remark, we would like to stress that all results depend quite strongly upon the general assumption which are made to perform the analysis, the *priors* in presently fashionable Bayesian language. In fact,

(1) there are too many constants which enter the BBN physics (the fine structure coupling, the Newton constant, the strong interaction scale, Λ_{QCD}, the Yukawa couplings, the Higgs vacuum expectation value), so that if they are all considered as free independent parameters to be fixed by data, one lacks predictive power;

(2) there is no unique theoretical framework which allows for an unambiguous determination of their relative evolutionary history.

For these reasons, there are two typical strategies which have been exploited. One may assume that only a single fundamental constant (or a subset of them) is promoted to the role of a free parameter to be constrained, keeping all the others as fixed. Several analyses of variation of the fine structure coupling, which we describe in the next section are based on this assumption. On the other hand one can consider a specific theoretical model, which reduces the number of independent parameter one starts with, and this typically allows for tighter constraints. Examples of this approach has been considered in the last decade in details, based on dilaton inspired theories, or rather on unified gauge theories, where all gauge coupling of the SMPP get unified at some high mass scale M_{GUT}.

To conclude this short introduction, let us stress that checking for a time (and space) variation of fundamental constants is only meaningful for *adimensional* quantities, such as α. This is due to the fact that measurement of *dimensional* parameters is strongly intertwined with both the system of units and the particular measurement technique which is employed, so that an absolute determination of, say, the time evolution of the speed of light, c, is meaningless.

This can be illustrated with a simple example. Suppose we want to measure the value of c by using a *light clock device*, a source S and a mirror placed at a distance D away from S, which reflects the light ray back to S. The value of c is then computed as the ratio of the distance $2D$ over the total time elapsed from emission to light collection, which is expressed in terms of an adimensional number, *once* units of length L and time T are specified. For example, we can choose an atomic clock to specify T, using the hyperfine splitting transition rate of caesium-133 atoms. In this case the particular combination

of fundamental parameters $m_e^2 c^2 \alpha^4 / m_p \hbar$ (the typical hyperfine frequency) is kept fixed by definition, m_p being the proton mass. If we choose the length unit L as the distance traveled by light in k units of time T, it is rather trivial that there is no possibility to detect the time variation of the speed of light, as also c in this case is kept fixed by definition. On the other hand we may use the standard prototype platinum–iridium bar as the value of L, which depends on the interatomic spacing of the material, and thus ultimately on the value of the Bohr radius $a_B = \hbar / m_e c \alpha$. In this case if we find that at different epochs the value of c has changed in these units, this amounts to say that the ratio

$$\frac{c}{L/T} \propto \frac{m_p}{m_e} \frac{1}{\alpha} \tag{118}$$

is time dependent. Therefore, either α or the adimensional ratio m_p/m_e or both, change with time.

As this simple example shows, evidences for time varying fundamental constants are in all cases evidences for particular combination of adimensional quantities, which depends upon the particular choice of units which is adopted. In the following, when time changes of dimensional parameters are considered, a ratio of two independent and homogenous constants will be always implicitly understood, as for example the ratio Λ_{QCD}/m_q, with m_q some quark mass, or $G_N M_{GUT}^2$.

8.2.2. Varying the fine structure constant

There are several direct measurements in the laboratory on the variation of α over a relatively short time period, using different techniques, see e.g. [379]. The geological limit from the Oklo natural reactor is about $|\delta\alpha/\alpha| \leq 10^{-8}$ over a period of few billion years [383–385]. Astrophysical observations of high red-shift quasar absorption lines provide the only evidence for a possible time variation of α [386–388],

$$\delta\alpha/\alpha = (-0.57 \pm 0.11) \times 10^{-5}. \tag{119}$$

A result compatible with zero is instead reported by [389,390], which however has been criticized in [391].

Over longer time scales, the value of α can be constrained by cosmological observables, such as CMB and BBN. Indeed, CMB anisotropies are a very good probe of α since its value is imprinted in the ionisation history of the universe. The main effects are a change in the redshift of recombination due to a change of hydrogen energy levels, the modification of the Thomson scattering cross-section which is proportional to α^2, and at subleading level a change of ^{4}He abundance [392–394]. If the value of α is increased, the last scattering surface moves towards larger redshifts, which correspond to a shift of first Doppler peak towards larger l's. Moreover, this shift produces a larger Integrated Sachs–Wolfe effect (i.e. more power around the first peak), while the high multipole diffusion damping is decreased by a larger α, thus increasing the power on very small scales. With present CMB data, including those from the first year release from WMAP Collaboration, one finds the bound $-0.06 \leq \delta\alpha/\alpha \leq 0.02$ at 95% C.L., while a Fisher matrix analysis shows that future experiments such as PLANCK should be able to constrain variations of α during CMB formation with an accuracy of 0.3% [395].

The value of α enters the physics of primordial nucleosynthesis in several ways and, remarkably, BBN represents the earliest reliable probe of possible variation of the fine structure coupling over cosmological times, though it suffers from being model dependent with respect to CMB analysis. This issue was first studied in [396–398], where the focus was on the abundance of ^{4}He, while a detailed analysis has been presented mainly in [399,400], which we follow for our discussion.

During the early stages of BBN, at the n/p ratio freeze out temperature, T_D, the fine structure coupling affects the weak n–p rates in two ways. First of all, it changes the neutron–proton mass difference Δm, which can be only phenomenologically parameterized as in [401], where the authors find

$$\Delta m \text{ (MeV)} \sim 2.05 - 0.76 \left(1 + \frac{\delta\alpha}{\alpha}\right). \tag{120}$$

This result is obtained by studying the the behavior of the nucleon masses versus α, which determines the electromagnetic quark masses and binding energy. The fact that this parametrization, though quite reasonable, is not deduced from first principles in a QCD-based calculation, is the main source of possible uncertainties and renders all predictions model-dependent. Furthermore, weak rates also depend upon α when QED radiative and thermal corrections are included. However, these corrections are at the level of few percent, see e.g. [51], so the effect is very small for moderate variation of α, i.e. $\delta\alpha/\alpha \ll 1$. Since the ^{4}He mass fraction is mainly sensitive to the n/p ratio at freeze out, while it depends more weakly on the whole set of nuclear reaction rates, this implies that at first approximation the whole dependence of Y_p upon α is through Δm, which also fixes the decoupling temperature,[18] since

$$Y_p \sim \frac{2}{1 + \exp(\Delta m / T_D(\Delta m))}. \tag{121}$$

The dependence of other nuclei on α is more involved, and one should scrutinize the way the fine structure constant appears in the set of nuclear reaction rates. The leading effect is due to the change of Coulomb barrier. Charged particle reactions at low energies take place via tunneling through a repulsive potential, and this produces most of the energy dependence in

[18] Notice that the Fermi coupling constant G_F does not depend upon the values of gauge couplings in the SMPP, but on the Higgs vacuum expectation value only.

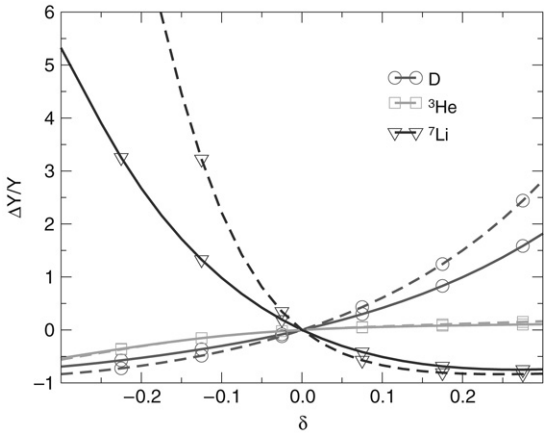

Fig. 21. The relative variation of ^{2}H, ^{3}He and ^{7}Li produced during BBN as a function of the variation of the fine structure coupling, $\delta = \delta\alpha/\alpha$. From [400].

the cross section,

$$\sigma(E) = \frac{S(E)}{E} e^{-2\pi\eta}, \tag{122}$$

where $\eta = \alpha Z_1 Z_2 \sqrt{\mu/2E}$, with Z_1 and Z_2 the charges of the incoming nuclei and μ the reduced mass. If one neglects the dependence on α of the astrophysical S-factor and of reduced mass, as in [399], then only the Sommerfeld parameter η would change linearly with α, and one can obtain the thermally averaged rates versus $\delta\alpha/\alpha$, see Tables 1 and 2 of [399], as well as the fractional variation of light nuclei abundances. Not surprisingly, the most dramatic changes are those of ^{7}Li, due to the strong Coulomb barrier in its production.

The analysis of [399] has been improved in [400], see Fig. 21, by including several corrections previously neglected, which accounts for the α dependence of the S-factor, namely the normalization of initial-state Coulomb penetrabilities, final state charged particle Coulomb interactions, linear dependence on α of photon coupling to nuclear currents in radiative processes, photon energy and barrier penetration in external direct captures and, finally, the electromagnetic contribution to the nuclear masses. All these corrections can amount to a third of the total dependence of ^{7}Li on $\delta\alpha/\alpha$, while they are smaller for ^{3}He and ^{2}H.

These results can be used to get bounds on $\delta\alpha/\alpha$ by comparing data with the results of a fully numerical computation of light nuclei versus α, using a modified version of public BBN codes. For example [393] reports at 95% C.L. $\delta\alpha/\alpha = -0.007 \pm 0.009$, using the experimental values of ^{4}He, $Y_p = 0.244 \pm 0.002$, and of deuterium, $^2\mathrm{H/H} = (3.0 \pm 0.4) \times 10^{-5}$, while [400] for the same experimental values obtain $\delta\alpha/\alpha = -0.007^{+0.010}_{-0.017}$. If we use the ^{2}H/H and Y_p of Section 4 and the response matrix formalism of [402] we find the updated bound $-0.007 \leq \delta\alpha/\alpha \leq 0.017$ at 95% C.L. It should be noticed that a varying value of α does not significantly improve the global fit of data when ^{7}Li is also included in the analysis. If one uses $\log_{10}(^7\mathrm{Li/H}) = -9.91^{+0.19}_{-0.13}$ [177], combined with the deuterium experimental result as above, one would find a reasonable agreement for $\delta\alpha/\alpha \sim 0.23$ (the standard value being excluded at more than 3-σ), but including ^{4}He gives a minimum χ^2 very far from this value but with a very low likelihood [400]. Stated differently, it seems difficult that the problem of the lower observed ^{7}Li with respect to theoretical expectation could be alleviated by allowing a different value of α at the BBN epoch, unless one also includes N_{eff} as a free parameter in the analysis. In this case, a larger value of α, which suppresses the theoretical value of ^{7}Li, and a slower expansion rate at BBN, $N_{\mathrm{eff}} < 3$ (which is degenerate with α and can compensate for the otherwise too large amount of ^{4}He for positive $\delta\alpha/\alpha$) can reasonably fit all nuclear abundances [403].

8.2.3. The role of Higgs vacuum expectation value, fermion masses and Λ_{QCD}

In the SMPP the vacuum expectation value, v, of the Higgs field provides the mass term to vector bosons $W^{\pm}$ and Z via the Higgs–Englert–Brout mechanism, as well as to all fermions via Yukawa couplings. Any variation of the weak scale, v, or better to say of the ratio of the weak to strong scales, v/Λ_{QCD}, and weak to gravitational scale over cosmological times can therefore, have a dramatic impact since it induces a time dependence of all massive particles after spontaneous symmetry breaking of the electroweak symmetry.

The main effects on BBN are the change of the Fermi coupling constant, the neutron–proton mass difference, the electron mass and finally, the binding energy of deuterium [404–407]. The change of $G_F = 1/\sqrt{2}v^2$ re-scales all weak reactions which keep neutron and proton in equilibrium, and thus shifts the decoupling temperature, T_D. Similarly, these rates are also affected by the variation of the neutron–proton mass difference, due to the u and d quark mass contribution to Δm. This contribution is proportional to the difference between the two corresponding Yukawa couplings and can be estimated once the electromagnetic contribution to Δm is singled out. Since the latter can be calculated with relatively little uncertainty,

being the Born term of the Cottingham formula [401], one obtains, see Eq. (120),

$$\Delta m\ (\mathrm{MeV}) = 1.29 + 2.053\frac{\delta v}{v}, \tag{123}$$

with the assumption that in this case only v is considered as a free parameter, while both α and the Yukawa couplings are fixed to their standard values. This estimate is consistent with recent lattice QCD calculation with dynamical quarks [408]. Finally, the electron mass is shifted linearly with v, $\delta m_e/m_e = \delta v/v$. The changes in G_F, Δm and m_e fixes the new value of $\Delta m/T_D$, which is a key parameter for Y_p, as we stressed already several times.[19] For example, if v is increased, the lower value of G_F and the larger m_e (which reduces the available phase space) implies a less efficient n–p rates, so that their freeze out occurs earlier (more ^{4}He), but the larger effect is due to the increased Δm, which reduces the n/p ratio, and therefore the final value of Y_p.

Finally, changing v alters the deuteron binding energy B_D[20] through the change in the pion mass m_π. Since the pion is a Goldstone boson, its mass scales as a geometric mean between weak and strong scales as found by Gell-Mann, Oakes and Renner [410], $m_\pi^2 \sim (m_u + m_d)\Lambda_{QCD} \propto v$. It is worth noticing that a change of B_D can be induced by a variation of v, as we are presently discussing, or a time evolving values of Yukawa couplings, y_i, with $i = u, d$, or finally by a change of the strong interaction scale, Λ_{QCD}, which we consider later on,

$$\frac{\delta m_\pi}{m_\pi} = \frac{1}{2}\left(\frac{\delta\Lambda_{QCD}}{\Lambda_{QCD}} + \frac{\delta v}{v} + \frac{\delta y_u + \delta y_d}{y_u + y_d}\right). \tag{124}$$

Therefore, the effects which we now describe of a modified value of B_D will be relevant when any of these parameters is assumed to be time-dependant.

The value of B_D fixes both the initial conditions for BBN, given by the Nuclear Statistical Equilibrium, as well as the cross-sections that burn deuterium into heavier nuclei. As B_D increases, deuterium becomes more stable, and BBN would start at a higher temperature epoch T_N. Interaction rates of the BBN network occur more rapidly at higher temperature (though the cross-sections have changed) leading to a more efficient ^{2}H processing. One thus expect in this case a decreased ^{2}H/H ratio and an increased Y_p [411,409], see also Table I in [402].

Static properties of nuclei and, in particular, binding energies depend strongly on m_π, which sets the length scale of attractive nuclear forces, and gives the dominant contribution to two- and three-body potential via the one and two pion-exchange terms. Though accurate calculations have been performed which reproduce several experimental properties [412–414], a numerical determination of the functional dependence of binding energies upon m_π is still lacking. On the other hand, this dependence has been studied extensively in the framework of low energy effective theory that respect the approximate $SU(2)_L \otimes SU(2)_R$ of QCD [415–418]. Depending on the values of the coefficients (fixed by data) which weight the s-wave four-nucleon operator expansion of the lagrangian density, the result seems to suggest that deuterium remains loosely bound for a wide range of m_π, or rather that the value of B_D strongly changes with m_π [417]. Despite the large uncertainties, the results are compatible with a linear dependence for small variations around the current value,

$$B_D\ (\mathrm{MeV}) = 2.22\left(1 + r\frac{\delta m_\pi}{m_\pi}\right), \tag{125}$$

with $-10 \leq r \leq -6$ [417,418].

One further caveat is represented by the fact that the role of strange quark mass in nuclear quantities such as binding energy is not fully understood, being so close to the non-perturbative scale, Λ_{QCD} [419,402]. The sensitivity of B_D to m_s has been estimated in [420], by inspecting the role of σ meson mass to nuclear potential. They find $\delta B_D/B_D \sim -17\delta m_s/m_s$. Some authors have also pointed out that large pion mass variation could also render deuterium an unbound system, and discussed the values of m_π which would lead to stable di-neutron (or di-proton) systems [419,421,265]. This would have dramatic consequences on the standard BBN picture, leading to a stable or long-lived ^{8}Be, and by-passing the $A = 5$ bottleneck through formation of ^{5}He. Both effects would produce a large enhancement of lithium or metallicity production in the early universe.

Implementing all changes described so far in a BBN numerical code, and assuming v as a free parameter, one can typically constrain $\delta v/v$ at the level of percent. In particular, one can estimate $\delta Y_p \sim \delta v/v(\%)$. Using both ^{2}H/H with an error of 30% and a rather low value for $Y_p = 0.238 \pm 0.005$, which seems presently disfavored, Yoo and Sherrer find $-0.7\% \leq \delta v/v \leq 2.0\%$ [407]. Interestingly, a looser bound (10%) is obtained from (pre-WMAP) data on CMB, by considering the effect of a varying electron mass in both the Thomson scattering cross-section and hydrogen binding energy. We have updated the bound from BBN of [407], using the data on ^{2}H/H and Y_p discussed in Section 4 and find $-0.005 \leq \delta v/v \leq 0.012$ at 95% C.L.

[19] The change in electron mass also produces a different value for the $e^+ - e^-$ energy density, and thus of the Hubble parameter, but the effect is sub-leading [407].

[20] Regardless of its expression in terms of fundamental parameters, the effect of changing B_D has been studied for example in [409]. Combining a full BBN data analysis, which also includes ^{7}Li abundance with the WMAP prior on η, they find $\delta B_D/B_D = -0.019 \pm 0.005$, and point out that this 4-σ shift of the D binding energy might reconcile the whole BBN picture with data, in particular the low value of observed ^{7}Li.

Table 12
A summary of BBN constraints on fundamental parameters discussed in Sections 8.2.2 and 8.2.3.

	Data	Range	Ref.
$\delta\alpha/\alpha$	$Y_p = 0.244 \pm 0.002$		
	$^2\mathrm{H/H} = (3.0 \pm 0.4) \times 10^{-5}$	-0.016–0.002 (95% C.L.)	[393]
$\delta\alpha/\alpha$	$Y_p = 0.244 \pm 0.002$		
	$^2\mathrm{H/H} = (3.0 \pm 0.4) \times 10^{-5}$	-0.024–0.003 (95% C.L.)	[400]
$\delta\alpha/\alpha$	$Y_p = 0.250 \pm 0.003$		This paper
	$^2\mathrm{H/H} = \left(2.87^{+0.022}_{-0.021}\right) \times 10^{-5}$	-0.015–0.014 (95% C.L.)	(using [402])
$\delta v/v$	$Y_p = 0.238 \pm 0.005$		
	$^2\mathrm{H/H} = \left(3.0^{+1.0}_{-0.5}\right) \times 10^{-5}$	-0.007–0.02	[407]
$\delta v/v$	$Y_p = 0.250 \pm 0.003$		
	$^2\mathrm{H/H} = \left(2.87^{+0.022}_{-0.021}\right) \times 10^{-5}$	-0.005–0.012 (95% C.L.)	This paper
$\delta\Lambda_{QCD}/\Lambda_{QCD}$	$Y_p = 0.238 \pm 0.005$		
	$^2\mathrm{H/H} = (2.6 \pm 0.4) \times 10^{-5}$	~ -0.1–~ 0.1	[411]
$\delta\Lambda_{QCD}/\Lambda_{QCD}$	$^2\mathrm{H/H} = (1\text{–}10) \times 10^{-5}$	~ -0.06–~ 0.06	[419]

The scenario with a varying strong interaction scale, Λ_{QCD}, can be described in quite a complete analogy. In this case, assuming that the weak scale is kept fixed, while v/Λ_{QCD} is time dependent, the effects are due to the change of neutron–proton mass difference, since the electromagnetic contribution is weighted by the strong scale,

$$\Delta m\ (\mathrm{MeV}) = 1.29 - 0.76\frac{\delta\Lambda_{QCD}}{\Lambda_{QCD}}, \tag{126}$$

and the shift in deuterium and heavier nuclei binding energy [419,411]. In particular, in [411] results are obtained by exploiting a simplified BBN network up to nuclei with $A = 3$. This introduces some systematics in the result, but it has the benefit of reducing the dependence on Λ_{QCD} only through the two parameters Δm and B_D. The result is a bound on Λ_{QCD} at the level of 10%, if one corrects for such a systematic effect.

The effect of ^{2}H binding energy on BBN is also considered in [419], where the authors quote $|\delta\Lambda_{QCD}/\Lambda_{QCD}| \leq 0.06$ as a conservative bound. Interestingly, they also point out that even when both the strong scale and quark masses are modified by the same amount, so that all binding energies remain unchanged (and so does the reference temperature, T_N), nevertheless the freezing temperature is changed, since it also involves the Planck mass scale which is assumed to be fixed. In this case one obtains a bound of the order of $(\delta\Lambda_{QCD}/M_P)/(\Lambda_{QCD}/M_P) \leq 0.1$ [419].

8.2.4. Correlated variation of fundamental constants in unified scenarios

A summary of bounds on fundamental parameters considered in the previous sections is presented in Table 12. As we mentioned already, they refer to a single parameter analysis, i.e. assuming that all but a single fundamental constant are held fixed. On general grounds, one could expect that this assumption is rather ad hoc. For example, in models with extra dimensions, or based on embedding of the SMPP into a larger gauge symmetry group, it is quite natural that more than a single coupling or fundamental scale, if not all, would be time dependent during the (homogeneous) expanding history of the universe. When using BBN to constrain such a variation (and CMB anisotropies to a lesser extent as they are not sensitive to strong interactions), one immediately faces the problem of several degeneracies among these parameters. This results in a much less predictive power, unless a specific theoretical framework is assumed in the analysis, which reduces the number of free parameters of the theory, and relates possible variations of different fundamental constants.

The purpose of this section is to describe the impact on the BBN of simultaneous variation of all involved fundamental parameters and discuss the constraints on these variations which can be obtained when some particular model is assumed (GUT theories, string-theory inspired dilaton scenario).

The first steps in this programme are basically the following: to identify those combination of fundamental parameters which influence the BBN dynamics and quantify how light nuclei abundances change when this parameters are left as a free input. In general, this task is very involved, as large variation of, say, the strong scale parameter, Λ_{QCD}, or quark masses can change the standard picture of BBN in quite a dramatic way (e.g. by rendering deuteron an unbound state or predicting bound (pp) or (nn) states which may add new paths to nucleosynthesis). On the other hand, it is easier to study the problem perturbatively, in the neighborhood of the standard values that all these couplings, mass scales, etc., take today as measured in laboratory. A comprehensive analysis of this sort was lacking until quite recently, and has been mainly pursued in a very detailed study of Dent, Stern and Wetterich [402] (see also a semi-analytical *tour de force* of [422] in the chiral limit of *QCD*). We will follow their approach in the following, and choose to work in the units for which the strong interaction scale is held fixed (see our discussion in Section 8.2.1). One can then identify the following set of fundamental constants playing a role at the BBN epoch, which we collectively denote by φ_k, $k = 1, \ldots, 7$: the Newton constant, G_N,[21] the fine structure coupling,

[21] The results of this section have some overlap with the analysis presented later of scenarios when one varies the gravitational action, including a time-evolving Newton constant.

Table 13
The response matrix R for ^{2}H, ^{3}He, ^{4}He, ^{6}Li and ^{7}Li (from [402]). The reference value for the baryon fraction is $\Omega_B h^2 = 0.022$.

	^{2}H	^{3}He	^{4}He	^{6}Li	^{7}Li
G_N	0.94	0.33	0.36	1.4	−0.72
α	3.6	0.95	1.9	6.6	−11
v	1.6	0.60	2.9	5.5	1.7
m_e	0.46	0.21	0.40	0.97	−0.17
Δ_q	−2.9	−1.1	−5.1	−9.7	−2.9
M_q	17	5.0	−2.7	−6	−61
$\Omega_B h^2$	−1.6	−0.57	0.04	−1.5	2.1

α, the Higgs vacuum expectation value, v, the electron mass, m_e,[22] the light quark mass difference, $\Delta_q = m_d - m_u$, the averaged light quark mass, $M_q = (m_d + m_u)/2 \propto m_\pi^2$ [402]. Finally, the baryon density parameter is also included. Notice that in this analysis variation of the strange quark mass, m_s/Λ_{QCD}, is not accounted for.

The leading linear dependence of nuclear abundances X_i ($i = {}^2$H, ^{3}H, ^{4}He, ^{6}Li, ^{7}Li) upon small changes of these parameters is then encoded in the response matrix R defined as

$$R_{ik} = \frac{\varphi_k}{\mathrm{X}_i}\frac{\partial \mathrm{X}_i}{\partial \varphi_k}. \tag{127}$$

This matrix can be evaluated by numerically integrating the BBN equations. In particular, in [402] this has been performed in two steps, by first varying a set of nuclear physics parameter r_j which includes binding energies of light nuclei up to ^{7}Be, nucleon mass, neutron–proton mass difference, neutron lifetime and a subset of the φ_k, (α, m_e, G_N and η) and computing the matrix

$$C_{ij} = \frac{r_j}{\mathrm{X}_i}\frac{\partial \mathrm{X}_i}{\partial r_j}, \tag{128}$$

and then relating the variation of the r_j to small changes of the φ_k,

$$F_{jk} = \frac{\varphi_k}{r_j}\frac{\partial r_j}{\partial \varphi_k}. \tag{129}$$

The response matrix R is therefore given by the matrix product $R = CF$. This decomposition turns out to be useful as the determination of C is rather robust, while computing F requires some theoretical assumption, as for example the dependence of binding energies on the pion mass. In Table 13 the entries for the R matrix are reported [402]. The last row is the logarithmic variation for small changes of the baryon fraction around the reference value $\Omega_B h^2 = 0.022$. We have checked that the result is very weakly dependent on the reference point in the range 0.015–0.025, the variation being of the order of 5% for ^{2}H and even smaller for ^{4}He.

Using these results one can construct the χ^2 function (we do not use ^{7}Li in this analysis)

$$\chi^2 = \frac{\left({}^2\mathrm{H}^{(th)}(\varphi) - {}^2\mathrm{H}^{(exp)}\right)^2}{\sigma_{^2H}^2} + \frac{\left(\mathrm{Y}_p^{(th)}(\varphi) - \mathrm{Y}_p^{(exp)}\right)^2}{\sigma_{\mathrm{Y}_p}^2}, \tag{130}$$

where the theoretical abundances are computed using the linear expansion in terms of R (but we have retained an exact dependence on the baryon fraction). In this way, one gets an estimate of the kind of constraints which can be obtained on all φ_j, and more importantly, it serves to illustrate the degeneracies which appear between the several pairs of fundamental constants, at least as long as we consider small variations with respect to the standard results, so that the linear expansion used in Eq. (130) is legitimate.

As an example, we have considered the experimental values and errors of Section 4. The results are shown in the figures of Table 14, where the various curves correspond to a Fisher matrix analysis around the reference model with $\Omega_B h^2 \sim 0.0209$ and all other parameters at their standard values (this is indeed, locally, the minimum of the total χ^2). When one of the two selected parameters is the baryon density, the plots correspond to the case where only one fundamental constant is varied while all others are fixed to the standard value. In this case, one can read from the contours the typical order of magnitude of the constraint which can be obtained in this single-parameter analysis, which is at the few percent level for α, v, Δ_q and M_q, while it is almost one order of magnitude larger for G_N and m_e. More interestingly, the other bidimensional contours show the degeneracies among pairs of parameters. In particular, notice the strong correlations of G_N with α and m_e and between the pairs v–α, m_e–α, Δ_q–α, v–m_e, and v–Δ_q.

[22] Differently than in our previous discussion, m_e is assumed an independent parameter with respect to v. This is equivalent to consider the lepton Yukawa couplings as varying parameters.

Table 14
The bidimensional 68% and 95% C.L. contours illustrating the correlation of fundamental parameters in a BBN analysis (^{2}H/H and Y_p as in Section 4).

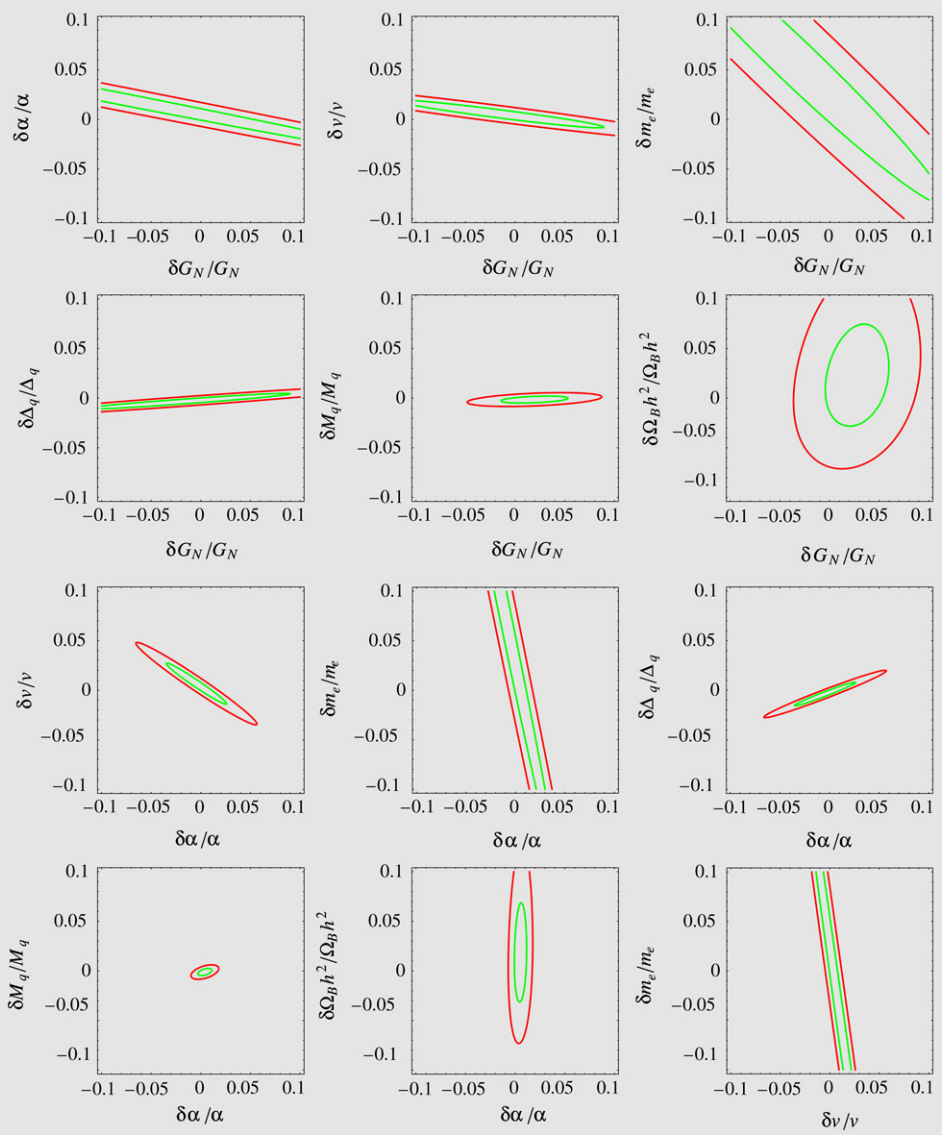

The difficulty of treating simultaneous variations of more than a single fundamental parameter is somehow alleviated if one works in the framework of a definite theoretical model beyond the SMPP, which imposes further relationships among (some) of them. A typical example is given by Grand Unified Theories (GUT) which assume that the three SMPP gauge couplings get unified at some high mass scale, M_G, where the dynamics is dictated by a larger (simple) symmetry group. This scenario and its implications for BBN has been worked out in details in [423–425,421,402,426]. The general argument is that in GUT theories unification of couplings implies that the various fundamental constants are likely to vary simultaneously and, for example, a change of the fine structure coupling implies a much larger variation of the strong interaction scale, Λ_{QCD}, at low energies.

If we denote by α_G the (common) value of the three $SU(3)_c \times SU(2)_L \times U(1)_Y$ couplings, α_i, at M_G (typically $M_G \sim 10^{16}$ GeV), then their running is given by Renormalization Group equations,

$$\alpha_i^{-1}(M_Z) = \alpha_G^{-1} + \frac{b_i}{2\pi} \log\left(\frac{M_G}{M_Z}\right), \tag{131}$$

where the coefficients b_i depend on the particle multiplets. If α_G undergoes time variation at a cosmic time above the unification scale, then one can traces the correlated variation of the SMPP couplings at low energies. Neglecting the threshold

Table 14 (*continued*)

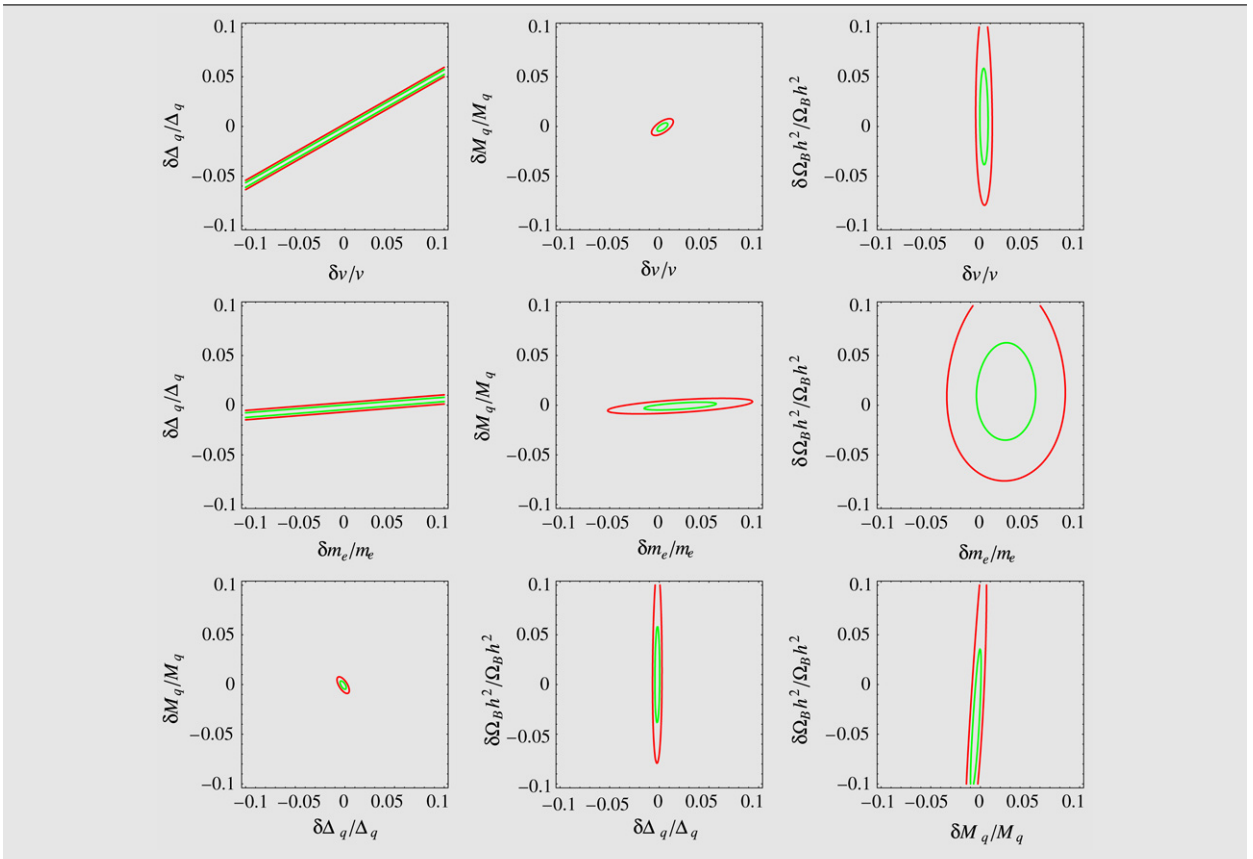

effect one obtains [423,424]

$$\frac{\delta \Lambda_{QCD}}{\Lambda_{QCD}} \sim (34\text{–}40)\frac{\delta\alpha}{\alpha}. \tag{132}$$

Also Yukawa couplings and the Higgs vacuum expectation value v (which is for example, tied to the supersymmetric breaking scale in most supersymmetric models) are expected to vary and to be related to time evolution of α. However, the size of the effect is model dependent, or simply unknown, so it is usually parameterized in terms of an unknown constant, $\delta y_i/y_i = c\delta\alpha/\alpha$, and similarly for v. In general, in addition to the time evolution of α_G, one could also consider other possibilities, where the GUT mass scale M_G also varies [425].

The BBN constraints in these scenarios on the variation of α (and all other related parameters) have been first analyzed in a qualitative manner in [424,421] and then worked out using a full BBN numerical study in [426,402], with two main results. On one hand, the constraints become typically tighter, $|\delta\alpha/\alpha| \leq 10^{-5} - 10^{-4}$. Moreover, in some cases the theoretical value of ^{7}Li is lowered and can be rendered compatible with the experimental result. This is the case, for example, when the weak scale, v, is determined by dimensional transmutation, so that variation of the largest top quark Yukawa coupling induces changes of v [398,426], or assuming that the variation of fundamental constants are triggered by an evolving dilaton scalar field [406,426].

8.2.5. *Varying the Newton constant and scalar-tensor theories of gravity*

The effect of a varying gravitational constant, G_N, on the BBN is through the expansion law, $H \propto \sqrt{G_N}$, which determines both the neutron–proton density ratio at freeze-out (Y_p), and the efficiency of ^{2}H burning abundance when nucleosynthesis starts. We have already seen in the previous section the typical constraints which can be put on $\delta G_N/G_N$, of the order of few percent. In particular, using the values of Y_p and ^{2}H/H already discussed, we find $-0.036 \leq \delta G_N/G_N \leq 0.086$, at 95% C.L., which is dominated by the effect on ^{4}He. In this case, the limit can be read off directly from the bound on $N_{\rm eff}$, since a change of G_N is equivalent to the change

$$\frac{\delta G_N}{G_N} = \frac{7}{43}\Delta N_{\rm eff}. \tag{133}$$

Recently, the effect of a varying G_N has been considered by several authors, with similar results, depending on the experimental values for light nuclei adopted in their analysis (for earlier studies see e.g. [427,428]). In [429] it is stressed the sensitivity of ^{2}H to the value of the Newton constant. In the pessimistic case of a large systematic error on Y_p, deuterium can provide a 20% bound. On the other hand, the results of [217], which adopt $Y_p = 0.249 \pm 0.009$, suggests that Y_p still gives the strongest possible constraint. If one makes the assumption of a monotonic behavior for the time dependence of the gravitational constant, $G_N \sim t^{-x}$, the bound on δG_N can also be cast in a constraint on the exponent x and thus on the present value of $\dot{G}_N/G_N$. In [217] it is found $-0.0029 < x < 0.0032$, and $-2.4 \times 10^{-13}\ \mathrm{yr}^{-1} < \dot{G}_N/G_N < 2.1 \times 10^{-13}\ \mathrm{yr}^{-1}$. Our estimate on $\delta G_N/G_N$ translates into $-0.6 \times 10^{-13}\ \mathrm{yr}^{-1} < \dot{G}_N/G_N < 1.6 \times 10^{-13}\ \mathrm{yr}^{-1}$ using $t_0 = 13.7$ Gyr for the lifetime of the Universe.

An interesting class of models which allows for a time dependent gravitational coupling is represented by scalar-tensor theories of gravity [430,431], where the latter is mediated, in addition to the usual spin-2 gravity field, by a spin-0 scalar φ which couples universally to matter fields. Its dynamics define the evolution of an effective Newton constant for ordinary matter, to which φ is "universally" coupled, as one can read by the action of the model in the "Einstein" frame,

$$S = \int \frac{\mathrm{d}^4x}{16\pi G_*}\sqrt{-g}\left[R - 2g_{\mu\nu}\partial^\mu\partial^\nu\varphi - V(\varphi)\right] + S_m\left[F^{-2}(\varphi)g_{\mu\nu};\Psi\right], \tag{134}$$

where G_* is the bare gravitational coupling, $V(\varphi)$ the scalar field potential, and $F(\varphi)$ a positive function, which enters the coupling of ordinary matter fields Ψ to the metric. Strong constraints on the present (denoted by the index 0) values of the (generally) φ post-Newtonian parameters [432],

$$\gamma - 1 = -2\frac{\alpha_0^2}{1+\alpha_0^2}, \qquad \beta - 1 = \frac{1}{2}\frac{\beta_0\alpha_0^2}{(1+\alpha_0^2)^2}, \tag{135}$$

where

$$\alpha(\varphi) = \frac{\mathrm{d}\log F^{-1/2}}{\mathrm{d}\varphi}, \qquad \beta(\varphi) = \frac{\mathrm{d}\alpha}{\mathrm{d}\varphi}, \tag{136}$$

are set by solar system experiments, as the shift of the Mercury perihelion or the Shapiro delay of radio signals from the Cassini spacecraft as it passes behind the Sun, $\gamma_0 - 1 = (2.1 \pm 2.3) \times 10^{-5}$ [433].[23] The value of α_0 should be thus, very small, while β_0 can still be large.

The implications of models described by the action in Eq. (134) have been discussed by several authors with different choices of the arbitrary functions $F(\varphi)$ and $V(\varphi)$, see e.g. [435–448,434,449–451]. In the case of a standard Brans–Dicke theory the value of primordial ^{4}He produced during BBN can be evaluated semi–analytically as a function of the Brans–Dicke parameter ω (which weights the scalar field kinetic term in the Jordan frame) [442], in case one consider the particular solution $\varphi = const$ during the radiation dominated epoch, giving the bound $\omega_0 \geq 100$. The fact that the BBN constraints on the model depend strongly on the particular scalar-tensor theory considered in the analysis, thus providing quite different bounds on ω_0, have been stressed in [444], while a quite general numerical code for BBN in scalar-tensor models is described in [447,434]. In particular, in [434] it is studied in details the case of a massless dilaton with a quadratic coupling, $V(\varphi) = 0$, $F(\varphi) = \exp(-\beta\varphi^2)$, including the mass threshold effects when the universe cools down. The latter is due to the variation of the trace of the energy momentum tensor of ordinary matter-radiation, $\rho - 3P$, whenever a single specie becomes non-relativistic, which changes the source term in the Klein Gordon equation for φ. The results of the study of [434] show that the strongest bound comes from ^{4}He and indeed it is stronger than from solar system experiments, $\alpha_0 \leq 10^{-3}$ for $\beta \geq 0.3$, see Fig. 22. Finally, we mention that particular choices of the scalar field potential $V(\varphi)$ (and of the initial conditions for φ before the BBN) can solve the lithium problem, yet leading to values of ^{2}H/H and Y_p compatible with the experimental values. One example is illustrated in Fig. 23, from [450], where the potential is chosen to be $V(\varphi) = \Lambda^2\varphi^4$, and $F(\varphi) = \exp(-\beta\varphi^2)$. We see that there is a region in the parameter space which corresponds to primordial abundances of all light nuclei in agreement with experimental data.

8.2.6. A varying cosmological constant: Quintessence models

Observations of type Ia supernovae [452,453], structure formation [454,455] and CMB [8] provide quite a strong evidence for an accelerated expansion of the Universe at recent times. The simplest explanation of this result is to invoke a new component of the total energy–momentum tensor in the form of a cosmological constant Λ (ΛCDM model), which is a nice fit of data, yet it gives rise to two related fine tuning problems. On one hand, the value of Λ happens to be extremely small with respect to the typical energy scale of any fundamental physics model, as the Planck mass (122 orders of magnitude larger), or supersymmetry breaking scale, or finally, the electroweak mass scale (54 orders of magnitude off). Moreover, it seems really a coincidence that the energy density stored in the form of Λ and matter appears to be of the same order of magnitude *just* today, $\Omega_\Lambda \sim 0.75$ and $\Omega_{B+DM} \sim 0.25$. If the cosmological constant had been larger it would have changed the whole structure formation history, while a smaller value would have been irrelevant for observations.

[23] This bound is also usually presented in terms of a lower limit on the Brans–Dicke parameter $\omega_0 \geq 400\,00$, the constant which weights the scalar field kinetic term in the Jordan frame and in the minimal model with $V(\varphi) = 0$, $F(\varphi) = \varphi$.

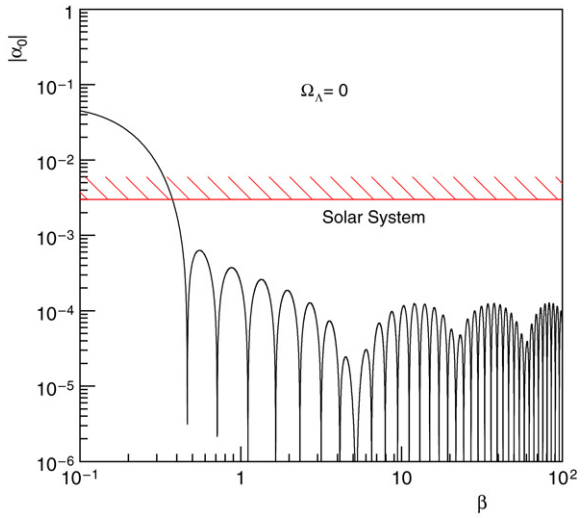

Fig. 22. Bounds on the post-newtonian parameters α_0 and β from ^{4}He in scalar-tensor theories in the case of a massless dilaton with quadratic coupling, $F(\varphi) = \exp(-\beta\varphi^2)$. The value of baryon density is $\Omega_B h^2 = 0.0224$. From [434].

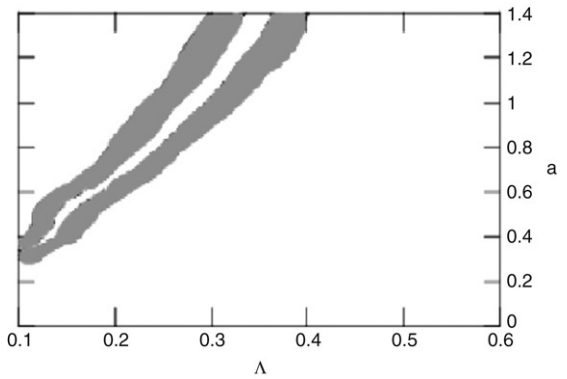

Fig. 23. Bounds on the parameters a and Λ which give acceptable results for ^{2}H/H, Y_p and ^{7}Li/H for a scalar-tensor theory defined by $\alpha = a\varphi^2$ and $V(\varphi) = \Lambda^2\varphi^4$. The initial conditions (pre-BBN) for φ are $\varphi_{in} = -1.3$, $\dot{\varphi}_{in} = 0$. From [450].

To solve (or to alleviate) these two related problems, many attempts have been made in the last two decades and based on the idea that the "dark energy" whose present value is given by Ω_Λ, is dynamically changing and is due to the evolution of a scalar field Q (the quintessence, k-essence, etc. field) see e.g. [456–467]. In particular, depending on the choice of the field potential, typically modeled as an exponential, $V(Q) = V_0 \exp(-\lambda Q/M_P)$ or an inverse power, $V(Q) = \lambda\Lambda^{4+a}/Q^a$, the field Q evolves according to an attractor-like solution of the equation of motions. This means that for a wide range of initial conditions at early times, the evolution of Q rapidly converges towards these solutions (tracker solutions), which lead naturally to a crossover from the radiation dominated epoch to a dark energy dominated era at late times.

If the Q-field provides a non-negligible contribution to the total energy density during radiation dominated regime, it follows that its early dynamics can be constrained by nucleosynthesis, and later on by CMB power spectrum. A first rough estimate can be obtained by requiring that at the neutron–proton decoupling temperature $T_D \sim$ MeV, the scalar field energy density Ω_Q should be small enough not to disturb the eventual amount of frozen neutrons, i.e. of the final ^{4}He mass fraction, see e.g. [460]. This bound can be cast in terms of the largest acceptable value for deviations of the effective number of neutrino from its standard value *at that particular temperature*, as in general the Q energy density would not scale simply as radiation

$$\Omega_Q(T_D) \leq \frac{7\Delta N_{\rm eff}/4}{10.75 + 7\Delta N_{\rm eff}/4} \leq 0.09, \tag{137}$$

where we have used our bound at 95% C.L. on $N_{\rm eff}$ of Section 5.

More detailed analysis have been presented in [468,445]. In [445], the authors consider as a model the particular potential of [469],

$$V(Q) = \left[(Q - Q_0)^2 + A\right]\exp(-\lambda Q), \tag{138}$$

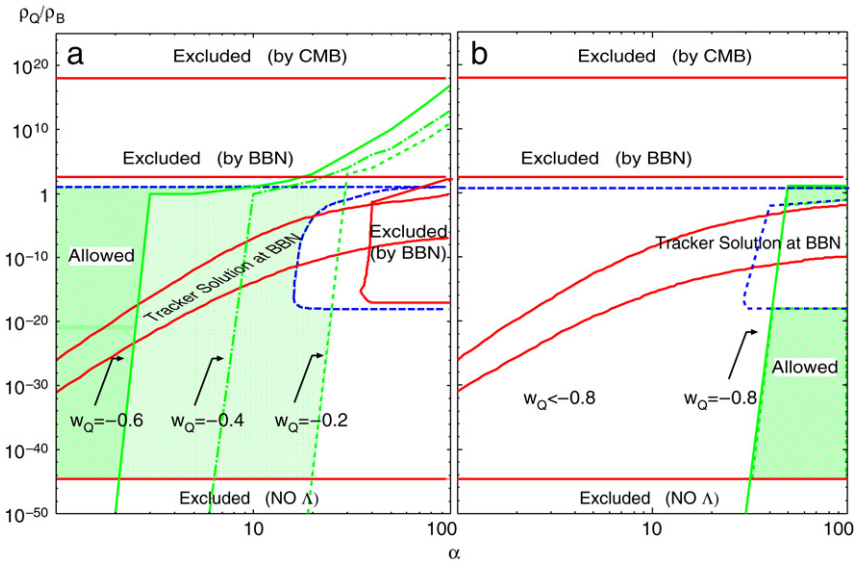

Fig. 24. Allowed values of the Q field potential parameter α and initial ρ_Q/ρ_B at $z = 10^{12}$ (B stands for "background", i.e. ordinary radiation and matter). The plots refer to power law (a) and SUGRA corrected potentials (b). Models in which the tracker solution is obtained by the BBN epoch are those in the band denoted by "Tracker Solution at BBN". Values of α to the right of the lines labeled $w_Q = -0.6, -0.4, -0.2$ are excluded by requiring that the present equation of state be sufficiently negative. The BBN constraint for a maximum energy density of the quintessence field of 0.1% and 5.6% are shown as dotted and solid lines, respectively. From [468].

and obtain the bound on the quintessence contribution to the total energy density during BBN $\Omega_Q \leq 0.12$, $\lambda \geq 5.7$ at 99% C.L. In [468] the analysis is performed for both the originally proposed inverse power potential of Ratra and Peebles [457],

$$V(Q) = M^{4+\alpha} Q^{-\alpha}, \tag{139}$$

and a modified version of it based on the hypothesis that the quintessence field be a part of supergravity models. In this case, for a flat Kähler potential, the potential receives an extra factor $\exp(3Q^2/2M_P^2)$. Their results are shown in Fig. 24, for the following choices of Y_p and ^{2}H/H

$$0.226 \leq Y_p \leq 0.247,$$
$$2.9 \times 10^{-5} \leq {}^2\mathrm{H/H} \leq 4.0 \times 10^{-5}. \tag{140}$$

The plots show the bound on the initial ratio of the Q field to background (B) (ordinary radiation and matter) energy density at initial redshift $z = 10^{12}$, assuming equipartition of Q energy at that epoch, $\dot{Q}^2/2 = V(Q)$, versus the potential parameter α. The regions denoted by "Tracker Solution at BBN" denotes models in which the evolution of Q has already reached the tracker solution. The main effect of BBN is to exclude a large family of possible kinetic-dominated solutions with a Q-energy density exceeding that of relativistic species prior or during nucleosynthesis.

8.3. Miscellanea

8.3.1. Testing Friedmann equation

We have already stressed several times that changing the expansion history in the early universe has a big impact on the BBN predictions for light nuclei abundance, in particular ^{4}He. Several modifications to the standard Friedmann equation have been already discussed, arising in a variety of contexts such as non-standard theory of gravity, time evolving Newton constant, or brane-world models. One may also try to perform somehow a *blind* test of the validity of Friedmann expansion law without a particular theoretical framework behind, and using a suitable parametrization of possible deviations from the standard behavior. This has been considered for example in [470], where the Hubble factor is expressed in terms of two parameters,

$$H(T) = H_1 \left(\frac{T}{1\ \mathrm{MeV}} \right)^{\alpha}, \tag{141}$$

where H_1 and the exponent α should be constrained by data, once we fix the baryon density parameter, η. A similar analysis has been performed in [471], with a slight different definition of $H(T)$. Using Eq. (141) one can compute the values of the three leading quantities which enter BBN dynamics: the freeze-out temperature, T_D, the time elapsed from T_D and the onset of BBN at T_N, and the value of the expansion rate at T_N. Interestingly, H_1 and α show a large degeneracy. The same Helium

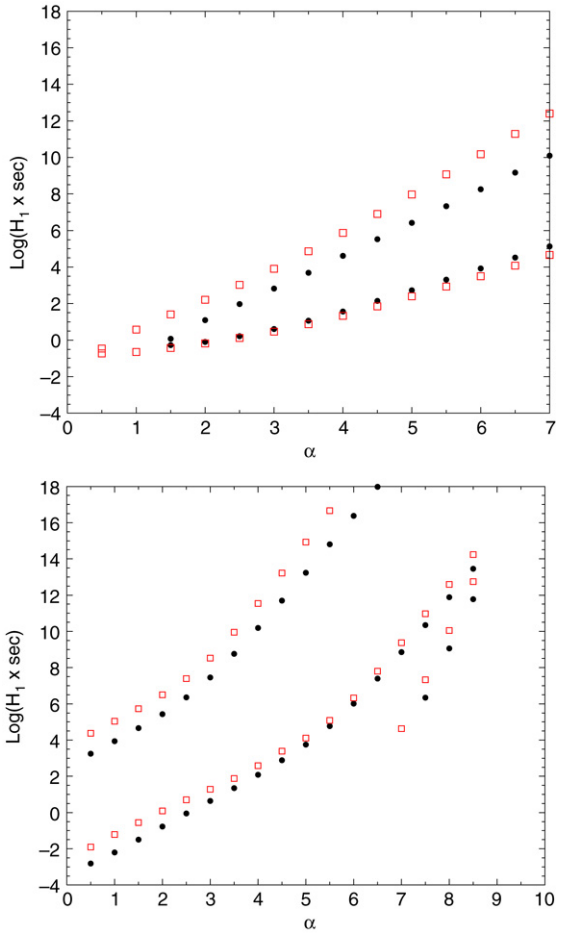

Fig. 25. Contours of constant helium (top) and deuterium (bottom) in the α-H_1 plane. Chosen values are $Y_p = 0.24$ and $^2\mathrm{H/H} = 3 \times 10^{-5}$. Squares and filled circles correspond to $\eta = 10^{-9}$ and $\eta = 10^{-10}$, respectively. From [470].

mass fraction and ^{2}H abundance can be obtained increasing at the same time the Hubble rate at every temperature (i.e. H_1), which raises the freezing temperature and thus leads to a larger initial neutron to proton density ratio, and the value of α (for a definite H_1 a larger α means a relatively lower expansion rate at T_N). Furthermore, for each nuclide there are two branches in the H_1–α plane for which Y_p or ^{2}H/H are the same, see Fig. 25: a lower branch, where also the standard result, $\alpha = 2$, $H_1 \sim$ MeV, is lying, and an upper branch, for higher values of H_1, which however cannot simultaneously fit both ^{4}He mass fraction and deuterium. The whole compatibility region is thus characterized by a single (almost) linear behavior, $\log(H_1) \propto \alpha$, with $1.5 \leq \alpha \leq 3$. This bound can also be used to constrain possible non-universal coupling of gravity to the three neutrino generations as considered in [471], where the study is also extended to the case of a degenerate BBN, or the possibility that matter and antimatter may have different couplings to gravity [472]. A different gravitational coupling to bosons and fermions, $G_{N,B}$ and $G_{N,F}$ respectively, has been instead considered in [473], with the result $0.33 \leq G_{N,B}/G_{N,F} \leq 1.10$ at 2-σ.

Similar analyses have been also applied in the framework of metric-affine gravity models, where the non-Riemaniann effects are encoded in a fictitious fluid with equation of state $P = \rho$ [474], or which account for the quantum gravity corrections for matter fields computed in a loop quantum gravity approach, with a non-canonical equation of state [475]. Finally, one can bound the values of parameters which measure departure from Lorentz invariance [476], see e.g. [477] for a review of the Lorentz- and CPT-violating extension of the SMPP.

The sensitivity of BBN to any modification of the Friedmann equation can be also exploited to test a specific prediction of general relativity, which has no analog in Newton theory, namely the fact that pressure contributes to the acceleration of the scale factor,

$$\frac{\ddot{a}}{a} = -\frac{4\pi G_N}{3}(\rho + 3P)\,. \tag{142}$$

Indeed the Friedmann equation *knows* about the pressure contribution in Eq. (142) via the Bianchi identity. If one allows for deviation from this distinctive feature of Einstein theory and introduces, as in [478], a free constant parameter, χ, which

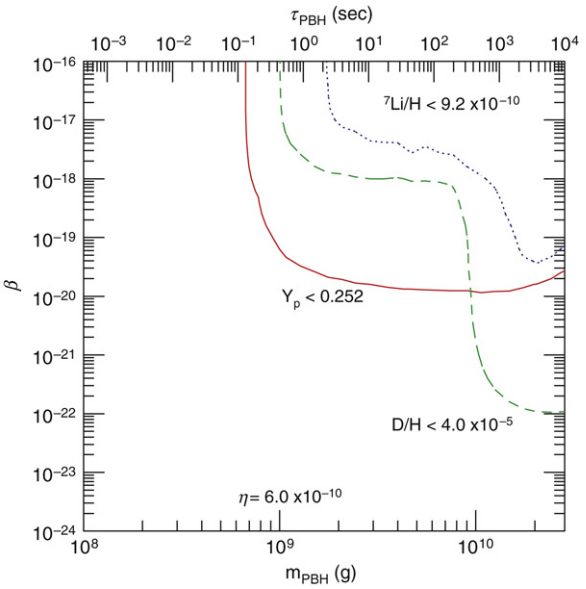

Fig. 26. The BBN bounds on the primordial black hole fraction versus their mass. Regions to the right and above the curves are excluded by primordial nucleosynthesis. From [491].

modifies the spatial component of Einstein's equations,

$$\frac{\ddot{a}}{a} = -\frac{4\pi G_N}{3}(\rho + 3\chi P)\,, \tag{143}$$

one obtains during a radiation dominated expansion (neglecting the spatial curvature term),

$$H^2 = \frac{1+\chi}{2}\frac{8\pi G_N}{3}\rho. \tag{144}$$

Bounds on χ can then be obtained from the BBN. Not surprisingly, the results of [478] show an excellent agreement with the standard expectation, $\chi = 1$. Notice that variation of this parameter is completely degenerate with a change of the Newton constant during the BBN, or a non-standard effective number of neutrinos $N_{\rm eff}$.

8.3.2. Primordial black holes and BBN

Primordial black holes may form in the early universe in presence of sub-horizon density perturbations of order unity [479–481]. Assessing cosmological constraints upon their density over some mass ranges can provide important information on the primordial density fluctuations. For a recent review see e.g. [482]. These constraints have been discussed by many authors in the 1970s [483–490], while updated analysis using BBN [491] and CMB data [492,493] have been presented quite recently. Primordial black holes evaporating by the BBN epoch ($t \leq 10^3$ s) have a mass lying in the range $M \leq 10^{10}$ g, since there is a simple relation between mass and lifetime, τ_{bh}, see e.g. [491],

$$M \sim 10^9 \left(\frac{\tau_{bh}}{\rm s}\right)^{1/3} {\rm g}. \tag{145}$$

They emit various particles such as neutrinos/antineutrinos, photons, quark-gluon jets which produce hadrons through fragmentation processes. All these (high energy) particles interact with species already present in the thermal bath, and induce several effects which can change the standard picture of light nuclei production. For example, production of high energy neutrinos and antineutrinos change the weak interaction freeze-out temperature, and thus the neutron to proton ratio. Similarly, large hadron injection after the weak process decoupling temperature T_D may revival chemical equilibrium between nucleons, thus leading to quite different amounts of ^{4}He and deuterium with respect to the standard case.

In Fig. 26 we report the results of [491] for $\beta(M)$, the primordial black hole initial fraction to the total energy density as function of their mass. The bound for 10^9 g $\leq M \leq 10^{10}$ g, $\beta(M) \leq 10^{-20}$ is strongly constrained by the upper bound on Y_p (they use $Y_p \leq 0.252$ in their analysis), since in this mass range the effect of black hole evaporation is to delay the freeze out of n–p chemical equilibrium. On the other hand, for larger masses and lifetimes, the extra produced neutrons cannot be burn into ^{4}He and thus contribute to deuterium abundance, which provides a stronger constraint in this region, $\beta(M) \leq 10^{-22}$.

8.3.3. Mirror world

The theory of a hidden mirror world, an exact duplicate of our visible world, is based on the product of two identical gauge symmetry group $G \times G'$, with G the SMPP group, $SU(3)_c \times SU(2)_L \times U(1)_Y$, in the minimal case. The two sectors

communicate through gravity and, possibly, by other interactions (kinetic mixing of photons and mirror photons,[24] neutrino mixing, common gauge symmetry of flavor) and are exchanged by the action of a discrete symmetry, the mirror parity, which implies that both particle sectors are described by the same action, and are characterized by the same particle content. For a review and a comprehensive list of references we address the reader to [495]. The mirror world would influence the whole evolution history of the universe through its contribution to the expansion rate, and can represent a natural candidate for dark matter, as well as providing a mechanism for baryogenesis. Of course, if mirror particles populate the primordial plasma with the same densities of ordinary particles, they would contribute to the effective neutrino number for a too large value $N_{\rm eff} \sim 6.14$ at the onset of BBN, which is excluded by light nuclei abundances. Thus, the mirror particle density should be reduced, and characterized by a plasma temperature, T', lower than the ordinary photon temperature, in order to be compatible with the bound on $\Delta N_{\rm eff}$. This can achieved if the inflationary reheating temperature is different in the two sectors, and all possible interactions between the two worlds are weak enough to ensure that they do not come into mutual thermal equilibrium.

The ratio T'/T can be computed by using entropy conservation. Use of the definition of Section 2 leads to

$$\frac{T'(t)}{T(t)} = \left(\frac{s'}{s}\right)^{1/3} \left(\frac{g_{*s}(T)}{g_{*s}(T')}\right)^{1/3} \equiv x \left(\frac{g_{*s}(T)}{g_{*s}(T')}\right)^{1/3}, \tag{146}$$

with s (s') the entropy density of ordinary (mirror) species. During the radiation dominated epoch we have

$$\begin{aligned} H(T) &= \left[\frac{8\pi G_N}{3}\frac{\pi^2}{30}\left(g_*(T)T^4 + g_*(T')T'^4\right)\right]^{1/2} \\ &\sim \left[\frac{8\pi G_N}{3}\frac{\pi^2}{30} g_*(T)(1+x^4)\right]^{1/2} T^2, \end{aligned} \tag{147}$$

where the last approximate equality holds as long as the value of x is not too small. On the other hand the parameter x can be re-expressed in terms of $\Delta N_{\rm eff}$. Since photons, electron/positron pairs and active neutrinos correspond to $g_* = 10.75$ we have

$$\Delta N_{\rm eff} = 6.14 x^4, \tag{148}$$

and thus the BBN bound $\Delta N_{\rm eff} \leq 0.4$ gives $x \leq 0.51$.

It is interesting to sketch how nucleosynthesis proceeds in the mirror world, in particular to compute the final yield of mirror ^{4}He. As usual one can use the limit that all (mirror) neutrons get bound in ^{4}He and compute the decoupling and deuterium formation time. In this case we have [496]

$$Y'_p \sim \frac{2\exp\left[-t(T_N)/\tau_n(1+x^{-4})^{1/2}\right]}{1+\exp\left[\Delta m/T_D(1+x^{-4})^{1/6}\right]}, \tag{149}$$

where it has been used the fact that the weak interaction decoupling temperature in the mirror world is larger than T_D by a factor $(1+x^{-4})^{1/6}$ and that, since $T'_N \sim T_N$ unless the mirror baryon density parameter η' is very different than η, the time of nucleosynthesis is $t\ (T' = T_N) = t(T_N)/(1+x^{-4})^{1/2}$. As noticed in [496], the estimate (149) is not valid for small x and $\eta' = 10^{-10} - 10^{-9} \sim \eta$, since in this case deuterium production can become ineffective, thus inhibiting the whole BBN reaction network. The result of Y'_p versus x as numerically computed in [496] is shown in Fig. 27. Notice that for large $\eta' \geq 10^{-8}$ the value of Y'_p is in good agreement with the estimate provided by Eq. (149). Indeed, this large η'/η regime is particularly interesting, since it corresponds to a sizeable contribution of mirror baryons to the present energy density of the universe,

$$\frac{\Omega'_B}{\Omega_B} = x^3 \frac{\eta'}{\eta}. \tag{150}$$

In this case mirror baryons might constitute the dark matter or one of its components.[25] In view of the bound on x, this requires a large value for the ratio $\eta'/\eta \geq 10$, so that the mirror world would contain a considerably bigger fraction of ^{4}He than the visible world. Further details on the thermodynamics of the early Universe with mirror dark matter are available in [499].

24 BBN and CMB bounds on the mixing of photon with a hidden light abelian gauge boson have been recently considered in [494].

25 The growth of perturbations and the power spectrum in presence of a sizeable mirror baryon density has been studied in [496,497] and in more detail in [498] and reference therein.

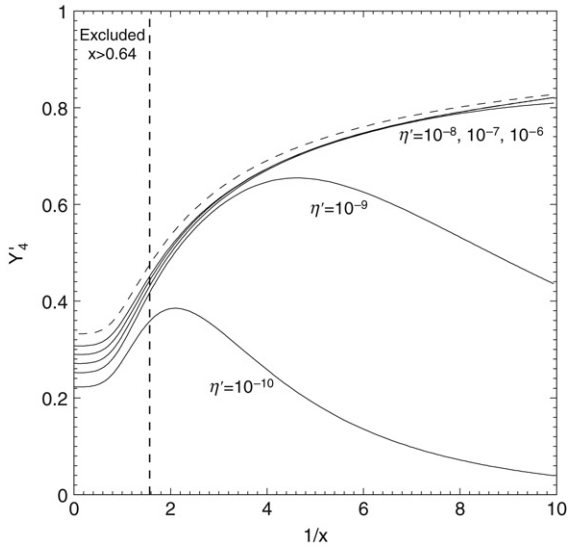

Fig. 27. The primordial mirror ^{4}He mass fraction as a function of x (see Eq. (146)). The dashed curve is the approximate result of Eq. (149). The solid curves are obtained via exact numerical calculation. From [496].

9. Massive particles & BBN

The existence in the primordial plasma of one or more species of massive particles ($m_X \gg m_e$) besides baryons is at very least a likely possibility, given the numerous pieces of evidence in favor of the existence of dark matter (DM). A wide variety of observations suggests that most of the matter in the universe is not in a visible form (with $\Omega_{DM} \simeq 5\Omega_B$), and several of them also imply that *DM* is non-baryonic and cold, i.e. made by particles with a non-relativistic momentum distribution. Direct and indirect evidence, starting more than seventy years ago with the orbital velocities of galaxies within clusters [500], now also includes the rotational speeds of galaxies [501], gravitational lensing [502,503], the cosmic microwave background [8], the large scale structure [455], and the light element abundances themselves [11].

At first sight, it might appear that *DM* has no impact on BBN since the expansion of the universe at the BBN epoch is dominated by radiation, and the presence of additional massive particles at the BBN epoch is thus dynamically irrelevant. We recall that, for example, the analysis of [470,471] without assuming strong priors on η show that the behavior of the Hubble parameter should be very close to the radiation dominated regime during the BBN, see Section 8.3. Once the WMAP prior on η is used, this result would narrow even further. Thus, even from an observational point of view, any effect due to massive particles at the BBN must be of non-gravitational nature.

Additional couplings for the *DM* particles are far from being a remote possibility: there are instead strong motivations which point to a connection between dark matter and the electroweak scale. A stable particle with an electroweak scale mass and couplings would naturally be produced in the thermal bath of the early universe in an amount similar to the observed matter abundance [504]. From a particle physics perspective, the hierarchy problem appears to require new physics at or above the electroweak scale. Furthermore, stringent constraints from electroweak precision measurements (and from the stability of the proton) indicate that these new particles respect symmetries which limit their interactions. Such symmetries can also lead to the stability of one or more of the new particles, such as the lightest exotic particle in the spectrum of R-parity conserving supersymmetry, K-parity in universal extra dimensional models, or T-parity in little Higgs models. For a review of *DM* models, see e.g. [505].

Dark matter cannot bring electric charge by definition (otherwise it would be visible) and – although the reason is less obvious – it appears that it cannot be strongly interacting (see [506] and reference therein for a recent overview of the stringent bounds on such scenarios). However, *DM* might be produced as a decay product of charged (or strongly interacting) progenitors, and there are also viable particle physics scenarios where this can take place, the most popular of which being the so-called super-WIMP scenario [507]. Charged or strongly interacting metastable particles at the BBN epoch may form bound systems with baryons, altering the nuclear reactions pattern and thus the yields of light elements. The analysis of this scenario, which goes under the name of "catalyzed nucleosynthesis", is addressed in Section 9.2. On the other hand, particles which decay (or annihilate) into Standard Model products, even if only weakly interacting, may affect BBN via the cascades they induced in the plasma: the injection of secondaries triggers directly or indirectly non-thermal reactions, altering again standard BBN predictions. Of course, if the lifetime satisfies $\tau_X \ll 1$ s, the particles have decayed well before the BBN and no meaningful bound can be derived.

In general, annihilations have a similar effect as decays, the main difference being the time (or redshift) distribution of the injection: for decays the rate per unit volume is n_X/τ_X, while for annihilations is given by $n_X n_{\bar{X}} \langle\sigma v\rangle$. If we parameterize $\langle\sigma v\rangle \propto \sigma_n (T/m_X)^n$ ($n = 0$, 1 correspond then to s-wave and p-wave annihilation respectively), in the early universe when

homogeneity is a good approximation, the former gives an injection rate scaling as $(1+z)^3$, or $(1+z)^{6+n}$ for annihilations. In the following, unless otherwise stated, we will generically refer to "decays" to indicate any mode of injection of energetic particles in the plasma, thus implicitly including the annihilating case. Some specific features of the annihilation injection mode will be discussed at the end of Section 9.1.2.

9.1. Cascade nucleosynthesis

The phenomenology of non-thermal BBN bounds strongly depends on the branching ratios of the secondaries the X particle decays into: the hadronic, electromagnetic (photons, $e^{\pm}$), neutrino or inert (exotic invisible) ones. The last case requires two or more (meta)stable particles, which does not happen very naturally in most realistic models of physics beyond the SMPP. Perhaps, one exception is provided by the case of the axino decaying into a gravitino and an axion, see e.g. [508]. In general, the only constraint in this case comes from the requirement that the universe at $T \sim 0.1$ MeV is radiation-dominated, which implies

$$\rho_X = m_X\, n_X \lesssim \rho_\gamma \Leftrightarrow \left(\frac{m_X}{0.1\ \mathrm{GeV}}\right)\left(\frac{n_X}{n_\gamma}\right) \lesssim 10^{-4}. \tag{151}$$

We do not treat this scenario and its constraints further. For more details, see for example [509].

It is worth noting that even a decay into neutrinos $X \to Y + \nu$ has effects on the BBN. The effects are two-fold: (i) energetic neutrinos can create charged leptons by annihilation onto the thermal neutrino background[26]; although with a suppressed efficiency, sufficiently high energy neutrinos can also produce pions via $\nu + \bar{\nu}_{th} \to \pi^+ + \pi^-$ which affect the p–n equilibrium. (ii) electromagnetic (and possibly hadronic) showers are induced by 3 or 4 body decay channels via a virtual or real weak boson propagator, like $X \to Y + \nu + e^+ + e^-$; the previous final state is always considered as kinematically allowed, when a tree level $X \to Y + \nu$ is included in the analysis, since – given the binding energies of nuclei – to induce any change to BBN the phase space available must be $\gg 1$ MeV anyway. The importance of these sub-leading channels for phenomenological constraints from astrophysical arguments has also been emphasized in other contexts [510,511]. We address the reader to [512] for a more thorough analysis. In the remainder of this section we describe electromagnetic cascades (Section 9.1.1) and hadronic ones (Section 9.1.2). It is worth noting that, for a very broad range of lifetimes involved ($0.1\ \mathrm{s} \lesssim \tau_X \lesssim 10^{12}$ s), the thermalization of the secondaries takes place in a time which is negligible with respect to the Hubble time, and therefore redshifting of particles can be safely neglected.

9.1.1. Development of the electromagnetic cascade

There are some features of the electromagnetic cascades in the primordial plasma which significantly simplify the treatment with respect to hadronic ones. When the injected e^+, e^-, γ are energetic enough, the cascade develops very rapidly by a combination of two processes: the pair-production on the CMB thermal distribution ($\gamma + \gamma_{\mathrm{CMB}} \to e^+ + e^-$) and the inverse Compton scattering of the non-thermal electrons and positrons ($e^{\pm} + \gamma_{\mathrm{CMB}} \to e^{\pm} + \gamma$) off the CMB photons [513–517]. There is a critical energy, $E_C(T)$, above which the non-thermal spectrum is quickly cutoff by pair-production, leaving virtually no photon available to photo-dissociate the few available nuclei.[27] Although the typical energy for pair-producing on the bulk of the CMB distribution is $m_e^2/\langle E_{\mathrm{CMB}}\rangle \simeq m_e^2/2.7\,T$, since reactions on the energetic tail of the distribution are also important, E_C turns out to be smaller: Numerical calculations estimate $E_C \simeq m_e^2/22\,T$ [517] or $E_C \simeq m_e^2/23.6\,T$ [516]. By equating E_C to the ^{2}H and ^{4}He binding energies of 2.2 MeV and 19.8 MeV respectively, one infers the keV-scale characteristic temperatures below which a small but non-negligible fraction of γ's (at the percent level) is available to photodisintegrate the light nuclei. This is why meta-stable particles with a too short lifetime cannot significantly affect thermal BBN yields. Meaningful bounds on electromagnetic cascades are only achieved if $\tau_X \gtrsim 10^5$ s for deuterium dissociation and $\tau_X \gtrsim 10^7$ s for the more tightly bound ^{4}He (in a radiation-dominated universe $t \propto T^{-2} \propto E_C^2$).

Another interesting feature is that the e.m. cascade develops so rapidly that most of the effect depends only on the total amount of injected energy E_0 and the time of injection, rather than the nature and energy of the primary. It is customary to define a parameter representing the energy stored in meta-stable particles before the cascade begins (hence the zero subscripts), for example $\zeta_X \equiv m_X\, n_{X,0}/n_{\gamma,0}$, which together with the decay time τ_X characterizes almost completely the process. A quasi-universal shape of non-thermal photons is reached very quickly. Numerical simulations have found a spectrum below E_C well approximated by [516,517]

$$\frac{\mathrm{d}N_\gamma}{\mathrm{d}E_\gamma} = \begin{cases} K_0 \left(\dfrac{E_\gamma}{E_X}\right)^{-3/2} & \text{for } E_\gamma < E_X \\ K_0 \left(\dfrac{E_\gamma}{E_X}\right)^{-2} & \text{for } E_X \le E_\gamma \le E_C, \end{cases} \tag{152}$$

[26] In principle, they can also upscatter $e^{\pm}$ in the plasma, but decays are only relevant when $T \ll 1$ MeV, when almost no charged particle populate the plasma.

[27] No e^+, e^- remain instead available for electro-disintegrations, since the cross-section with the abundant CMB photons is effective to quickly cool them down to thermal energies.

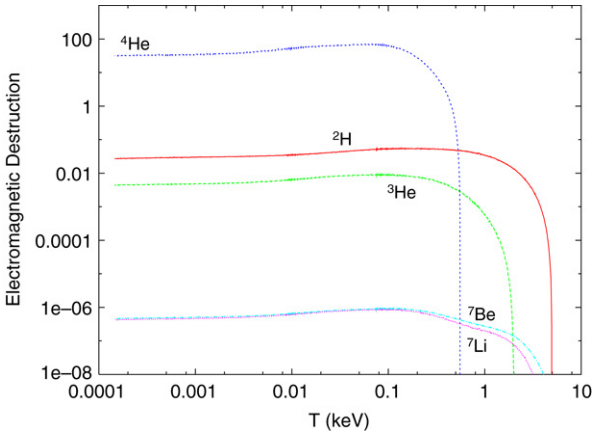

Fig. 28. Number of destroyed nuclei per TeV of electromagnetically interacting energy injected in the plasma at temperature T. From [518].

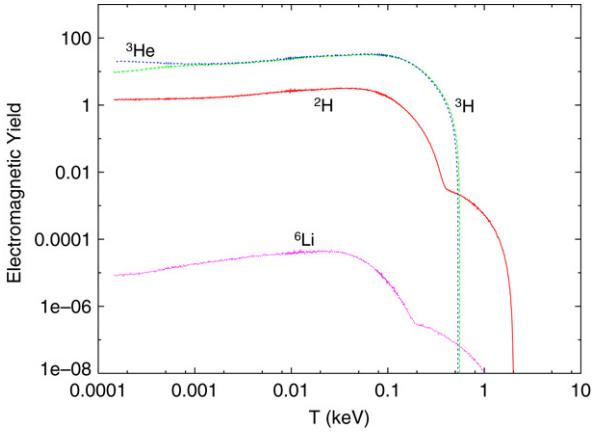

Fig. 29. Number of produced nuclei per TeV of electromagnetically interacting energy injected in the plasma at temperature T, due to photodisintegration and fusion reactions. From [518].

where $K_0 = E_0/(E_X^2[2 + \ln(E_C/E_X)])$ is a normalization constant such that the total energy in γ-rays below E_C equals the total energy E_0 injected. One has $E_X \approx 0.0264E_C$ according to Ref. [516], or $E_X \approx 0.03E_C$ according to [514]. A more accurate calculation of the evolution of this spectrum should include interactions of these "break-out" photons via photon–photon scattering $\gamma + \gamma_{\rm CMB} \to \gamma + \gamma$, (mainly redistributing the energy of energetic γ-rays right below energy E_C), Bethe–Heitler pair production $\gamma + p(^4\mathrm{He}) \to p(^4\mathrm{He}) + \mathrm{e}^- + \mathrm{e}^+$, Compton scattering off thermal electrons $\gamma + \mathrm{e}^- \to \gamma + \mathrm{e}^-$ (with the produced energetic e^- in turn inducing inverse Compton scattering and thus further low-energy γ's) and, of course, nuclear photodisintegration, which directly affects BBN.

In Fig. 28 we show the amounts of destroyed nuclei per TeV of injected electromagnetic energy, E_0, at a temperature T. The sharp rises at characteristic temperatures are due to the pair production threshold effect for energetic γ, which depend on the binding energy. In Fig. 29 we show a similar plot for the nuclei *produced* as a result of the dissociations. It is evident that, although a minor amount of ^{2}H starts to be produced from spallation of ^{3}He already at $T \simeq 1$ keV, a major secondary production of ^{2}H, ^{3}H and ^{3}He happens at $T \lesssim 0.5$ keV, when ^{4}He photodisintegration becomes relevant. In this range, not only does ^{2}H, ^{3}H and ^{3}He production over-compensate their photodisintegration (which takes place at a slower rate) but a significant synthesis of ^{6}Li is induced by the non-thermally produced ^{3}H and ^{3}He, with a subleading contribution from direct photodisintegration of ^{7}Li and ^{7}Be. For a compilation of the reactions involved in the cascade nucleosynthesis calculations, we address the reader to the excellent review [518]. Also, some relevant new nuclear astrophysics data and their implications for BBN have been presented in [519].

In Fig. 30 we show a typical result for the excluded regions in the plane ζ_X–τ_X (where 0 refers to a time $t \ll \tau_X$), in this case taken from [189]. In the left panel only deuterium constraints are considered, in the right panel constraints from all elements are included. The light blue regions are excluded due to underproduction of deuterium: in the left shoulder at relatively small τ_X this is due to the fact that direct photodestruction of ^{2}H dominates. For $\tau \gtrsim 10^7$ s ^{4}He destruction is important, and leads typically to over-production of ^{2}H, unless the injected energy is so high that in turn even this secondary deuterium is destroyed (upper-right corner of the plot). In this parameter range, typically even ^{4}He and ^{7}Li are destroyed to a level inconsistent with observations, but these additional constraints basically overlap with the deuterium ones. On the

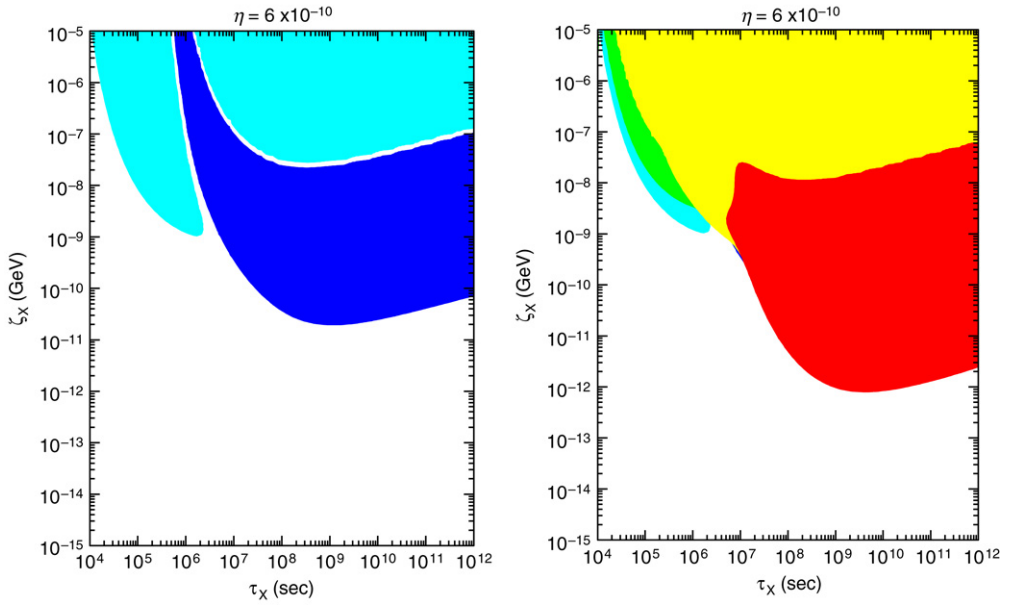

Fig. 30. Regions of the parameter space ζ_X–τ_X excluded by: left panel: ^{2}H overproduction (dark blue) or ^{2}H under-production (light blue); right panel: including also the constraints from overproduction of ^{6}Li (dark red), shown on the top of the ^{7}Li (yellow) and ^{4}He (green) constraints. From [189].

other hand, if one considers ^{6}Li production from non-thermally produced $A = 3$ nuclei, one can also disfavor the red region shown in the right panel due to over-production of ^{6}Li, which is however less robust due to the likely reprocessing of this fragile isotope in the observed stellar systems. Note that if the metastable particle is the progenitor of the *DM* candidate, it must fulfill the condition $m_X\, n_X \gtrsim 4\, m_p\, n_B$, i.e. a typical value for ζ_X fulfills $\zeta_X \gtrsim 2 \times 10^{-9}$ GeV. Larger values imply a very large mass difference between the X particle and the *DM* candidate, smaller values refer to metastable particles which account at most for a sub-leading fraction of the *DM* today. So, a way to summarize previous constraints is to say that BBN excludes electromagnetically decaying particles as progenitors of *DM* when their lifetime is longer than $\tau_X \gtrsim$ few $\times\, 10^5$ s.

9.1.2. Including hadronic channels

Generally, in the decay of the X particles one expects both hadronic and electromagnetic channels. The treatment of cascades in presence of hadrons is significantly more involved, since it introduces more particles, more timescales and more processes to take into account. The flow-chart in Fig. 31 summarizes the decay scheme and physical processes involved. Note that a hadronic branching ratio unavoidably leads to secondary electromagnetic showers, which affect BBN along the lines described in Section 9.1.1. To have a first qualitative understanding of the effects of hadronic particles, it is worth recalling that different hadronic species interact in the plasma via a few reactions, which assume different relevance at different times:

- *mesons*, mostly $\pi^\pm$ and kaons (with rest frame lifetime in the 10^{-8} s range), have only an effect at times $t \approx 1$–10 s, when ordinary weak interactions are not efficient anymore, but they still have time to interact before decaying. They mostly act by enhancing the n/p ratio and thus the final value of Y_p.
- *antinucleons*, by the preferred tendency to annihilate onto protons, have a similar final effect of increasing n/p. Compared with mesons, they also have an additional peculiar effect at later times ($t \simeq 10^2$ s) by annihilating onto Y_p and leaving ^{2}H, ^{3}H, and ^{3}He among secondaries.
- *nucleons*, at early times, nucleons thermalize via electromagnetic processes: magnetic moment scattering off $e^\pm$ for neutrons, Coulomb stopping off $e^\pm$ and Thomson scattering off thermal photons for protons. However, at late times other energy loss mechanisms start to dominate for high energy nucleons, namely nucleon–nucleon collision and nuclear spallation reactions. Due to the different electric charge, these nuclear processes are already dominant for neutrons at $t \gtrsim 200$ s, while for protons only at $t \gtrsim 10^4$ s. When they are effective, a cascade nucleosynthesis can take place: each nucleon–nucleon scattering will produce another energetic nucleon (a single 100 GeV nucleon can produce several tens of 10 MeV nucleons) and their effect of spallation over ^{4}He will produce many ^{2}H, ^{3}H, and ^{3}He nuclei. The total effect will be more efficient than for antinucleons: a single 100 GeV antimatter particle has a much shorter mean free path before annihilating with a ^{4}He nucleus and produce the mentioned secondaries, and nucleon induced production is therefore much more efficient. Non-thermal nucleon injection lead to an increased Y_p abundance at $t \leq 200$ s, increased ^{2}H abundance at 200 s $\leq t \leq 10^4$ s, or decreased ^{7}Li abundance at $t \approx 10^3$s. Spallation of ^{4}He to produce ^{2}H, ^{3}H, and ^{3}He may have as a secondary effect the synthesis of ^{6}Li.

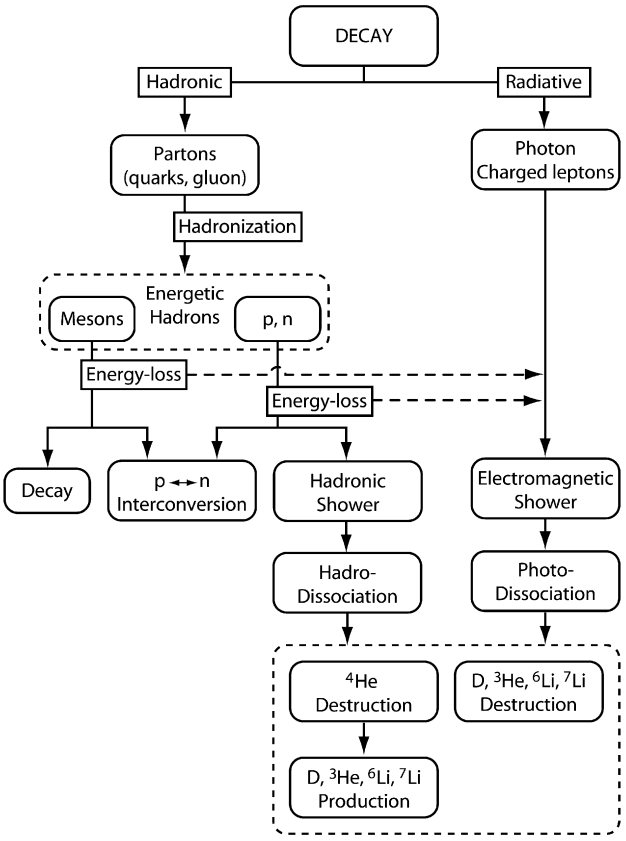

Fig. 31. Flow-chart of the decay effects on BBN. From [520].

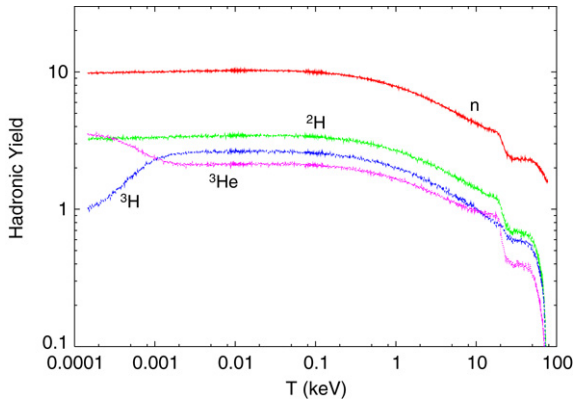

Fig. 32. Light element nuclei yields for a particle of mass $m_X = 1$ TeV decaying as $X \to q\bar{q}$ as a function of the temperature T of the cascade injection in the plasma. From [518].

To illustrate this point, in Fig. 32, we report the light element yields produced by the decay $X \to q\bar{q}$ of a single metastable particle with mass $m_X = 1$ TeV, as a function of the photon temperature at which the injection takes place. It is interesting that initially, after hadronization of the quark–antiquark state, on average only 1.56 neutrons result; all others are created at $T \leq 90$ keV by the thermalization of injected neutrons and protons due to inelastic nucleon–nucleon scattering and ^{4}He spallation. Similarly, all the ^{2}H, ^{3}H, and ^{3}He nuclei are due to ^{4}He spallation processes and n–p nonthermal fusion reactions (for ^{2}H) induced by the thermalization of the injected energetic nucleons.

For a more quantitative analysis, a numerical treatment is required. Technically, the problem of solving cascade nucleosynthesis is highly non-trivial, especially in presence of significant hadronic branching ratios. One major difficulty is that one cannot study the non-thermal effects independently of the earlier standard BBN stage, as it is possible (at least as first approximation) in the case of electromagnetic cascades. Although already in the 80's several authors have

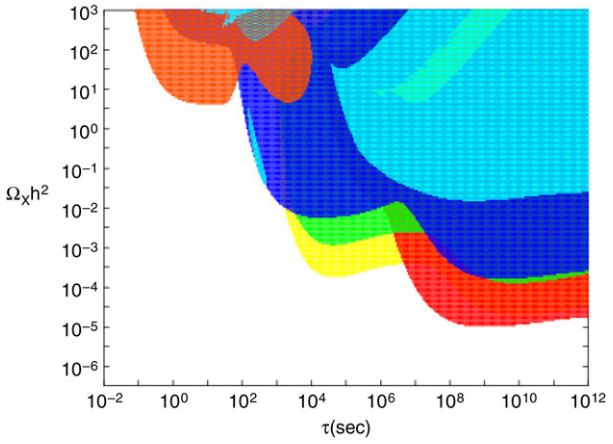

Fig. 33. Conservative BBN constraints on the abundance of relic decaying neutral particles as a function of their lifetime; particle mass is $m_\chi = 1$ TeV and the hadronic branching ratio $B_h = 3.33 \times 10^{-2}$. $\Omega_\chi h^2$ is the contribution neutral particles would have given to the total relic density today, would they have not decayed. Colored regions are excluded and correspond to constraints imposed by observations (see text). From [518].

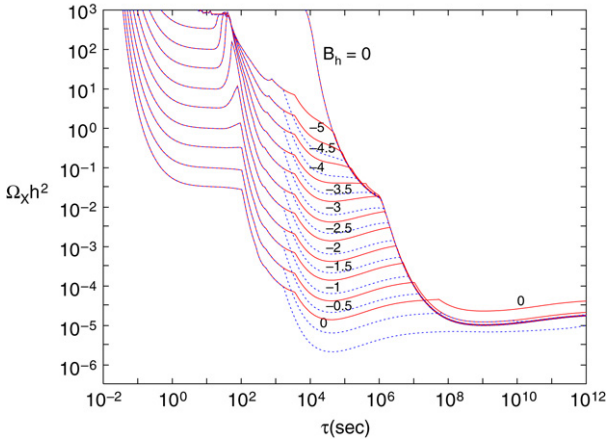

Fig. 34. Constraints on the relic abundance of neutral decaying particles as a function of their decay time, for a particle mass $m_\chi = 100$ GeV and varying branching ratio, B_h. Numbers in the picture refer to the solid line above and stand for the corresponding $\log_{10} B_h$. Dotted lines are the actual constraints if one considers the less conservative ^{6}Li/^{7}Li. From [518].

estimated the effects of injecting a non-thermal population of particles in the plasma at the BBN epoch, only recently several authors have followed *self-consistently* the reactions taking place during their thermalization and coupled them to the simultaneously ongoing thermal nuclear network [521–523,518]. The latest treatments typically adopt a Monte Carlo technique to calculate the interaction probability of the particle shower, and codes such as PYTHIA are employed to determine the energy distribution of the shower particles given the initial branching ratios in the decay. Nucleon energy losses must be taken into account as well. For a more detailed overview of the scheme and techniques of the numerical treatment, see e.g. [520,518].

The resulting constraints can be presented similarly to the ones for e.m. decays, still it is crucial to specify not only the injected energy, but also the hadronic branching ratio, B_h. For example, in Fig. 33 we report the BBN constraints derived in [518] for the decay of particle of mass $m_X = 1$ TeV and hadronic branching ratio, $B_h = 3.33 \times 10^{-2}$. The quantity $\Omega_X h^2$ is the contribution that neutral particles would have given to the total energy density today, would they have not decayed, and is proportional to the parameter ζ_X introduced in the previous section ($\Omega_X h^2 = (M_X n_X^0 h^2)/\rho_{cr} = (n_\gamma^0 h^2/\rho_{cr})\zeta_X \simeq 3.9 \times 10^7 \zeta_X$/ GeV). Colored regions are excluded and correspond to constraints imposed by upper limit for Y_p (orange area), upper limit on ^{2}H (blue), upper limit on ^{3}He/^{2}H (red), and lower limit on ^{7}Li (light blue). The yellow region violates the less conservative bound from ^{6}Li/^{7}Li. References for observational abundances used to get these constraints, which partly differ from the ones we have compiled in Section 4, can be found in the original paper [518].

As a consequence of the different mechanisms dominating at different times, the most stringent constraints are given by: the overproduction of ^{4}He at early times ($\tau_\chi \leq 10^2$ s), overproduction of ^{2}H for 10^2 s $\leq \tau_\chi \leq 10^3$ s, overproduction of ^{6}Li for 10^3 s $\leq \tau_\chi \leq 10^7$ s, and an overproduction of the ^{3}He/^{2}H ratio for $\tau_\chi \geq 10^7$ s. Fig. 34 illustrates how the constraints

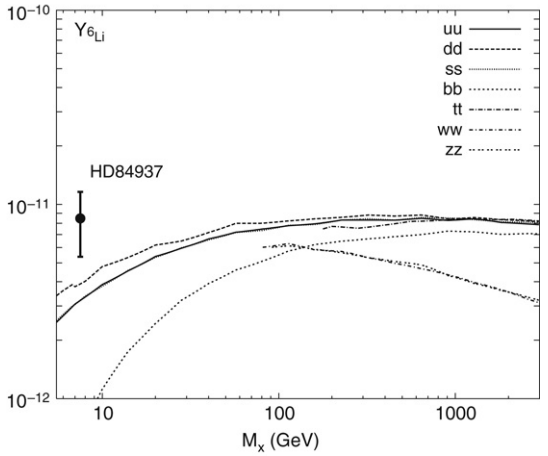

Fig. 35. The abundances of ^{6}Li as produced in scenarios with hadronic cascades injected by neutralino annihilation, for different channels, as labeled. The annihilation rate is taken to be $\langle\sigma v\rangle = 10^{-25}$ cm^3/s. From [522].

depend on the branching ratio, B_h, this time for a particle mass, $m_\chi = 100$ GeV, with the allowed region below the lines. In the limit $B_h \to 0$, one recovers bounds due to the e.m. channels, while even for $B_h \sim 1\%$ metastable particles with a relic abundance comparable to today's *DM* one are excluded if $\tau_X \gtrsim 10^2$ s. Of course, one can turn the argument around and explore the possibility that decays may *explain* some discrepancies existing between the SBBN model and observation. In particular, both "lithium problems" mentioned in Section 4.5 may be solved by hadronically decaying particles with lifetime ∼2000 s (see e.g. Fig. 2 in [560,524]). It is worth mentioning that in some of these scenarios "low-energy" observables (like the properties of gravitino dark matter) would be linked to very high energy physical scales, as the reheating temperature and the leptogenesis scale, see for example [559,561,525].

In case of an annihilation mode, the major peculiarity is that in order to have the same injection rate of a decay at an epoch $z_{\rm inj}$, a very large annihilation rate at epochs $z > z_{\rm inj}$ is required. Typically, in order to produce significant modifications of the light element yields, often an unphysically large $\langle\sigma v\rangle$ is required. Stronger bounds follow then from non-BBN considerations, unless a relatively light particle ($m_X \lesssim$ few GeV) is considered (see e.g. [526]). A possible exception is provided by the ^{6}Li nuclide. It has been shown that, for typical electroweak-scale WIMP masses, the primordial ^{6}Li yield from DM annihilation exceeds the SBBN abundance for any $\langle\sigma v\rangle > 10^{-27}$ cm^3/s [527,522].

This is illustrated in Fig. 35: interestingly for the annihilation rate required to produce the correct WIMP DM thermal relic abundance, an $\mathcal{O}(100)$ GeV DM particle produces an amount of ^{6}Li in the same range required to explain observational claims of ^{6}Li.

9.2. Catalyzed BBN

The constraints derived in the previous section assume that, before decaying, the meta-stable particle *X* is "inert". While *DM* can not be charged or strongly interacting, there is no a priori reason why its parent particle should bring no electric or strong charge. Whenever this happens, the possibility arises that *X* particles may form bound systems with baryons, altering the nuclear reaction pattern and thus the yield of light elements. This scenario is currently known as catalyzed BBN (CBBN). The cosmological role of charged massive particles (CHAMPs) was already considered in the late 80's [528–530], but the influence of bound states in BBN has only been fully appreciated recently. In 2006, within a few weeks three papers appeared pointing out the importance of CBBN [531–533] and identifying the main physical mechanisms responsible for the alteration in the nuclear network. In the last two years, several articles have followed, clarifying the physical ingredients regulating this complex scenario, including refinement in the calculation of catalyzed reactions, late-time nucleosynthesis, etc. [523, 534–537,524,538–543]. A quite complete review of the physics can be found in [524], which we shall mainly follow for the present summary. We limit ourselves to consider singly charged CHAMPs, although it has been argued that negative doubly charged and *stable* CHAMPs bound to ^{4}He^{++} may be viable as *DM* candidates in walking technicolor theories [544]. It is worth noting that, at least qualitatively, one expects similar catalytic mechanisms if the particle *X* is strongly interacting, rather than being electrically charged. One physically motivated scenario of this kind is the long-lived gluino in split-SUSY [545–547]. Some calculations of the primordial nucleosynthesis in presence of massive, strongly interacting particles have been performed in the past (see [548,549]), where bound states with "ordinary" nuclei were considered. The main difficulty with this scenario is that the nuclear physics of such bound states is very hard to treat reliably. For example, analogies with toy-models used to describe hypernuclei are employed [550] and the description of the bound systems is at best parametric. An accurate treatment is made highly non-trivial by the effects of non-perturbative physics, and we shall not consider them

Table 15
Binding energies E_b in the Bohr approximation $|E_b| \simeq Z^2\,\alpha\,m_A/2$ and photo-dissociation decoupling temperatures T_{ph} in keV (as calculated in [531]) for exotic bound states AX.

Bound state	pX	^{2}HX	^{3}HX	^{3}HeX	^{4}HeX	^{7}LiX	^{7}BeX	^{8}BeX
$\lvert E_b\rvert$	25	50	75	299	397	1566	2787	3178
T_{ph}	0.6	1.2	1.8	6.3	8.2	21	32	34

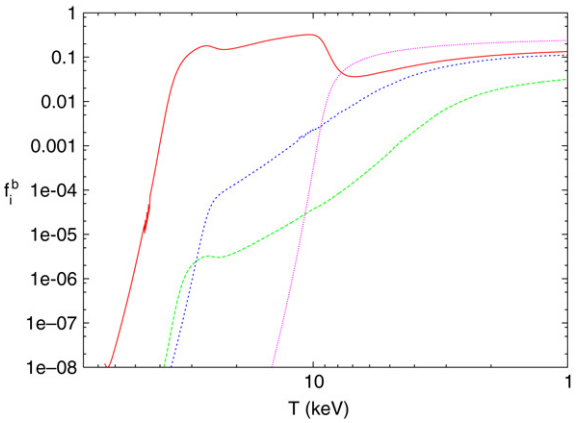

Fig. 36. Bound state fractions $f_A^b \equiv n_{AX}/n_A^{tot}$ of nuclei A bound to CHAMP X^- as a function of temperature T, for a model with $M_X = 100$ GeV and $\Omega_X h^2 = 0.1$. Shown are f_A^b for ^{7}Be solid (red), ^{7}Li long-dashed (green), ^{6}Li short-dashed (blue), and ^{4}He dotted (purple), respectively. From [524].

further. We want to remark, however, that the BBN cascade bounds that are sometimes considered in the literature for such particles (see [551]) may be altered, since catalytic effects are completely neglected.

9.2.1. Early time CBBN: Formation of bound states and catalysis

A negatively charged, long lived particle X (or CHAMP) with mass $M_X \gg m_p$ would form bound-states with nuclei and alter the network of reactions leading to the synthesis of light elements. Compared with a generic nucleus A of charge Z and mass m_A, its corresponding bound state with a CHAMP, AX, has a mass higher by $\sim m_X$, a charge lower by one unit $(Z-1)$, and it is characterized by an AX binding energy given by $E_b \simeq Z^2\,\alpha\,m_A/2$ in the limit $m_A \ll m_X$. Another interesting quantity is the photo-dissociation temperature T_{ph} of the AX system, defined as the temperature at which the photodissociation rate, $\Gamma_{ph}(T)$, for the bound nucleus becomes smaller than the Hubble rate, $H(T)$. Roughly speaking, below T_{ph} the AX system is stable against photodestruction. In Table 15 we report binding energies in the Bohr-like atom approximation (corrections are of order $\sim$10% for ^{4}HeX, up to 50% for ^{7}BeX) and the T_{ph}, as originally calculated in [531]. A precise calculation of the fractional abundance of bound nuclei requires solving the Boltzmann equation, including all relevant reactions for the AX state. The inadequacy of simple approaches based on the Saha equation to determine the evolution of the AX abundance was realized immediately in [531] and further analyzed e.g. in [532,523]. However, even the latter analysis had to rely on strong approximations on the reaction rates for bound nuclei (that the bound state nucleus would be destroyed in the interaction, and that standard BBN is over at the time CBBN takes place, etc.). Fig. 36, which we take from the more recent and accurate analysis in [524], shows the evolution of bound state fractions $f_A^b \equiv n_{AX}/n_A^{tot}$ of nuclei A bound to X as a function of temperature T, for a model with $m_X = 100$ GeV and $\Omega_X h^2 = 0.1$. It confirms that the behavior of f_A^b is significantly different than that expected from simple estimates by the Saha equation due to nuclear destruction of bound states and slow recombination rates (with respect to the Hubble time). This is particularly relevant in $f_{^7\mathrm{Li}}^b$ due to the ^{7}Li$X(p,X)\,2^4$He reaction.

Once CHAMP-nuclei states XA are formed in the plasma, each nuclear reaction will have its CHAMP homologue:

$$\begin{aligned} \text{standard BBN:}\quad & A + A_1 \to A_2 + A_3, \\ \text{CBBN:}\quad & AX + A_1 \to A_2 + A_3 + X. \end{aligned} \tag{153}$$

At first sight, the main advantage of CBBN reactions is the smaller Coulomb barrier. However, there is a more subtle effect – whose importance was already recognized in [531] – which acts on homologues of radiative captures, i.e. of reactions of the kind $A(A_1,\gamma)A_2$. If we denote by λ_γ the wavelength of the emitted photon, in general of the order of 100 fm, electric dipole (E1) reaction rates scale as λ_γ^{-3}, whereas electric quadrupole (E2) ones scale as λ_γ^{-5}. The introduction of the photonless state in the CHAMP-mediated reaction replaces λ_γ with the Bohr radius of the bound system, approximately 5 fm for ^{4}He. In terms of the usual parameterization of low-energy nuclear reaction (see Eq. (122)), the former Coulomb effect enters the exponential barrier-factor, the latter – when present – influences the S-factor, which can be indeed enhanced by orders

Table 16
Dipole amplitude, Q-values, and catalyzed S-factor enhancement in the cross-section for relevant (α, γ) reactions. Modified from [523], taking into account the values recently reported by [540].

Reaction	EM Transition	$N(\alpha,\gamma)C$ Q_{SPN} (MeV)	$NX(B,C)X^-$ Q_{CBBN} (MeV)	Enhancement S_{CBBN}/S_{SBBN}
$^2H(\alpha,\gamma)^6Li$	E2	1.474	1.124	$\sim 10^7$
$^3H(\alpha,\gamma)^7Li$	E1	2.467	2.117	~ 30
$^3He(\alpha,\gamma)^7Be$	E1	1.587	1.237	~ 30

of magnitude, as reported in Table 16. Another, usually sub-leading effect in the direction of decreasing S is a decrease of phase–space due to the reduction of the reaction Q-value.

The most important alteration to the standard scenario in catalyzed BBN is mainly due to the enhancement of the single ^{6}Li producing process,

$$\text{standard BBN: } Y_p + {}^2\text{H} \rightarrow {}^6\text{Li} + \gamma; \qquad Q = 1.47 \text{ MeV}, \tag{154}$$

replaced by the process

$$\text{CBBN: } {}^4\text{He}X + {}^2\text{H} \rightarrow {}^6\text{Li} + X; \qquad Q \simeq 1.13 \text{ MeV}, \tag{155}$$

which in [531] was identified to be very effective even for a small fraction of X particles bound with nuclei. The usual BBN process of Eq. (154) is indeed only allowed at the quadrupole level (due to the almost identical mass to charge ratio of ^{2}H and Y_p), which is the reason for the very small value of ^{6}Li/^{7}Li, as already discussed in Section 4. Another possible path to enhance the ^{6}Li yield in CBBN was proposed in [533], who noticed that the decay of X when still in a bound state with Y_p could result in a break-up of the Y_p nucleus, producing ^{3}He and ^{3}H that would eventually fuse into ^{6}Li when reacting with Y_p. However, the possibility that this would happen is estimated to be very low and the $^2H(^4HeX,\ ^6Li)X$ appears to be in all cases still dominating the production of ^{6}Li [533,523]. The enhancement of the ^{6}Li yield in CBBN due to the process in Eq. (155) has been confirmed by all the published analysis as the most remarkable effect of CBBN and in particular by [540], who performed an accurate quantum three-body calculation of the cross-section of the reactions involved in CBBN. The observational hints of a plateau in ^{6}Li at a value well above standard BBN predictions, as well as the persisting discrepancy between ^{7}Li observations in the Spite Plateau and the (apparently overproduced) ^{7}Li yield has motivated several authors to explore the CBBN scenario further, trying to also explain the ^{7}Li "problem". A mechanism to address this issue was pointed out in [532]. Since significant fractions of ^{7}Li and (mostly) ^{7}Be are in bound states with CHAMPs, ^{7}Be can be depleted by the enhancement of the CBBN analogues of ^{7}Li(p, α)^{4}He, ^{7}Be(n, p)^{7}Li, and ^{7}Be(n, α)^{4}He. The authors of Ref. [538] performed a CBBN analysis also adding the effect of X decay cascades. They concluded that in presence of strong showers from decaying relic particles, bound-state effects on nucleosynthesis are negligible, and both Li problems are solved (if at all) in a way very similar to the cascade BBN case in absence of catalysis. [535] proposed a more elaborate solution of the ^{7}Li problem: the $^7BeX(p,\ \gamma)^8BX$, and the subsequent beta-decay of $^8\text{B} \rightarrow {}^8\text{Be} + \text{e}^+ + \nu_e$ would deplete the final ^{7}Li abundance, with little consequence on Y_p. The $^7BeX(p,\ \gamma)$ reaction would happen through a shifting of the resonance as an effect of the X presence, which would lead to a huge rate enhancement.

To a large extent, the reason why settling these issues is far from trivial is that significant uncertainties remain in the estimates of binding energies and CBBN reaction rates, due to the use of very simplified nuclear models and of the Born approximation. An account of the situation has been given in Section III of [524], which we address the reader to for further technical details. [524] also contains the most systematic and up-to-date analysis of CBBN, including calculations of rates of AX recombination–photodisintegration and CBBN analogues of BBN nuclear reaction rates. As long as the range $10 \text{ keV} > T > 0.8 \text{ keV}$ is concerned, the author confirms that the most relevant role is played by reaction (155), even when using the detailed calculation for its rate obtained in [534]. Moreover, in this regime only nine reactions (reported in Table II of [524]) are sufficient to describe the physics of CBBN. The evolution of light nuclide abundances in presence of bound-state reactions is shown in Fig. 37, where the enhancement of ^{6}Li abundance is clearly visible (note however that the role of X decays has been "switched off").

9.2.2. Late time CBBN: HX bound states, CHAMP-exchange, and decays

The authors of [532] suggested the possibility that the formation of bound state nuclei of CHAMPs with ^{3}H, ^{2}H and p at very late times might induce the suppression of synthesized ^{6}Li. Bound states of $Z = 1$ nuclei with X form at 1–2 keV temperatures, see Table 15. These bound states behave essentially as "long-lived" neutrons, which can dissociate Li and ^{7}Be Coulomb-unsuppressed. [524] carried on an extensive analysis of these effects, making use of reaction rates derived in the Born approximation, identifying nineteen reactions as relevant when late time CBBN effects are taken into account. These early results indicated that bound states of CHAMPs with $Z = 1$ WOULD induce at late times the destruction of most of the synthesized ^{6}Li and some ^{7}Li. Initially, it appeared that the stringent constraints initially put on the abundance of CHAMPs, e.g. in [531,536] loosen significantly. To add another layer of complication, an additional late time effect was pointed out in [524], which somewhat compensates the previous one. It is due to exothermal transfer of CHAMPs from $Z = 1$ nuclei into heavier nuclei (CHAMP-exchange reactions), i.e. $HX(^4\text{He}, \text{H})^4\text{He}X$. By lowering the abundance of neutral states HX, more of

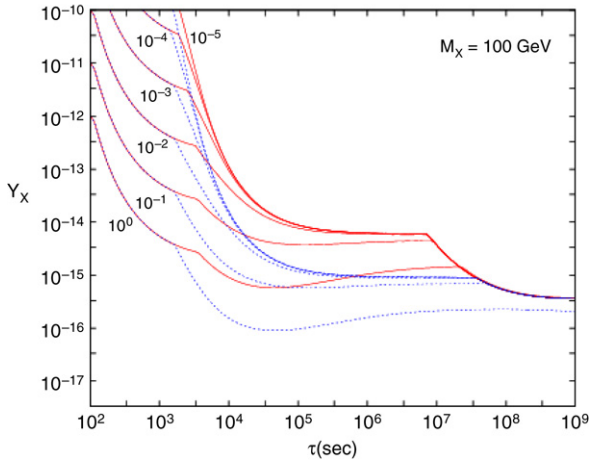

Fig. 37. Limits on the primordial CHAMP to entropy ratio $Y_x = n_X/s$ for CHAMPs with intermediate lifetimes. Shown are constraint lines for CHAMPs of mass $m_X = 100$ GeV and a variety of hadronic branching ratios, $B_h = 10^{-5}$–1, as labelled in the Figure. Solid (red) lines correspond to the conservative limit $^6\text{Li}/^7\text{Li} < 0.66$, whereas dashed (blue) lines correspond to $^6\text{Li}/^7\text{Li} < 0.1$. From [518], updated (courtesy of K. Jedamzik).

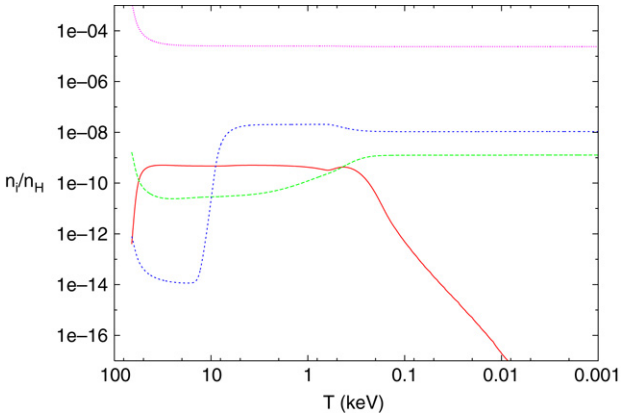

Fig. 38. Evolution of light-element number ratios $^7\text{Be/H}$ (solid-red), $^7\text{Li/H}$ (long-dashed-green), $^6\text{Li/H}$ (short-dashed-blue), and $^2\text{H/H}$ (dotted-purple), for a CHAMP model with $M_X = 100$ GeV, $\Omega_X h2 = 0.01$, and $\tau_X = 10^{10}$ s. Neither effects due to electromagnetic and hadronic energy release during CHAMP decay nor charge exchange effects have been taken into account. From [524], updated (courtesy of K. Jedamzik).

the ^{6}Li and ^{7}Be produced can survive. The detailed study of bound state reaction rates performed by [540] has finally shown that CHAMP-exchange reactions dominate the late time CBBN, thus "protecting" the abundances of Li and ^{7}Be produced at earlier times, as it can be seen in Fig. 38. The late-time drop in ^{7}Be is due to electronic capture decays.

9.2.3. ^{9}Be from CBBN

Finally, we want to point out here that modifications to the yields of heavier than ^{7}Li elements can take place in CBBN. As we have summarized in Section 3.4, one robust prediction of the standard BBN is the absence of sizeable yields of $A > 7$ elements. Roughly speaking, this is due to the lack of stable $A = 8$ elements, and to the inefficiency of the $3\,\alpha \rightarrow {}^{12}C$, which would respectively allow a slow light element chain to produce heavier elements or "bridge" it, as it happens in stars. The very short lifetime of ^{8}Be is a problem that can be overcome in CBBN, where sizeable amounts of meta-stable bound states $^8\text{Be}X$ can be created through the mechanism $^4\text{He}X(\alpha, \gamma)^8\text{Be}X$ at $T \lesssim 30$ keV, as showed by [552]. Once this bound state has been produced, the neutron capture reaction $^8\text{Be}X(\text{n}, ^9\text{Be})X$ can take place and ^{9}Be be efficiently produced in CBBN, whereas the analogue SBBN mechanism is suppressed as a consequence of the lifetime of ^{8}Be, shorter than a femtosecond. Although the absolute abundance of ^{9}Be produced by this mechanism is sensitive to the CHAMP abundance in the plasma, Y_X, [552] argued that an enhanced production of ^{9}Be and ^{6}Li are peculiar signatures of CBBN, and found that their ratio is independent of Y_X. The author derives the conclusion that the primordial ratio $^9\text{Be}/^6\text{Li} \sim 10^{-3}$ should therefore be a "signature" of CBBN, as it dramatically differs from $^9\text{Be}/^6\text{Li} \sim 10^{-5}$ ($^9\text{Be/H} \sim 10^{-19}$, [95]) which one obtains in SBBN. In their detailed study, [540] have challenged this result by arguing that the rate estimate of $^8\text{Be}X(\text{n}, ^9\text{Be})X$ by [552] is too high; although strong conclusions would require a careful examination of all the nuclear effects involved, they hint toward a much lower efficiency of the process proposed by [552]. While this issue is yet to be clarified, the kind of constraints to supersymmetric scenarios that might follow from a peculiar ^{9}Be production in CBBN has preliminarily been studied in [553,554].

9.2.4. Constraints in CHAMP parameter space

If the lifetime of the CHAMP is $\tau_X \leq 3 \times 10^2$ s, i.e. before that bound states can form, clearly its only effect on BBN is equivalent to injecting electromagnetically and hadronically interacting particles into the plasma. For intermediate lifetimes, 3×10^2 s $\leq \tau_X \leq 5 \times 10^5$ s, the main novel constraint is due to the possible overproduction of ^{6}Li via ^{4}He$X(^2$H, $X)^6$Li. Fortunately, as this reaction is now known within a factor three in light of the dedicated calculations of [534], this range of lifetimes is relatively well constrained. However the decay of a CHAMP at this time induces again a cascade nucleosynthesis; in hadronic cascades from a neutral particle decaying at the same time, it is well known that ^{6}Li overproduction is the main effect. Thus, unexpectedly, for hadronic branching ratios $B_h \geq 0.01$ (and e.g. $M_X = 1$ TeV) the effects of a charged particle decay do not differ much from those of a neutral one [539]. The results of the previous section apply since the ^{6}Li produced by the hadronic shower induced reactions dominates over the effect of catalyzed ^{6}Li production. Only for $B_h \lesssim 10^{-2}$ and for sufficiently large decay times τ_X the CBBN mechanism provides new bounds.

Finally, for longer lifetimes, $\tau_X \geq 5 \times 10^5$ s, the conservative limits on charged decaying particles initially derived in [539] appeared to be no stronger than those on neutral particles, due to the large uncertainties in nucleosynthesis at $T \leq 3$ keV. However, the nuclear rate calculations for CBBN presented in [540] strongly reduce those uncertainties. A recent application of these updated calculations has been performed in [554] with an analysis restricted to a minimal SUGRA model with heavy gravitino, which we address for further details.

10. Conclusions

In this review we have reported the current status of BBN, focusing in the first part on precision calculations possible in the standard scenario, which provide a tool for current cosmological framework, in the second part on the constraints to new physics, which become particularly important in the forthcoming LHC era. The "classical parameter" constrained by BBN is the baryon to photon ratio, η, or equivalently the baryon abundance, $\Omega_B h^2$. At present, the constraint is dominated by the deuterium determination, and we find $\Omega_B h^2 = 0.021 \pm 0.001 (1\sigma)$. This determination is consistent with the upper limit on primordial ^{3}He/H (which provides a lower limit to η), as well as with the range selected by ^{4}He determinations, which however provides a constraint almost one order of magnitude weaker. The agreement within $2\,\sigma$ with the WMAP determination, $\Omega_B h^2 = 0.02273 \pm 0.00062$, represents a remarkable success of the Standard Cosmological Model. On the other hand, using this value as an input, a factor $\gtrsim 3$ discrepancy remains with ^{7}Li determinations, which can hardly be reconciled even accounting for a conservative error budget in both observations and nuclear inputs. Even more puzzling are some detections of traces of ^{6}Li at a level far above the one expected from the Standard BBN. If the observational determinations are solid, both nuclides indicate that either their present observations do not reflect their primordial values, and should thus be discarded for cosmological purposes, or that the early cosmology is more complicated and exciting than the Standard BBN lore. Neither a non-standard number of massless degrees of freedom in the plasma (parameterized via $N_{\rm eff}$) or a lepton asymmetry ξ_e (all asymmetries assumed equal) can reconcile the discrepancy. Current bounds on both quantities come basically from the ^{4}He measurement, $N_{\rm eff} = 3.2 \pm 0.4\,(1\sigma)$ and $\xi_e = -0.008 \pm 0.013\,(1\sigma)$.

On the other hand, other exotic proposals have been invoked to reconcile this discrepancy. Typically they involve massive meta-stable particles with weak scale interactions, which should be soon produced at the LHC. In Supersymmetric scenarios, long-lived particles are possible whenever the Next to Lightest Supersymmetric Particle (NLSP) decays into the Lightest Supersymmetric Particle (LSP) are gravity-mediated, or "disfavored" by phase space arguments, with a modest mass splitting between NLSP and LSP. Cases frequently considered in the recent literature are neutralino $\rightarrow$ gravitino decays, for example, or stau $\rightarrow$ gravitino. The phenomenology associated with the catalysis of reactions due to bound states of charged particles (as the stau) with ordinary nuclei is a particularly new topic in recent investigations. Also, the importance of a possible primordial origin of the ^{6}Li measured in a few systems of the ^{7}Li plateau has been recognized: first, the bounds in parameter space tighten significantly if lithium constraints are used, especially ^{6}Li [555–557,527]; second, because these exotic BBN scenarios may accommodate for a cosmological origin for ^{6}Li while solving the ^{7}Li excess problem as well, their phenomenology is very appealing. Although these links among primordial nucleosynthesis, dark matter, and perhaps SUSY phenomenology are quite fascinating, it is worth stressing that BBN bounds on cascade decays or annihilations of massive particles apply well beyond the restricted class of SUSY-inspired models. For example, the electromagnetic cascades following heavy sterile neutrino decays are constrained by these kinds of arguments, as well as decays of massive pseudo Nambu–Goldstone bosons, as considered in [558,472].

There are two directions along which we can expect the BBN field to develop in the future. On one hand, BBN is an important tool for precision cosmology, especially if its priors are used in combination with other cosmological observables. Already BBN provides the best bounds on parameters as $N_{\rm eff}$ and ξ_e (and bounds on η comparable to the CMB); yet, since theoretical uncertainties are at the moment well below observational ones, there is surely room to refine its power, provided that significantly greater efforts are devoted to determine light element abundances, and in particular Y_p. It is instructive in this sense to look back to what S. Sarkar wrote in his review [12] thirteen years ago:

Thousands of person years of effort have been invested in obtaining the precise parameters of the Z^0 resonance in $e^+ - e^-$ collisions, which measures the number of light neutrino species (and other particles) which couple to the Z^0. In comparison, a modest amount of work has been done, by a few small teams, on measuring the primordial light element abundances, which provide a complementary check of this number as well as a probe of new superweakly interacting particles which do not couple to the Z^0.

Despite the improvements reported in this article, we feel that unfortunately insufficient attention has been devoted to this problem, if compared to other areas of observational cosmology. In particular, the ^{4}He determination is still plagued by systematic uncertainties. Although their importance has been recently recognized and assessed more carefully, the fact that this reanalysis was triggered after the independent determination of η from CMB (and its agreement with the "low deuterium determinations" in QSO spectra) shows that there is still a long way to go towards a precision era for primordial elements. On the other hand, a significant improvement has taken place in assessing and reducing theoretical uncertainties, mostly related to nuclear reaction data. BBN has benefit from a wealth of new nuclear astrophysics measurements at low energies and covering large dynamical ranges. Given the much larger observational uncertainties, in this sector an effort in reassessing the systematic errors in older datasets might be more useful in reducing remaining discrepancies in the nuclear rates error budget. This is in particular the case for reactions involving ^{7}Be.

The other direction of development follows from the interplay with Lab experiments. Neutrinos have reserved many surprises, and it is not excluded that exotic properties may show up in future experiments with important implications for BBN, as we illustrated in Section 6. However, it is in particular from LHC that one expects a better understanding of high energy scales, and thus of the cosmology at earlier times and higher temperatures. Most theories that go beyond the Standard Model of Particle Physics require new states to appear at or above the electroweak scale and, as already reported, they might have implications for the phenomenology at the BBN epoch. If the LHC should provide indication for the existence of the SMPP Higgs and nothing else, there will be no natural scale to explore. In this case, albeit sad, BBN and other cosmological tools might be the only practical means to explore very high energy phenomena leaving their imprint on the cosmos. One example treated here is the effect of variations of fundamental "constants" on cosmological time-scales that emerge in extra dimensional scenarios, possibly embedded in grand unified theories or string theories. If, as hopefully more likely, the LHC will reveal new dynamics above the electroweak scale, we might be able to infer from the empirical evidence the presence of cosmological effects before the BBN epoch. A new Standard Cosmological Model would emerge as well, perhaps making the BBN one more step in the ladder back to the Big Bang, rather than the first one.

Acknowledgements

We would like to thank C. Abia, A.D. Dolgov, J. Lesgourgues, S. Pastor and G.G. Raffelt for valuable comments and suggestions, and G.L. Fogli for having particularly encouraged this work. We also thank M. Kamimura, and especially K. Jedamzik, for suggestions and clarifying remarks which much improved the manuscript, and K. Jedamzik for providing also the updated version of some Figures. F. Iocco is supported by MIUR through grant PRIN-2006, and acknowledges hospitality at Fermilab during some stage of this work. G. Miele acknowledges supports by Generalitat Valenciana (Grant No. AINV/2007/080) and by the Spanish MICINN (grants SAB2006-0171 and FPA2005-01269). G. Mangano, G. Miele, and O. Pisanti acknowledge supports by INFN - I.S. FA51 and by PRIN 2006 "Fisica Astroparticellare: Neutrini ed Universo Primordiale" of Italian MIUR. P.D. Serpico is supported by the US Department of Energy and by NASA grant NAG5-10842. Fermilab is operated by Fermi Research Alliance, LLC under Contract No. DE-AC02-07CH11359 with the United States Department of Energy.

References

[1] R.A. Alpher, H.A. Bethe, G. Gamow, Phys. Rev. 73 (1948) 803.
[2] E.M. Burbidge, G.R. Burbidge, W.A. Fowler, F. Hoyle, Rev. Modern Phys. 29 (1957) 547.
[3] H. Kragh, Cosmology and Controversy, Princeton Univ. Press, 1996.
[4] A. Meiksin, P. Madau, Astrophys. J. 412 (1993) 34.
[5] M. Rauch, et al., arxiv:astro-ph/9612245.
[6] D.H. Weinberg, J. Miralda-Escude, L. Hernquist, N. Katz, arxiv:astro-ph/9701012.
[7] A.E. Evrard, MNRAS 292 (1997) 289.
[8] J. Dunkley, et al., [WMAP Collaboration], 2008. arXiv:0803.0586 [astro-ph].
[9] R. Malaney, G. Mathews, Phys. Rep. 229 (1993) 145.
[10] C.J. Copi, D.N. Schramm, M.S. Turner, Science 267 (1995) 192.
[11] K.A. Olive, G. Steigman, T.P. Walker, Phys. Rep. 333–334 (2000) 389.
[12] S. Sarkar, Rep. Progr. Phys. 59 (1996) 1493.
[13] D.N. Schramm, M.S. Turner, Rev. Modern Phys. 70 (1998) 303.
[14] G. Steigman, Ann. Rev. Nucl. Part. Sci. 57 (2007) 463.
[15] P.J.E. Peebles, The Large-Scale Structure of the Universe, Princeton University Press, 1980.
[16] P.J.E. Peebles, Principles of Physical Cosmology, Princeton University Press., 1993.
[17] W.M. Yao, et al., J. Phys. G 33 (2006) 1.
[18] P.D. Serpico, et al., JCAP 0412 (2004) 010.
[19] E.W. Kolb, M.S. Turner, The Early Universe, Addison-Wesley Publishing Company, New York, 1990.
[20] V.F. Mukhanov, Int. J. Theor. Phys. 43 (2004) 669.
[21] R.A. Lyttleton, H. Bondi, Proc. Roy. Soc. A 252 (1959) 313.
[22] S. Sengupta, P.B. Pal, Phys. Lett. B 365 (1996) 175.
[23] A.D. Dolgov, et al., Nuclear Phys. B 632 (2002) 363.
[24] K.N. Abazajian, J.F. Beacom, N.F. Bell, Phys. Rev. D 66 (2002) 013008.
[25] Y.Y.Y. Wong, Phys. Rev. D 66 (2002) 025015.
[26] R.V. Wagoner, W.A. Fowler, F. Hoyle, Astrophys. J. 148 (1967) 3.
[27] R.V. Wagoner, Astrophys. J. Suppl. 18 (1969) 247.
[28] R.V. Wagoner, Astrophys. J. 179 (1973) 343.
[29] S. Esposito, G. Mangano, G. Miele, O. Pisanti, Nuclear Phys. B 568 (2000) 421.

[30] S. Esposito, G. Mangano, G. Miele, O. Pisanti, JHEP 0009 (2000) 038.
[31] A.F. Heckler, Phys. Rev. D 49 (1994) 611.
[32] R.E. Lopez, M.S. Turner, Phys. Rev. D 59 (1999) 103502.
[33] G. Mangano, G. Miele, S. Pastor, M. Peloso, Phys. Lett. B 534 (2002) 8.
[34] L.H. Kawano, 1988. Preprint FERMILAB-Pub-88/34-A.
[35] L.H. Kawano, 1992. Preprint FERMILAB-Pub-92/04-A.
[36] K. Enqvist, K. Kainulainen, V. Semikoz, Nuclear Phys. B 374 (1992) 392.
[37] V.F. Shvartsman, Pisma Zh. Eksp. Teor. Fiz. 9 (1969) 315 [JETP Lett. 9, 184].
[38] G. Steigman, D.N. Schramm, J.R. Gunn, Phys. Lett. B 66 (1977) 202.
[39] The ALEPH, DELPHI, L3, OPAL and SLD Collaborations, Phys. Rep. 427 (2005) 257.
[40] L. Cucurull, J.A. Grifols, R. Toldra, Astropart. Phys. 4 (1996) 391.
[41] A.D. Dolgov, S.H. Hansen, A.Y. Smirnov, JCAP 0506 (2005) 004.
[42] A.D. Dolgov, Phys. Rep. 370 (2002) 333.
[43] G. Mangano, et al., Nuclear Phys. B 729 (2005) 221.
[44] M.Yu. Khlopov, S.T. Petkov, Phys. Lett. B 99 (1981) 117.
[45] S. Hannestad, Phys. Rev. D 64 (2001) 023515.
[46] A. Dolgov, Sov. J. Nucl. Phys. 33 (1981) 700.
[47] G. Raffelt, G. Sigl, L. Stodolsky, Phys. Rev. D 45 (1992) 1782.
[48] G. Sigl, G. Raffelt, Nuclear Phys. B 406 (1993) 423.
[49] B.H. Mckellar, M.J. Thomson, Phys. Rev. D 49 (1994) 2710.
[50] A.D. Dolgov, S.H. Hansen, D.V. Semikoz, Nuclear Phys. B 503 (1997) 426.
[51] S. Esposito, G. Mangano, G. Miele, O. Pisanti, Nuclear Phys. B 540 (1999) 3.
[52] S. Weinberg, Gravitation and Cosmology, Wiley, New York, 1972.
[53] D.M. Wilkinson, Nuclear Phys. A 377 (1982) 474.
[54] A. Sirlin, Phys. Rev. 164 (1967) 1767.
[55] W.J. Marciano, A. Sirlin, Phys. Rev. Lett. 56 (1986) 22.
[56] D.A. Dicus, et al., Phys. Rev. D 26 (1982) 2694.
[57] J.L. Cambier, J.R. Primack, M. Sher, Nuclear Phys. B 209 (1982) 372.
[58] R. Baier, E. Pilon, B. Pire, D. Schiff, Nuclear Phys. B 336 (1990) 157.
[59] D. Seckel, Nuclear mass corrections to the p–n rates during Big Bang Nucleosynthesis, 1993. hep-ph/9305311.
[60] R.E. Lopez, M.S. Turner, G. Gyuk, Phys. Rev. D 56 (1997) 3191.
[61] M. Le Bellac, Finite Temperature Field Theory, Cambridge University Press, 1996.
[62] J.F. Donoghue, B.R. Holstein, Phys. Rev. D 28 (1983) 340.
[63] J.F. Donoghue, B.R. Holstein, Phys. Rev. D 29 (1984) 3004.
[64] J.F. Donoghue, B.R. Holstein, R.W. Robinett, Ann. Phys. 164 (1985) 233.
[65] A.E. Johansson, G. Peressutti, B.S. Skagerstam, Nuclear Phys. B 278 (1986) 324.
[66] W. Keil, Phys. Rev. D 40 (1989) 1176.
[67] W. Keil, R.L. Kobes, Physica A 158 (1989) 47.
[68] M. Le Bellac, D. Poizat, Z. Phys. C 47 (1990) 125.
[69] T. Altherr, P. Aurenche, Phys. Rev. D 40 (1989) 4171.
[70] R.L. Kobes, G.W. Semeneff, Nuclear Phys. B 260 (1985) 714.
[71] R.L. Kobes, G.W. Semeneff, Nuclear Phys. B 272 (1986) 329.
[72] R.F. Sawyer, Phys. Rev. D 53 (1996) 4232.
[73] I.A. Chapman, Phys. Rev. D 55 (1997) 6287.
[74] S. Esposito, G. Mangano, G. Miele, O. Pisanti, Phys. Rev. D 58 (1998) 105023.
[75] L.S. Brown, R.F. Sawyer, Phys. Rev. D 63 (2001) 083503.
[76] A. Serebrov, et al., Phys. Lett. B 605 (2005) 72.
[77] G.J. Mathews, T. Kajino, T. Shima, Phys. Rev. D 71 (2005) 021302.
[78] N. Severijns, M. Beck, O. Naviliat-Cuncic, Rev. Modern Phys. 78 (2006) 991.
[79] B.D. Fields, S. Dodelson, M.S. Turner, Phys. Rev. D 47 (1993) 4309.
[80] M.S. Smith, L.H. Kawano, R.A. Malaney, Astrophys. J. Suppl 85 (1993) 219.
[81] C. Angulo, et al., Nuclear Phys. A 656 (1999) 3.
[82] R.H. Cyburt, Phys. Rev. D 70 (2004) 023505.
[83] P. Descouvemont, A. Adahchour, C. Angulo, A. Coc, E. Vangioni-Flam, At. Data Nucl. Data Tables 88 (2004) 203.
[84] L. Krauss, P. Romanelli, Astrophys. J. 358 (1990) 47.
[85] G.R. Caughlan, R. Fowler, At. Data Nucl. Data Tables 40 (1988) 291.
[86] D.D. Clayton, Principles of Stellar Evolution and Nucleosynthesis, The University of Chicago Press, 1983.
[87] C.E. Rolfs, W.S. Rodney, Cauldrons in the Cosmos, The University of Chicago Press, 1988.
[88] G. D'Agostini, Nucl. Instrum. Methods A 346 (1994) 306.
[89] K.M. Nollet, S. Burles, Phys. Rev. D 61 (2000) 123505.
[90] G. Fiorentini, E. Lisi, S. Sarkar, F.L. Villante, Phys. Rev. D 58 (1998) 063506.
[91] A. Cuoco, et al., Internat. J. Modern Phys. A 19 (2004) 4431.
[92] R.H. Cyburt, B.D. Fields, K.A. Olive, 2008. arXiv:0808.2818v1 [astro-ph].
[93] PArthENoPE, website: http://parthenope.na.infn.it/.
[94] E. Fermi, A. Turkevich, quoted in R.A. Alpher, R.C. Herman, Rev. Modern Phys. 22 (1950) 153.
[95] F. Iocco, et al., Phys. Rev. D 75 (2007) 087304.
[96] First Stars III, AIP Conf. Proc. 990 (2008).
[97] S. Burles, K.M. Nollett, M.S. Turner, Astrophys. J. 552 (2000) L1.
[98] R.H. Cyburt, B.D. Fields, K.A. Olive, New Astron. 6 (2001) 215.
[99] R.H. Cyburt, Nuclear Phys. A 718 (2003) 380.
[100] A. Coc, E. Vangioni-Flam, P. Descouvemont, A. Adahchour, C. Angulo, Astrophys. J. 600 (2004) 544.
[101] O. Pisanti, et al., Comp. Phys. Comm. 178 (2008) 956.
[102] R.I. Epstein, J.M. Lattimer, D.N. Schramm, Nature 263 (1976) 198.
[103] T. Prodanovic, B.D. Fields, Astrophys. J. 597 (2003) 48.
[104] M. Linsky, et al., Astrophys. J. 647 (2006) 1106.
[105] FUSE, website: http://fuse.pha.jhu.edu/.
[106] B.E. Wood, et al., Astrophys. J. 609 (2004) 838.
[107] E.B. Jenkins, et al., Astrophys. J. 520 (1999) 182.
[108] S.L. Ellison, J.X. Prochaska, S. Lopez, MNRAS 380 (2007) 1245.
[109] D. Romano, M. Tosi, C. Chiappini, F. Matteucci, MNRAS 369 (2006) 295.
[110] B.D. Savage, et al., Astrophys. J. 659 (2007) 1222.

[111] N. Prantzos, EAS Publications Series 32 (2008) 311. arXiv:0709.0833.
[112] T. Prodanovic, B.D. Fields, JCAP 0809 (2008) 003.
[113] E. Lellouch, B. Bezard, T. Fouchet, H. Feuchtgruber, T. Encrenaz, T. de Graauw, Astron. Astrophys. 670 (2001) 610.
[114] T.F. Adams, Astron. Astrophys. 50 (1976) 461.
[115] B.D. Fields, Astrophys. J. 456 (1996) 478.
[116] M. Pettini, B.J. Zych, M.T. Murphy, A. Lewis, C.C. Steidel, 2008. arXiv:0805.0594 [astro-ph].
[117] S. Burles, D. Tytler, Astrophys. J. 499 (1998) 699.
[118] D. Kirkman, D. Tytler, N. Suzuki, J. O'Meara, D. Lubin, Astrophys. J. Suppl. 149 (2003) 1.
[119] J.M. O'Meara, et al., Astrophys. J. 552 (2001) 718.
[120] M. Pettini, D. Bowen, Astrophys. J. 560 (2001) 41.
[121] S.A. Levshakov, M. Dessauges-Zavadsky, S. D'Odorico, P. Molaro, 2001. astro-ph/0105529.
[122] S. D'Odorico, M. Dessauges-Zavadsky, P. Molaro, Astron. Astrophys. 368 (2001) L21.
[123] N.H.M. Crighton, J.K. Webb, A. Ortiz-Gill, A. Fernandez-Soto, MNRAS 355 (2004) 1042.
[124] J.M. O'Meara, et al., Astrophys. J. 649 (2006) L61.
[125] M. Rugers, C.J. Hogan, Astrophys. J. 459 (1996) L1.
[126] R.F. Carswell, et al., MNRAS 268 (1994) L1.
[127] S. Burles, D. Kirkman, D. Tytler, Astrophys. J. 519 (1999) 18.
[128] R.F. Carswell, et al., MNRAS 278 (1996) 506.
[129] E.J. Wampler, et al., Astron. Astrophys. 316 (1996) 33.
[130] J.K. Webb, et al., Nature 388 (1997) 250.
[131] D. Tytler, et al., Astron. J. 117 (1999) 63.
[132] D. Kirkman, et al., Astrophys. J. 559 (2001) 23.
[133] N.H.M. Crighton, J.K. Webb, R.F. Carswell, K.M. Lanzetta, MNRAS 345 (2003) 243.
[134] D. Kirkman, et al., Astrophys. J. 529 (2000) 655.
[135] B.D. Fields, S. Sarkar, PDG Mini-review, in W.M. Yao, et al., J. Phys. G 33 (2006) 1.
[136] R. Barlow, 2004. arXiv:physics/0401042.
[137] K. Sigurdson, S.R. Furlanetto, Phys. Rev. Lett. 97 (2006) 091301.
[138] L. Chuzhoy, P.R. Shapiro, Astrophys. J. 651 (2006) 1.
[139] D.L. Anderson, Science 261 (1993) 170.
[140] R.T. Rood, T.M. Bania, D.S. Balser, Science 295 (2002) 804.
[141] G. Gloeckler, J. Geiss, in: L. Da Silva, M. Spite, J.R. Medieros (Eds.), The Light Elements and Their Evolution, Astronomical Society of the Pacific, San Francisco, CA, 2000.
[142] P.R. Mahaffy, Space Sci. Rev. 84 (1998) 251.
[143] D.C. Black, Geochim. Cosmochim. Acta 36 (1972) 347.
[144] P. Eberhardt, Earth Planet. Sci. Lett. 24 (1974) 182.
[145] J. Geiss, H. Reeves, Astron. Astrophys. 18 (1972) 126.
[146] J. Geiss, Primordial abundance of hydrogen and helium isotopes, in: N. Prantzos, E. Vangioni-Flam, M. Cassè (Eds.), Origin and Evolution of the Elements, Cambridge University Press, Cambridge, 1993.
[147] G. Gloeckler, J. Geiss, Space Sci. Rev. 84 (1998) 275.
[148] T.M. Bania, R.T. Rood, D.S. Balser, Nature 415 (2002) 54.
[149] M. Asplund, N. Grevesse, A.J. Sauval, ASP Conf. Ser. 336 (2005) 25.
[150] D. Romano, M. Tosi, F. Matteucci, C. Chiappini, MNRAS 346 (2003) 295.
[151] P.P. Eggleton, D.S.P. Dearborn, J.C. Lattanzio, Science 314 (2006) 1580.
[152] J. Geiss, G. Gloeckler, Space Sci. Rev. 130 (2007) 5.
[153] J. Geiss, G. Gloeckler, Space Sci. Rev. 84 (1998) 239.
[154] M. Peimbert, S. Torres-Peimbert, Astrophys. J. 193 (1974) 327.
[155] M. Peimbert, S. Torres-Peimbert, Astrophys. J. 203 (1976) 581.
[156] B.E.J. Pagel, R.J. Terlevich, J. Melnick, PASP 98 (1986) 1005.
[157] Y.I. Izotov, T.X. Thuan, Astrophys. J. 500 (1998) 188.
[158] Y.I. Izotov, T.X. Thuan, Astrophys. J. 602 (2004) 200.
[159] A. Peimbert, Astrophys. J. 584 (2003) 735.
[160] M. Peimbert, A. Peimbert, V. Luridiana, M.T. Ruiz, in: E. Pérez, R. González Delgado, G. Tenorio-Tagle (Eds.), Star Formation through Time, in: ASP Conf. Ser., vol. 297, ASP, San Francisco, 2003.
[161] V. Luridiana, A. Peimbert, M. Peimbert, M. Cerviño, Astrophys. J. 592 (2003) 846.
[162] M. Peimbert, V. Luridiana, A. Peimbert, Astrophys. J. 666 (2007) 636.
[163] R.L. Porter, R.P. Bauman, G.J. Ferland, K.B. MaCadam, Astrophys. J. 622 (2005) L73.
[164] R.L. Porter, G.J. Ferland, K.B. MaCadam, Astrophys. J. 657 (2007) 327.
[165] K.A. Olive, E.D. Skillman, Astrophys. J. 617 (2004) 29.
[166] M. Fukugita, M. Kawasaki, Astrophys. J. 646 (2006) 691.
[167] Y.I. Izotov, T.X. Thuan, G. Stasinska, Astrophys. J. 662 (2007) 15.
[168] M. Salaris, M. Riello, S. Cassisi, G. Piotto, Astron. Astrophys. 420 (2004) 911.
[169] R. Trotta, S.H. Hansen, Phys. Rev. D 69 (2004) 023509.
[170] G. Huey, R.H. Urt, B.D. Wandelt, Phys. Rev. D 69 (2004) 103503.
[171] K. Ichikawa, T. Takahashi, Phys. Rev. D 73 (2006) 063528.
[172] K. Ichikawa, T. Sekiguchi, T. Takahashi, Phys. Rev. D 78 (2008) 043509.
[173] J. Hamann, J. Lesgourgues, G. Mangano, JCAP 0803 (2008) 004.
[174] M. Asplund, et al., Astrophys. J. 644 (2006) 229.
[175] F. Spite, M. Spite, Astron. Astrophys. 115 (1982) 357.
[176] S.G. Ryan, J.E. Norris, T.C. Beers, Astrophys. J. 523 (1999) 654.
[177] S. Ryan, T. Beers, K. Olive, B. Fields, J. Norris, Astrophys. J. 530 (2000) L57.
[178] P. Bonifacio, P. Molaro, MNRAS 285 (1997) 847.
[179] P. Bonifacio, P. Molaro, L. Pasquini, MNRAS 292 (1997) L1.
[180] P. Bonifacio, et al., Astron. Astrophys. 390 (2002) 91.
[181] J. Melendez, I. Ramirez, Astrophys. J. 615 (2004) L33.
[182] C. Charbonnel, F. Primas, Astron. Astrophys. 442 (2005) 961.
[183] A.J. Korn, et al., Nature 442 (2006) 657.
[184] D.L. Lambert, AIP Conf. Proc. 743 (2005) 206.
[185] B.S. Nara Singh, M. Hass, Y. Nir-El, G. Haquin, Phys. Rev. Lett. 93 (2004) 262503.
[186] D. Bemmerer, et al., Phys. Rev. Lett. 97 (2006) 122502.
[187] F. Confortola, et al., [LUNA Collaboration], Phys. Rev. C 75 (2007) 065803. Phys. Rev. C 75, 069903.
[188] T.A.D. Brown, et al., Phys. Rev. C 76 (2007) 055801.

[189] R.H. Cyburt, J.R. Ellis, B.D. Fields, K.A. Olive, Phys. Rev. D 67 (2003) 103521.
[190] C. Angulo, et al., Astrophys. J. 630 (2005) L105.
[191] O. Richard, G. Michaud, J. Richer, Astrophys. J. 580 (2002) 1100.
[192] O. Richard, G. Michaud, J. Richer, Astrophys. J. 619 (2005) 538.
[193] V.V. Smith, D.L. Lambert, P.E. Nissen, Astrophys. J. 408 (1993) 262.
[194] V.V. Smith, D.L. Lambert, P.E. Nissen, Astrophys. J. 506 (1998) 405.
[195] L.M. Hobbs, J.A. Thorburn, Astrophys. J. 491 (1997) 772.
[196] R. Cayrel, M. Spite, F. Spite, E. VangioniFlam, M. Cassè, J. Audouze, Astron. Astrophys. 343 (1999) 923.
[197] P.E. Nissen, M. Asplund, V. Hill, S. D'Odorico, Astron. Astrophys. 357 (2000) L49.
[198] R. Cayrel, et al., Astron. Astrophys. 473 (2007) L37.
[199] R. Cayrel, et al., 2008. arXiv:0810.4290.
[200] E. Vangioni-Flam, M. Casse, J. Audouze, Phys. Rep. 333 (2000) 365.
[201] N. Prantzos, Astron. Astrophys. 448 (2006) 665.
[202] B.B. Nath, P. Madau, J. Silk, MNRAS 366 (2006) L35.
[203] E. Rollinde, E. Vangioni-Flam, K.A. Olive, Astrophys. J. 627 (2005) 666.
[204] E. Rollinde, E. Vangioni, K.A. Olive, Astrophys. J. 651 (2006) 658.
[205] L. Piau, T.C. Beers, D.S. Balsara, T. Sivarani, J.W. Truran, J.W. Ferguson, Astrophys. J. 653 (2006) 300.
[206] C. Evoli, S. Salvadori, A. Ferrara, 2008. arXiv:0806.4184 [astro-ph].
[207] S. Inoue, T.K. Suzuki, Nuclear Phys. A 718 (2003) 69.
[208] T. Prodanovic, B.D. Fields, Phys. Rev. D 76 (2007) 083003.
[209] V. Tatischeff, J.P. Thibaud, Astron. Astrophys. 469 (2007) 265T.
[210] T. Prodanovic, B.D. Fields, Astrophys. J. 616 (2004) L115.
[211] P.C. Stancil, A. Loeb, M. Zaldarriaga, A. Dalgarno, S. Lepp, Astrophys. J. 580 (2002) 29.
[212] E.R. Switzer, C.M. Hirata, Phys. Rev. D 72 (2005) 083002.
[213] E. Lisi, S. Sarkar, F.L. Villante, Phys. Rev. D 59 (1999) 123520.
[214] S. Burles, K.M. Nollett, J.N. Truran, M.S. Turner, Phys. Rev. Lett. 82 (1999) 4176.
[215] V. Barger, J.P. Kneller, P. Langacker, D. Marfatia, G. Steigman, Phys. Lett. B 569 (2003) 123.
[216] R.H. Cyburt, B.D. Fields, K.A. Olive, Phys. Lett. B 567 (2003) 227.
[217] R.H. Cyburt, B.D. Fields, K.A. Olive, E. Skillman, Astropart. Phys. 23 (2005) 313.
[218] S.H. Hansen, et al., Phys. Rev. D 65 (2002) 023511.
[219] G. Mangano, et al., JCAP 0703 (2007) 006.
[220] V. Simha, G. Steigman, JCAP 0806 (2008) 016.
[221] G.G. Raffelt, Phys. Rep. 320 (1999) 319.
[222] R. Foot, G.C. Joshi, H. Lew, R.R. Volkas, Modern Phys. Lett. A 5 (1990) 95;
R. Foot, G.C. Joshi, H. Lew, R.R. Volkas, Modern Phys. Lett. A 5 (1990) 2085 (erratum).
[223] S. Davidson, S. Hannestad, G. Raffelt, JHEP 0005 (2000) 003.
[224] J. Bernabeu, L.G. Cabral-Rosetti, J. Papavassiliou, J. Vidal, Phys. Rev. D 62 (2000) 113012.
[225] J. Bernabeu, J. Papavassiliou, J. Vidal, Phys. Rev. Lett. 89 (2002) 101802;
J. Bernabeu, J. Papavassiliou, J. Vidal, Phys. Rev. Lett. 89 (2005) 229902 (erratum).
[226] J. Bernabeu, J. Papavassiliou, J. Vidal, Nuclear Phys. B 680 (2004) 450.
[227] J.A. Grifols, E. Masso, Phys. Rev. D 40 (1989) 3819.
[228] J.A. Grifols, E. Masso, Modern Phys. Lett. A 2 (1987) 205.
[229] M. Hirsch, E. Nardi, D. Restrepo, Phys. Rev. D 67 (2003) 033005.
[230] A. Mirizzi, D. Montanino, P.D. Serpico, Phys. Rev. D 76 (2007) 053007.
[231] K. Enqvist, A.I. Rez, V.B. Semikoz, Nuclear Phys. B 436 (1995) 49.
[232] G. Mangano, et al., Nuclear Phys. B 756 (2006) 100.
[233] Y. Chikashige, R.N. Mohapatra, R.D. Peccei, Phys. Lett. B 98 (1981) 265.
[234] G.B. Gelmini, M. Roncadelli, Phys. Lett. B 99 (1981) 411.
[235] H.M. Georgi, S.L. Glashow, S. Nussinov, Nuclear Phys. B 193 (1981) 297.
[236] S. Chang, K. Choi, Phys. Rev. D 49 (1994) 12.
[237] J.F. Beacom, N.F. Bell, S. Dodelson, Phys. Rev. Lett. 93 (2004) 121302.
[238] M. Lattanzi, J.W.F. Valle, Phys. Rev. Lett. 99 (2007) 121301.
[239] A. Cuoco, J. Lesgourgues, G. Mangano, S. Pastor, Phys. Rev. D 71 (2005) 123501.
[240] S. Hannestad, Phys. Rev. D 70 (2004) 043506.
[241] K. Ichikawa, M. Kawasaki, F. Takahashi, Phys. Rev. D 72 (2005) 043522.
[242] M. Kawasaki, K. Kohri, N. Sugiyama, Phys. Rev. Lett. 82 (1999) 4168.
[243] M. Kawasaki, K. Kohri, N. Sugiyama, Phys. Rev. D 62 (2000) 023506.
[244] P.D. Serpico, G.G. Raffelt, Phys. Rev. D 70 (2004) 043526.
[245] C. Boehm, D. Hooper, J. Silk, M. Casse, Phys. Rev. Lett. 92 (2004) 101301.
[246] G. Steigman, K.A. Olive, D.N. Schramm, Phys. Rev. Lett. 43 (1979) 239.
[247] V. Barger, P. Langacker, H.S. Lee, Phys. Rev. D 67 (2003) 075009.
[248] A.D. Sakharov, JETP 5 (1967) 24.
[249] J.A. Harvey, M.S. Turner, Phys. Rev. D 42 (1990) 3344.
[250] M. Dine, A. Kusenko, Rev. Modern Phys. 76 (2004) 1.
[251] A. Riotto, M. Trodden, Ann. Rev. Nucl. Part. Sci. 49 (1999) 35.
[252] W. Buchmüller, R.D. Peccei, T. Yanagida, Ann. Rev. Nucl. Part. Sci. 55 (2005) 311.
[253] S. Davidson, E. Nardi, Y. Nir, 2008. arXiv:0802.2962 [hep-ph].
[254] A. Casas, W.Y. Cheng, G. Gelmini, Nuclear Phys. B 538 (1999) 297.
[255] J. March-Russell, H. Murayama, A. Riotto, JHEP 9911 (1999) 015.
[256] J. McDonald, Phys. Rev. Lett. 84 (2000) 4798.
[257] M. Kawasaki, F. Takahashi, M. Yamaguchi, Phys. Rev. D 66 (2002) 043516.
[258] K. Freese, E.W. Kolb, M.S. Turner, Phys. Rev. D 27 (1983) 1689.
[259] H.S. Kang, G. Steigman, Nuclear Phys. B 372 (1992) 494.
[260] K. Kohri, M. Kawasaki, K. Sato, Astrophys. J. 490 (1997) 72.
[261] S.E. Whitmire, R.J. Scherrer, Phys. Rev. D 61 (2000) 083508.
[262] S. Esposito, et al., Phys. Rev. D 63 (2001) 043004.
[263] M. Orito, T. Kajino, G.J. Mathews, Y. Wang, Phys. Rev. D 65 (2002) 123504.
[264] S.D. Stirling, R.J. Scherrer, Phys. Rev. D 66 (2002) 043531.
[265] J.P. Kneller, G.C. McLaughlin, Phys. Rev. D 70 (2004) 043512.
[266] L.A. Popa, A. Vasile, 2008. arXiv:0801.3928 [astro-ph].
[267] L.A. Popa, A. Vasile, JCAP 0806 (2008) 028.

[268] V. Simha, G. Steigman, JCAP 0808 (2008) 011.
[269] S. Pastor, T. Pinto, G. Raffelt, 2008. arXiv:0808.3137 [astro-ph].
[270] A.D. Dolgov, F. Takahashi, Nuclear Phys. B 688 (2004) 189.
[271] P.D. Serpico, G.G. Raffelt, Phys. Rev. D 71 (2005) 127301.
[272] D.N. Spergel, et al., [WMAP Collaboration], Astrophys. J. Suppl. 148 (2003) 175.
[273] W.J. Marciano, A.I. Sanda, Phys. Lett. B 67 (1977) 303.
[274] D.P. Kirilova, 1988. Dubna preprint JINR E2-88-301.
[275] R. Barbieri, A. Dolgov, Phys. Lett. B 237 (1990) 440.
[276] K. Enqvist, K. Kainulainen, J. Maalampi, Phys. Lett. B 249 (1990) 531.
[277] K. Kainulainen, Phys. Lett. B 244 (1990) 191.
[278] R. Barbieri, A. Dolgov, Nuclear Phys. B 349 (1991) 743.
[279] K. Enqvist, K. Kainulainen, M.J. Thomson, Nuclear Phys. B 373 (1992) 498.
[280] J.M. Cline, Phys. Rev. Lett. 68 (1992) 3137.
[281] X. Shi, D.N. Schramm, B.D. Fields, Phys. Rev. D 48 (1993) 2563.
[282] K.N. Abazajian, Astropart. Phys. 19 (2003) 303.
[283] A. Franklin, Rev. Modern Phys. 67 (1995) 457.
[284] F.E. Wietfeldt, E.B. Norman, Phys. Rep. 273 (1996) 149.
[285] B. Armbruster, et al., [KARMEN Collaboration], Phys. Lett. B 348 (1995) 19.
[286] A. Aguilar, et al., [LSND Collaboration], Phys. Rev. D 64 (2001) 112007.
[287] A.A. Aguilar-Arevalo, et al., [The MiniBooNE Collaboration], Phys. Rev. Lett. 98 (2007) 231801.
[288] M. Cirelli, G. Marandella, A. Strumia, F. Vissani, Nuclear Phys. B 708 (2005) 215.
[289] D. Kirilova, Internat. J. Modern Phys. D 13 (2004) 831.
[290] D.P. Kirilova, Internat. J. Modern Phys. D 16 (2007) 1197.
[291] D.P. Kirilova, M.P. Panayotova, JCAP 0612 (2006) 014.
[292] A.D. Dolgov, F.L. Villante, Nuclear Phys. B 679 (2004) 261.
[293] R. Foot, R.R. Volkas, Phys. Rev. Lett. 75 (1995) 4350.
[294] D.P. Kirilova, M.V. Chizhov, Nuclear Phys. B 534 (1998) 447.
[295] K. Abazajian, N.F. Bell, G.M. Fuller, Y.Y.Y. Wong, Phys. Rev. D 72 (2005) 063004.
[296] C.J. Smith, G.M. Fuller, C.T. Kishimoto, K.N. Abazajian, Phys. Rev. D 74 (2006) 085008.
[297] K. Abazajian, G.M. Fuller, M. Patel, Phys. Rev. D 64 (2001) 023501.
[298] E. Witten, Phys. Rev. D 30 (1984) 272.
[299] H. Kurki-Suonio, Phys. Rev. D 37 (1988) 2104.
[300] K. Sumiyoshi, T. Kajino, C. Alcock, G. Mathews, Phys. Rev. D 42 (1990) 3963.
[301] G. Fuller, K. Jedamzik, G. Mathews, A. Olinto, Phys. Lett. B 333 (1994) 135.
[302] A.F. Heckler, Phys. Rev. D 51 (1995) 405.
[303] K. Kainulainen, H. Kurki-Suonio, E. Sihvola, Phys. Rev. D 59 (1999) 083505.
[304] A. Megevand, F. Astorga, Phys. Rev. D 71 (2005) 023502.
[305] A.D. Dolgov, J. Silk, Phys. Rev. D 47 (1993) 4244.
[306] A. Nelson, Phys. Lett. B 240 (1990) 179.
[307] K.E. Sale, G.J. Mathews, Astrophys. J. 309L (1986) 1S.
[308] D.J. Schwarz, Ann. Phys. 12 (2003) 220.
[309] J. Barrow, J. Morgan, MNRAS 203 (1983) 393.
[310] Y. Zeldovich, Sov. Astron. Lett. 1 (1975) 5.
[311] R. Epstein, V. Petrosian, Astrophys. J. 197 (1975) 281.
[312] J. Applegate, C. Hogan, R. Scherrer, Phys. Rev. D 35 (1987) 1151.
[313] C. Alcock, G. Fuller, G. Mathews, Astrophys. J. 320 (1987) 439.
[314] T. Kajino, R. Boyd, Astrophys. J. 359 (1990) 267.
[315] H. Kurki-Suonio, R. Matzner, J. Centralla, T. Rothman, J. Wilson, Phys. Rev. D 38 (1988) 1091.
[316] H. Kurki-Suonio, R. Matzner, Phys. Rev. D 39 (1989) 1046.
[317] H. Kurki-Suonio, R. Matzner, K. Olive, D. Schramm, Astrophys. J. 353 (1989) 406.
[318] H. Kurki-Suonio, Matzner, Phys. Rev. D 42 (1990) 1047.
[319] G. Mathews, B. Meyer, C. Alcock, G. Fuller, Astrophys. J. 358 (1990) 36.
[320] G. Mathews, T. Kajino, M. Orito, Astrophys. J. 456 (1996) 98.
[321] M. Orito, T. Kajino, R. Boyd, G. Mathews, Astrophys. J. 488 (1997) 515.
[322] J.F. Lara, Phys. Rev. D 72 (2005) 023509.
[323] C.R. Alcock, D.S. Dearborn, G.M. Fuller, G.J. Mathews, B.S. Meyer, Phys. Rev. Lett. 64 (1990) 2607.
[324] K. Jedamzik, G.M. Fuller, Astrophys. J. 423 (1994) 33.
[325] E. Keihanen, Phys. Rev. D 66 (2002) 043512.
[326] J.F. Lara, T. Kajino, G.J. Mathews, Phys. Rev. D 73 (2006) 083501.
[327] K. Jedamzik, G.M. Fuller, G.J. Mathews, T. Kajino, Astrophys. J. 422 (1994) 423.
[328] S. Matsuura, S. Fujimoto, S. Nishimura, M. Hashimoto, K. Sato, Phys. Rev. D 72 (2005) 123505.
[329] S. Matsuura, S. Fujimoto, M. Hashimoto, K. Sato, Phys. Rev. D 75 (2007) 068302.
[330] M. Giovannini, E. Keihanen, H. Kurki-Suonio, Phys. Rev. D 66 (2002) 043504.
[331] G. Steigman, Ann. Rev. Astron. Astrophys. 14 (1976) 339.
[332] J.B. Rehm, K. Jedamzik, Phys. Rev. Lett. 81 (1998) 3307.
[333] J.B. Rehm, K. Jedamzik, Phys. Rev. D 63 (1998) 043509.
[334] H. Kurki-Suonio, E. Sihvola, Phys. Rev. Lett. 84 (2000) 3756.
[335] H. Kurki-Suonio, E. Sihvola, Phys. Rev. D 62 (2000) 103508.
[336] E. Sihvola, Phys. Rev. D 63 (2001) 103001.
[337] M. Giovannini, M.E. Shaposhnikov, Phys. Rev. Lett. 80 (1998) 22.
[338] A.D. Dolgov, Phys. Rep. 222 (1992) 309.
[339] M.Yu. Khlopov, S.G. Rubin, A.S. Sakharov, Phys. Rev. D 62 (2000) 083505.
[340] M.Yu. Khlopov, R.V. Konoplich, R. Mignani, S.G. Rubin, A.S. Sakharov, Astropart. Phys. 12 (2000) 367.
[341] S. Matsuura, A.D. Dolgov, S. Nagataki, K. Sato, Progr. Theoret. Phys. 112 (2004) 971.
[342] A.D. Dolgov, M. Kawasaki, N. Kevlishvili, arxiv:08062986.
[343] T. Kaluza, Sitzungsber. Preuss. Akad. Wiss. Berlin. (Math. Phys.) 966 (1921).
[344] O. Klein, Z. Phys. 37 (1926) 895.
[345] D. Bailin, A. Love, Rep. Progr. Phys. 50 (1987) 1087.
[346] N. Arkani-Hamed, S. Dimopoulos, G. Dvali, Phys. Lett. B 429 (1998) 263.
[347] I. Antoniadis, N. Arkani-Hamed, S. Dimopoulos, G. Dvali, Phys. Lett. B 436 (1998) 257.
[348] L. Randall, R. Sundrum, Phys. Rev. Lett. 83 (1999) 3370.

[349] L. Randall, R. Sundrum, Phys. Rev. Lett. 83 (1999) 4690.
[350] G.F. Giudice, J.D. Wells, PDG Mini-review in Yao W.M et al., J. Phys. G 33 (2006) 1.
[351] R. Sundrum, 2005. hep-th/0508134.
[352] P. Binetruy, C. Deffayet, D. Langlois, Nuclear Phys. B 565 (2000) 269.
[353] D.J.H. Chung, K. Freese, Phys. Rev. D 61 (2000) 023511.
[354] P. Binetruy, C. Deffayet, U. Ellwanger, D. Langlois, Phys. Lett. B 477 (2000) 285.
[355] M.J. Fairbarn, Phys. Lett. B 508 (2001) 335.
[356] J.M. Cline, C. Grojean, G. Servant, Phys. Rev. Lett. 83 (1999) 4245.
[357] C. Csaki, M. Graesser, C. Kolda, J. Terning, Phys. Lett. B 462 (1999) 34.
[358] T. Shiromizu, K. Maeda, M. Sasaki, Phys. Rev. D 62 (2000) 024012.
[359] R. Maartens, D. Wands, B. Bassett, I. Heards, Phys. Rev. D 62 (2000) 041301.
[360] D. Langlois, R. Maartens, M. Sasaki, D. Wands, Phys. Rev. D 63 (2001) 084009.
[361] S. Mizuno, K. Maeda, Phys. Rev. D 64 (2001) 123521.
[362] J.D. Barrow, R. Maartens, Phys. Lett. B 532 (2002) 155.
[363] V.V. Flambaun, E.V. Shuryak, Europhys. Lett. 74 (2006) 813.
[364] K. Ichiki, M. Yahiro, T. Kajino, M. Orito, G.J. Mathews, Phys. Rev. D 66 (2002) 043521.
[365] J.D. Bratt, A.C. Gault, R.J. Sherrer, T.P. Walker, Phys. Lett. B 546 (2002) 19.
[366] W.D. Goldberger, M.B. Wise, Phys. Rev. Lett. 83 (1999) 4922.
[367] B. Li, M.C. Chu, Phys. Rev. D 73 (2006) 023509.
[368] K.R. Dienes, E. Dudas, T. Gherghetta, Nuclear Phys. B 557 (1999) 25.
[369] R.N. Mohapatra, S. Nandi, A. Perez-Lorenzana, Phys. Lett. B 466 (1999) 115.
[370] Mohapatra, A. Perez-Lorenzana, Nuclear Phys. B 576 (2000) 466.
[371] N. Arkani-Hamed, S. Dimopoulos, G. Dvali, J. March-Russell, Phys. Rev. D 65 (2001) 024032.
[372] D.O. Caldwell, R.N. Mohapatra, S. Yellin, Phys. Rev. Lett. 87 (2001) 041601.
[373] D.O. Caldwell, R.N. Mohapatra, S. Yellin, Phys. Rev. D 64 (2001) 073001.
[374] C.S. Lam, 2001. hep-ph/0108198.
[375] R. Barbieri, P. Creminelli, A. Strumia, Nuclear Phys. B 585 (2000) 28.
[376] K.N. Abazajian, G.M. Fuller, M. Patel, Phys. Rev. Lett. 90 (2003) 061301.
[377] H.S. Goh, R.N. Mohapatra, Phys. Rev. D 65 (2002) 085018.
[378] P.A.M. Dirac, Nature 139 (1937) 323.
[379] J.P. Uzan, Rev. Modern Phys. 75 (2003) 403.
[380] J.D. Barrow, H.B. Sandvik, J. Magueijo, Phys. Rev. D 65 (2002) 063504.
[381] H.B. Sandvik, J.D. Barrow, J. Magueijo, Phys. Rev. Lett. 88 (2002) 031302.
[382] D.J. Shaw, J.D. Barrow, Phys. Rev. D 71 (2004) 063525.
[383] T. Damour, F.J. Dyson, Nuclear Phys. B 480 (1996) 37.
[384] Y. Fujii, et al., Nuclear Phys. B 573 (2000) 377.
[385] K.A. Olive, et al., Phys. Rev. D 66 (2002) 045022.
[386] J.K. Webb, et al., Phys. Rev. Lett. 82 (1999) 884.
[387] M.T. Murphy, J.K. Webb, V.V. Flambaum, MNRAS 345 (2003) 609.
[388] M.T. Murphy, et al., Lect. Notes Phys. 648 (2004) 131.
[389] R. Srianand, H. Chand, P. Petitjean, B. Aracil, Phys. Rev. Lett. 92 (2004) 121302.
[390] H. Chand, R. Srianand, P. Petitjean, B. Aracil, Astron. Astrophys. 417 (2004) 853.
[391] M.T. Murphy, J.K. Webb, V.V. Flambaum, Phys. Rev. Lett. 99 (2007) 239001.
[392] P.P. Avelino, C.J.A.P. Martins, G. Rocha, P. Viana, Phys. Rev. D 62 (2000) 123508.
[393] P.P. Avelino, et al., Phys. Rev. D 64 (2001) 103505.
[394] J.C.A.P. Martins, et al., Phys. Rev. D 66 (2002) 023505.
[395] G. Rocha, et al., MNRAS 352 (2004) 20.
[396] E. Kolb, M. Perry, T. Walker, Phys. Rev. D 33 (1986) 869.
[397] J.D. Barrow, Phys. Rev. D 35 (1987) 1805.
[398] B.A. Campbell, K.A. Olive, Phys. Lett. B 345 (1995) 429.
[399] L. Bergstrom, S. Iguri, H. Rubinstein, Phys. Rev. D 60 (1999) 045005.
[400] K.M. Nollett, R.E. Lopez, Phys. Rev. D 66 (2002) 063507.
[401] J. Gasser, H. Leutwyler, Phys. Rep. 87 (1982) 77.
[402] T. Dent, S. Stern, C. Wetterich, Phys. Rev. D 76 (2007) 063513.
[403] K. Ichikawa, M. Kawasaki, Phys. Rev. D 69 (2004) 123506.
[404] V.V. Dixit, M. Sher, Phys. Rev. D 37 (1988) 1097.
[405] R.J. Scherrer, D.N. Spergel, Phys. Rev. D 47 (1993) 4774.
[406] K. Ichikawa, M. Kawasaki, Phys. Rev. D 65 (2002) 123511.
[407] J.J. Yoo, R.J. Scherrer, Phys. Rev. D 67 (2003) 043517.
[408] S.R. Beane, K. Orginos, M.J. Savage, Nuclear Phys. B 768 (2007) 38.
[409] V.F. Dmitriev, V.V. Flambaum, J.K. Webb, Phys. Rev. D 69 (2003) 063506.
[410] M. Gell-Mann, R.J. Oakes, B. Renner, Phys. Rev. 175 (1968) 2195.
[411] J.P. Kneller, G.C. McLaughlin, Phys. Rev. D 68 (2003) 103508.
[412] B.S. Pudliner, et al., Phys. Rev. C 56 (1997) 1720.
[413] S.C. Pieper, R.B. Wiringa, Ann. Rev. Nucl. Part. Sci. 51 (2001) 53.
[414] V.V. Flambaum, R.B. Wiringa, Phys. Rev. C 76 (2007) 054002.
[415] A. Bulgac, G.A. Miller, M. Strikma, Phys. Rev. C 56 (1997) 3307.
[416] S.R. Beane, P.F. Bedaque, M.J. Savage, U. van Kolck, Nuclear Phys. A 700 (2002) 377.
[417] S.R. Beane, M.J. Savage, Nuclear Phys. A 717 (2003) 91.
[418] E. Epelbaum, U.G. Meissner, W. Gloeckle, Nuclear Phys. A 714 (2003) 535.
[419] V.V. Flambaum, E.V. Shuryak, Phys. Rev. D 65 (2002) 103503.
[420] V.V. Flambaum, E.V. Shuryak, Phys. Rev. D 67 (2002) 083507.
[421] T. Dent, Fairbarn, Nuclear Phys. B 653 (2003) 256.
[422] S.J. Landau, M.E. Mosquera, H. Vucetich, Astrophys. J. 637 (2006) 38.
[423] X. Calmet, H. Fritzsch, Eur. Phys. J. 24 (2002) 639.
[424] P. Langacker, G. Segre, M. Strassler, Phys. Lett. B 528 (2002) 121.
[425] X. Calmet, H. Fritzsch, Phys. Lett. B 540 (2002) 173.
[426] A. Coc, et al., Phys. Rev. D 76 (2007) 023511.
[427] J.M. Yang, D.N. Schramm, G. Steigman, R.T. Rood, Astrophys. J. 227 (1979) 697.
[428] F.S. Accetta, L.M. Krauss, P. Romanelli, Phys. Lett. B 248 (1990) 146.
[429] C.J. Copi, A.N. Davis, L.M. Krauss, Phys. Rev. Lett. 92 (2004) 171301.

[430] P. Jordan, Nature 164 (1949) 637.
[431] C. Brans, R.H. Dicke, Phys. Rev. 124 (1961) 925.
[432] C. Will, Theory and Experiments in Gravitational Physicss, in: Living Rev. Relativity, vol. 4, Cambridge University press, Cambridge, 1993, p. 4, 2001.
[433] B. Bertotti, L. Iess, P. Tortora, Nature 425 (2003) 374.
[434] A. Coc, K.A. Olive, J.P. Uzan, E. Vangioni, Phys. Rev. D 73 (2006) 083525.
[435] J.A. Casas, J. Garcia-Bellido, M. Quiros, Modern Phys. Lett. A 7 (1992) 447.
[436] J.A. Casas, J. Garcia-Bellido, M. Quiros, Phys. Lett. B 278 (1992) 94.
[437] A. Serna, R. Dominguez-Tenreiro, G. Yepes, Astrophys. J. 391 (1992) 433.
[438] A. Serna, J.M. Alimi, Phys. Rev. D 53 (1996) 3087.
[439] T. Etoh, M. Hashimoto, K. Arai, S. Fujimoto, Astron. Astrophys. 325 (1997) 893.
[440] D.I. Santiago, D. Kalligas, R.V. Wagoner, Phys. Rev. D 56 (1997) 7627.
[441] T. Damour, B. Pichon, Phys. Rev. D 59 (1999) 123502.
[442] F.G. Alvarenga, J.C. Fabris, S.V.B. Goncalves, J.A.O. Marinho, Bras. J. Phys. 31 (2001) 546.
[443] X. Chen, R.J. Scherrer, G. Steigman, Phys. Rev. D 63 (2001) 123504.
[444] A. Serna, J.M. Alimi, A. Navarro, Classical Quantum Gravity 19 (2002) 857.
[445] J.P. Kneller, G. Steigman, Phys. Rev. D 67 (2003) 063501.
[446] R. Nagata, T. Chiba, N. Sugiyama, Phys. Rev. D 69 (2004) 083512.
[447] T. Clifton, J.D. Barrow, R.J. Scherrer, Phys. Rev. D 71 (2005) 123526.
[448] V. Pettorino, C. Baccigalupi, G. Mangano, JCAP 0501 (2005) 014.
[449] A. De Felice, G. Mangano, P.D. Serpico, M. Trodden, Phys. Rev. D 74 (2006) 103005.
[450] J. Larena, J.M. Alimi, A. Serna, Astrophys. J. 658 (2007) 1.
[451] R. Nakamura, M. Hashimoto, S. Gamow, K. Arai, Astron. Astrophys. 448 (2006) 23.
[452] P. Astier, et al., [SNLS Collaboration], Astron. Astrophys. 447 (2006) 31.
[453] A.G. Riess, et al., [Supernova Search Team Collaboration], Astrophys. J. 607 (2004) 665.
[454] S. Cole, et al., [2dFGRS Collaboration], MNRAS 362 (2005) 505.
[455] M. Tegmark, et al., [SDSS Collaboration], Phys. Rev. D 74 (2006) 123507.
[456] C. Wetterich, Nuclear Phys. B 302 (1988) 668.
[457] B. Ratra, P.J. Peebles, Phys. Rev. D 37 (1988) 3406.
[458] R.R. Caldwell, R. Dave, P.J. Steinhardt, Phys. Rev. Lett. 80 (1998) 1582.
[459] E.J. Copeland, A.R. Liddle, D. Wands, Phys. Rev. D 57 (1998) 4686.
[460] P.G. Ferreira, M. Joyce, Phys. Rev. D 58 (1998) 023503.
[461] A.R. Liddle, R.J. Scherrer, Phys. Rev. D 59 (1999) 023509.
[462] P.J. Steinhardt, L. Wang, I. Zlatev, Phys. Rev. D 59 (1999) 123504.
[463] I. Zlatev, L. Wang, P.J. Steinhard, Phys. Rev. Lett. 82 (1999) 896.
[464] P. Brax, J. Martin, A. Riazuelo, Phys. Rev. D 62 (2000) 103505.
[465] T. Chiba, T. Okabe, M. Yamaguchi, Phys. Rev. D 62 (2000) 023511.
[466] C. Armendariz-Picon, V. Mukhanov, P.J. Steinhardt, Phys. Rev. Lett. 85 (2000) 4438.
[467] C. Armendariz-Picon, V. Mukhanov, P.J. Steinhardt, Phys. Rev. D 63 (2000) 103510.
[468] M. Yahiro, G.J. Mathews, K. Ichiki, T. Kajino, M. Orito, Phys. Rev. D 65 (2002) 063502.
[469] A. Albrecht, C. Skordis, Phys. Rev. Lett. 84 (2000) 2076.
[470] S.M. Carroll, M. Kaplinghat, Phys. Rev. D 65 (2002) 063507.
[471] E. Masso, F. Rota, Phys. Rev. D 68 (2003) 123504.
[472] E. Masso, F. Rota, Phys. Lett. B 600 (2004) 197.
[473] J.D. Barrow, R.J. Scherrer, Phys. Rev. D 70 (2004) 103515.
[474] A. Krawiec, M. Szydlowski, W. Godlowski, Phys. Lett. B 619 (2005) 219.
[475] M. Bojovald, R. Das, R.J. Scherrer, Phys. Rev. D 77 (2008) 084003.
[476] G. Lambiase, Phys. Rev. D 72 (2005) 087702.
[477] V.A. Kostelecky, Phys. Rev. D 69 (2005) 105009.
[478] S. Rappaport, J. Schwab, S. Burles, G. Steigman, Phys. Rev. D 77 (2008) 023515.
[479] Ya.B. Zel'dovich, I.D. Novikov, Sov. Astron. 10 (1967) 602.
[480] S.W. Hawking, MNRAS 152 (1971) 75.
[481] B.J. Carr, Astrophys. J. 201 (1975) 1.
[482] M.Yu. Khlopov, 2008. arXiv:0801.0116 [astro-ph].
[483] S.W. Hawking, Nature 248 (1974) 30.
[484] B.J. Carr, Astrophys. J. 206 (1976) 8.
[485] Ya.B. Zel'dovich, A.A. Starobinskii, JETP Lett. 24 (1976) 571.
[486] Ya.B. Zel'dovich, A.A. Starobinskii, M.Yu. Khlopov, V.M. Chechetkin, Sov. Astron. Lett. 3 (1977) 110.
[487] B.V. Vainer, P.D. Nasel'skii, Sov. Astron. 22 (1978) 138.
[488] S. Miyama, K. Sato, Progr. Theoret. Phys. 55 (1978) 1012.
[489] B.V. Vainer, O.V. Dryzhakova, P.D. Nasel'skii, Sov. Astron. Lett. 3 (1978) 185.
[490] D. Lindley, MNRAS 193 (1980) 593.
[491] K. Kohri, J. Yokoyama, Phys. Rev. D 61 (1999) 023501.
[492] M. Ricotti, J.P. Ostriker, K.J. Mack, 2007. arXiv:0709.0524 [astro-ph].
[493] H. Tashiro, N. Sugiyama, Phys. Rev. D 78 (2008) 023004.
[494] J. Jaeckel, J. Redondo, A. Ringwald, Phys. Rev. Lett. 101 (2008) 131801.
[495] Z. Berezhiani, Internat. J. Modern Phys. A 19 (2003) 107.
[496] Z. Berezhiani, D. Comelli, F. Villante, Phys. Lett. B 503 (2001) 362.
[497] A.Yu. Ignatiev, R.R. Volkas, Phys. Rev. D 68 (2003) 023518.
[498] P. Ciarcelluti, Ph.D. Thesis, 2003. arXiv:astro-ph/0312607.
[499] P. Ciarcelluti, A. Lepidi, Phys. Rev. D 78 (2008) 123003.
[500] F. Zwicky, Helv. Phys. Acta 6 (1933) 110.
[501] A. Borriello, P. Salucci, MNRAS 323 (2001) 285.
[502] H. Dahle, 2007. arXiv:astro-ph/0701598.
[503] D. Clowe, M. Bradac, A.H. Gonzalez, M. Markevitch, S.W. Randall, C. Jones, D. Zaritsky, Astrophys. J. 648 (2006) L109.
[504] B.W. Lee, S. Weinberg, Phys. Rev. Lett. 39 (1977) 165.
[505] G. Bertone, D. Hooper, J. Silk, Phys. Rep. 405 (2005) 279.
[506] G.D. Mack, J.F. Beacom, G. Bertone, Phys. Rev. D 76 (2007) 043523.
[507] J.L. Feng, A. Rajaraman, F. Takayama, Phys. Rev. D 68 (2003) 063504.
[508] E.J. Chun, H.B. Kim, J.E. Kim, Phys. Rev. Lett. 72 (1994) 1956.
[509] R.J. Scherrer, M.S. Turner, Astrophys. J. 331 (1988) 19; Astrophys. J. 331, 33.
[510] M. Kachelrieß, P.D. Serpico, Phys. Rev. D 76 (2007) 063516.

[511] G.D. Mack, T.D. Jacques, J.F. Beacom, N.F. Bell, H. Yuksel, 2008. arXiv:0803.0157 [astro-ph].
[512] T. Kanzaki, M. Kawasaki, K. Kohri, T. Moroi, Phys. Rev. D 76 (2007) 105017.
[513] F.A. Aharonian, V.G. Kirillov-Ugryumov, V.V. Vardanian, Astrophys. Space Sci. 115 (1985) 201.
[514] A.A. Zdziarski, R. Svensson, Astrophys. J. 344 (1989) 551.
[515] R. Svensson, A.A. Zdziarski, Astrophys. J. 349 (1990) 415.
[516] R.J. Protheroe, T. Stanev, V.S. Berezinsky, Phys. Rev. D 51 (1995) 4134.
[517] M. Kawasaki, T. Moroi, Astrophys. J. 452 (1995) 506.
[518] K. Jedamzik, Phys. Rev. D 74 (2006) 103509.
[519] M. Kusakabe, et al., 2008. arXiv:0806.4040 [astro-ph].
[520] M. Kawasaki, K. Kohri, T. Moroi, Phys. Rev. D 71 (2005) 083502.
[521] M. Kawasaki, K. Kohri, T. Moroi, Phys. Lett. B 625 (2005) 7.
[522] K. Jedamzik, Phys. Rev. D 70 (2004) 083510.
[523] R.H. Cyburt, J.R. Ellis, B.D. Fields, K.A. Olive, V.C. Spanos, JCAP 0611 (2006) 014.
[524] K. Jedamzik, Phys. Rev. D 77 (2008) 063524.
[525] F.D. Steffen, Phys. Lett. B 669 (2008) 74.
[526] P. McDonald, R.J. Scherrer, T.P. Walker, Phys. Rev. D 63 (2001) 023001.
[527] K. Jedamzik, Phys. Rev. D 70 (2004) 063524.
[528] A. De Rujula, S.L. Glashow, U. Sarid, Nuclear Phys. B 333 (1990) 173.
[529] S. Dimopoulos, D. Eichler, R. Esmailzadeh, G.D. Starkman, Phys. Rev. D 41 (1990) 2388.
[530] J. Rafelski, M. Sawicki, M. Gajda, D. Harley, Phys. Rev. A 44 (1991) 4345.
[531] M. Pospelov, Phys. Rev. Lett. 98 (2007) 231301.
[532] K. Kohri, F. Takayama, Phys. Rev. D 76 (2007) 063507.
[533] M. Kaplinghat, A. Rajaraman, Phys. Rev. D 74 (2006) 103004.
[534] K. Hamaguchi, T. Hatsuda, M. Kamimura, Y. Kino, T.T. Yanagida, Phys. Lett. B 650 (2007) 268.
[535] C. Bird, K. Koopmans, M. Pospelov, Phys. Rev. D 78 (2008) 083010.
[536] M. Kawasaki, K. Kohri, T. Moroi, Phys. Lett. B 649 (2007) 436.
[537] T. Jittoh, K. Kohri, M. Koike, J. Sato, T. Shimomura, M. Yamanaka, Phys. Rev. D 76 (2007) 125023.
[538] D. Cumberbatch, K. Ichikawa, M. Kawasaki, K. Kohri, J. Silk, G.D. Starkman, Phys. Rev. D 76 (2007) 123005.
[539] K. Jedamzik, JCAP 0803 (2008) 008.
[540] M. Kamimura, Y. Kino, E. Hiyama, 2008. arXiv:0809.4772 [nucl-th].
[541] M. Kusakabe, T. Kajino, R.N. Boyd, T. Yoshida, G.J. Mathews, Phys. Rev. D 76 (2007) 121302.
[542] M. Kusakabe, T. Kajino, R.N. Boyd, T. Yoshida, G.J. Mathews, 2007. arXiv:0711.3858 [astro-ph].
[543] T. Jittoh, et al., Phys. Rev. D 78 (2008) 055007.
[544] M.Y. Khlopov, C. Kouvaris, Phys. Rev. D 77 (2008) 065002.
[545] N. Arkani-Hamed, S. Dimopoulos, JHEP 0506 (2005) 073.
[546] G.F. Giudice, A. Romanino, Nuclear Phys. B 699 (2004) 65;
G.F. Giudice, A. Romanino, Nuclear Phys. B 706 (2005) 65 (erratum).
[547] N. Arkani-Hamed, S. Dimopoulos, G.F. Giudice, A. Romanino, Nuclear Phys. B 709 (2005) 3.
[548] D.A. Dicus, V.L. Teplitz, Phys. Rev. Lett. 44 (1980) 218.
[549] R. Plaga, Phys. Rev. D 51 (1995) 6504.
[550] R.N. Mohapatra, V.L. Teplitz, Phys. Rev. Lett. 81 (1998) 3079.
[551] A. Arvanitaki, C. Davis, P.W. Graham, A. Pierce, J.G. Wacker, Phys. Rev. D 72 (2005) 075011.
[552] M. Pospelov, 2007. arXiv:0712.0647 [hep-ph].
[553] J. Pradler, F.D. Steffen, Nuclear Phys. B 809 (2009) 318.
[554] S. Bailly, K. Jedamzik, G. Moultaka, 2008. arXiv:0812.0788 [hep-ph].
[555] E. Holtmann, M. Kawasaki, T. Moroi, Phys. Rev. Lett. 77 (1996) 3712.
[556] K. Jedamzik, Phys. Rev. Lett. 84 (2000) 3248.
[557] E. Holtmann, M. Kawasaki, K. Kohri, T. Moroi, Phys. Rev. D 60 (1999) 023506.
[558] E. Masso, R. Toldra, Phys. Rev. D 55 (1997) 7967.
[559] D.G. Cerdeno, K.Y. Choi, K. Jedamzik, L. Roszkowski, R. Ruiz de Austri, JCAP 0606 (2006) 005.
[560] K. Jedamzik, K.Y. Choi, L. Roszkowski, R. Ruiz de Austri, JCAP 0607 (2006) 007.
[561] T. Kanzaki, M. Kawasaki, K. Kohri, T. Moroi, Phys. Rev. D 75 (2007) 025011.